UNIVERSITÀ DEGLI STUDI DI CATANIA

in convenzione con

UNIVERSITÀ DEGLI STUDI DI PALERMO

Dottorato di Ricerca in
Scienza dei Materiali e Nanotecnologie - XXIX ciclo

Maria Cantarella

Polymer strategies for water purification based on photocatalysis and molecular imprinting

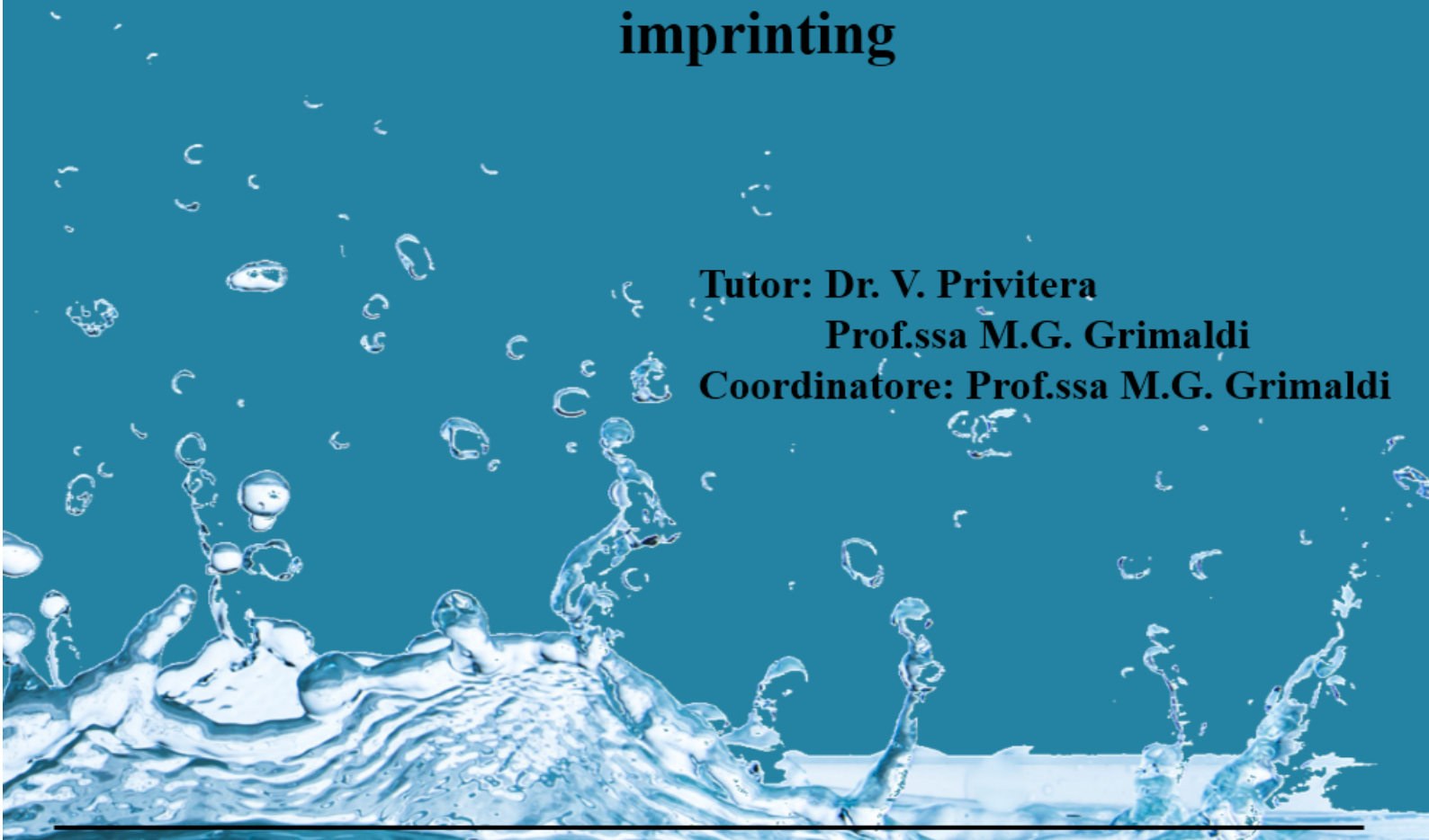

Tutor: Dr. V. Privitera
Prof.ssa M.G. Grimaldi
Coordinatore: Prof.ssa M.G. Grimaldi

Tesi per il conseguimento del titolo di Dottore di Ricerca

UNIVERSITÀ DEGLI STUDI DI CATANIA

IN CONVENZIONE CON

UNIVERSITÀ DEGLI STUDI DI PALERMO

DOTTORATO DI RICERCA IN
SCIENZA DEI MATERIALI E NANOTECNOLOGIE - XXIX CICLO

Maria Cantarella

Polymer strategies for water purification based on photocatalysis and molecular imprinting

TUTOR: DR. V. PRIVITERA

PROF.SSA M.G. GRIMALDI

COORDINATORE: PROF.SSA M.G. GRIMALDI

TESI PER IL CONSEGUIMENTO DEL TITOLO DI DOTTORE DI RICERCA

Contents

Preface 1

Chapter 1: Theory of photocatalysis **5**

1.1 Fundamentals of photocatalysis 6

1.1.1 *Heterogeneous photocatalysis* 8

1.1.2 *TiO_2 as photocatalyst* 12

1.1.3 *Operational parameters affecting photo-activity* 15

1.2 Development of visible light active TiO_2 photocatalysts 17

1.2.1 M*etal deposition* 18

1.2.2 *Non-metal doping* 19

1.2.3 *Dye sensitization* 21

1.2.4 *Semiconductor coupling* 22

1.3 Nanostructured photocatalysts 24

1.4 Conclusions 25

References 25

Chapter 2: Polymer nanocomposites **29**

2.1 Hybrid nanocomposites 30

2.1.1 *Polymer-matrix nanocomposites* 31

2.2 Polymer nanocomposites synthesis methods 34

2.2.1 *Ex situ synthesis methods* 34

2.2.2 In *situ synthesis methods* 35

2.3 Polymer-supported TiO_2 nanomaterials as photocatalysts 37

2.3.1 *Overview of some examples of polymer-TiO_2 nanocomposites* 41

2.4 Future research 43

References 45

Chapter 3: Immobilization of TiO_2-based nanomaterials in PMMA 49

3.1 Experimental section 50

3.1.1 *Synthesis method* 50

3.1.2 *Photocatalytic activity tests* 51

3.1.3 *Antibacterial activity tests* 55

3.2 PMMA/TiO_2 composites 56

3.2.1 *Preparation of PMMA/TiO_2 NPs nanocomposites and characterization* 56

3.2.2 *Photocatalytic activity: results and discussion* 60

3.2.3 *Antibacterial activity: results and discussion* 65

3.2.4 *Stability of the PMMA/TiO_2 NPs photocatalysts* 66

3.2.5 *PMMA/TiO_2 nanotubes composites* 70

3.3 PMMA/TiO_2 NPs/SWCNTs composites 74

3.3.1 *Results and discussion* 76

3.4 PMMA/TiO_2-TCPP nanocomposites 79

3.4.1 *Results and discussion* 81

3.5 Conclusions 86

References 87

Chapter 4: Future perspectives: molecularly imprinted polymers 89

4.1 Emerging contaminants in water 90

4.2 Molecular imprinting 93

4.2.1 *MIPs for water treatment* 96

4.3 Experimental section 98

4.3.1 *MIP film synthesis* 99

4.3.2 *Quartz Crystal Microbalance analysis* 101

4.4 Results and discussion 102
4.5 Conclusions and future perspectives 107
References 108

Conclusion 111

Appendix: Characterization techniques 113
A.1 Scanning Electron Microscopy 115
A.2 Atomic Force Microscopy 119
A.3 Quartz Crystal Microbalance 123

Curriculum vitae 127

List of publications 129

Acknowledgements 131

Preface

Water is a natural resource essential for life, but many factors prevent access to safe drinking water. Today, 1 billion people in the world have a limited access to it.

Earth's population could grow by three billion in the next 50 to 75 years and by 2050 the global water demand is estimated to increase by 55% (*The United Nations World Water Development Report, 2015*). Furthermore, this growth implies a greater risk that existing water sources will become polluted. In fact, the industrial and agricultural growth related to such population increase, will add their own pollutants to many water supplies.

Much of the world's freshwater is contaminated by natural or human causes. Some contaminants are organisms that include pathogens like bacteria, viruses and parasites. These living organisms can be spread by human and animal waste. Other pollutants are the man-made byproducts of industry and agriculture including harmful heavy metal ions, insecticides, fertilizers, dye molecules, radionuclides, pharmaceuticals, personal care products and endocrine disruptor compounds. Water-related diseases cause millions of mortalities every year.

For too long time water was generally taken as granted until increasing pollution and diminishment of potable water supplies delineated a need to protect our water provisions and develop technologies to purify water, in order to avoid side effects and consequences for the human health and for the environment. Wastewater effluents are high in nutrients and may cause algal blooms that release toxins into source water. For this reason, it is mandatory that pollutants in wastewater effluents from both industrial and domestic origin be removed before discharge into the environment. However, the current water treatment methods for securing clean water will be unable to meet the needs of our growing population; in fact, many of the methods used today were already established in the beginning of the twentieth century and they fail to satisfy many requirements. For example, adsorption or coagulation merely concentrate the pollutants present by

transferring them to other phases, not being completely eliminated or destroyed *(Padmanabhan et al., 2006)*. Other conventional processes including sedimentation, filtration, chemical and membrane technologies, such as the widely used reverse osmosis, involve high operating costs and could generate toxic secondary pollutants into the ecosystem *(Gaya and Abdullah, 2008)*. Chlorination has been the most commonly and widely used disinfection process, but the by-products generated from chlorination are mutagenic and carcinogenic to human health *(Yang and Cheng, 2007)*. Considering current and future problems, new methods and technologies of purifying water at lower cost, energy and environmental impact than current methods are required.

Since the end of the twentieth century, a great amount of effort has been pointed to the development of advanced oxidation processes (AOPs) as innovative water treatment technologies. The goal of these AOPs is to mineralize organic pollutants into inorganic compounds via highly reactive transitory species, such as hydroxyl radicals (OH·). Among these AOPs, heterogeneous photocatalysis, employing semiconductor catalysts irradiated by light (TiO_2, ZnO, Fe_2O_3, CdS, GaP and ZnS), has demonstrated its efficiency in degrading a wide range of refractory organics into readily biodegradable compounds, mineralized to innocuous carbon dioxide and water, and in destroying bacteria. Considering the several photocatalysts, the most promising and widespread material is the titanium dioxide (TiO_2), because of its photocatalytic efficiency under UV light. Furthermore, it is abundant, inexpensive and stable. In addition, nanosized particles are preferred to bulk TiO_2 because they are significantly more reactive due to their enormous surface-to-volume ratio. Currently, the main goal of the research in this field is the development of different strategies to modify the photoresponse of TiO_2, for example by non metal and/or metal doping, dye sensitization or coupling with a second semiconductor, in order to obtain visible light active materials. The use of solar photocatalysis technology is inexpensive, environmentally friendly and universally applicable. The equipment needed is minimal, therefore it can be appropriate for developing countries or remote sites with no access to electricity.

Although the nanoscale TiO_2 shows greater surface in contact with water than simple bulk materials and consequently a higher efficiency, it

suffers of several limits for a real application due to their impact on human health and ecosystems. Many side effects associated to the use of nanomaterials have been confirmed, many others are still under study. Therefore, if nanomaterials are applied in the form of dispersion, efficient separation processes are necessary after water treatment. To overcome the above mentioned drawbacks, continuous efforts are being made to immobilize the nanomaterials on different substrates. Considering the various substrates that have been tested for supporting photocatalysts, polymers seem to be very promising.

Recently, there is an increasing interest on a large number of substances that have been detected in the environment, but which are currently not included in routine monitoring programs. Such substances, like non-steroidal anti-inflammatory drugs (NSAIDs) or endocrine-disrupting compounds, are identified as emerging contaminants. Their concentrations are extremely low to be removed by traditional methods, but their presence may cause severe problems. In addition, the traditional techniques may remove various pollutants simultaneously but cannot effectively remove specific pollutants from wastewater. For these reasons, new methods that are both selective and cost-effective to remove the low-level organic pollutants are urgently needed. In this challenge, the central point is to prepare synthetic materials with specific molecular recognition ability targeted toward the pollutants. Recently, molecularly imprinted polymers (MIPs) are attracting extensive attention; MIPs are synthetic polymers possessing specific cavities designed for target molecules. In this field, molecular imprinting provides potential opportunities for efficient removal of low abundance pollutants with low cost, low energy consumption and low environmental impact.

Aim of this dissertation is to propose innovative polymeric materials for water treatment as potential alternative to the traditional methods. Two types of materials have been studied: TiO_2 based polymeric nanocomposites, using poly (methyl methacrylate) (PMMA) as matrix, with high photocatalytic and antibacterial activities both under UV light and visible light; molecularly imprinted polymer films synthesized by electrochemical polymerization for the selective removal of NSAIDs from water.

Chapter 1 introduces the fundamental processes involved in TiO_2 photocatalysis, with particular attention to the recent development in the use of nanostructured TiO_2 for water purification.

Chapter 2 summarizes the synthesis methods for the realization of polymeric nanocomposites; it illustrates their typical application and their use for water treatment.

Chapter 3 describes the synthesis, the characterization, and the photocatalytic and antibacterial properties under UV light of the PMMA/TiO_2 nanocomposites. It reports also the combination of these nanocomposites with carbon nanotubes to increase their photocatalytic efficiency and the functionalization of the TiO_2 surface with a porphyrin, in order to obtain active systems under visible light.

Chapter 4 presents the preliminary results and the future perspectives of the molecularly imprinted polymers for the removal of emerging contaminants in wastewater, such as the NSAIDs.

At the end, in the appendix, the characterization techniques used in this work have been described.

Chapter 1

Theory of photocatalysis

Remediation of contaminated water is an area of great interest. In the recent years, numerous techniques have been applied to improve the quality of naturally available water to the level suitable for human consumption. However, most of these methods involve high operating costs or generate toxic by-products. Heterogeneous photocatalysis using metal oxide semiconductors for water purification is an attractive option because no harmful by-products are created. It can degrade organic molecules, which are usually toxic, into innocuous species (CO_2, H_2O, NO_3^-, PO_4^{3-} and halide ions) as well as immobilize microbial cells by fracturing the cell walls. Among the several inorganic semiconductor, TiO_2 is the most studied and probably the most suitable for industrial use. The reason lies in its very efficient photoactivity, high stability and low cost. In addition, nanostructured TiO_2 materials offer large surface to volume ratios allowing higher adsorption of the target molecules. Another interesting aspect of photocatalysis is the potential utilization of sunlight, which could permit energy-efficient water treatment in remote locations; the development of visible-light active titanium dioxide is one of the key challenges in the field of semiconductor photocatalysis.

In this chapter, the fundamentals of heterogeneous photocatalysis are described, with particular attention to the application of TiO_2 as photocatalyst. The strategies used to improve its efficiency and to enhance its photocatalytic performance in the visible region are showed. The most important recent progresses in the field of nanostructured TiO_2 for water treatment applications are also illustrated.

1.1 Fundamentals of photocatalysis

The seminal article by Fujishima and Honda published in 1972 [Fujishima and Honda, 1972] is considered the origin of the impressive development of research on photocatalysis. This work revealed the possibility of water splitting by photoelectrochemical cell having an inert cathode and rutile titania anode. Consequently, Frank and Bard [Frank and Bard, 1977] for the first time reported the application of TiO_2 in photocatalytic oxidation of CN^- and SO_3^{2-} in aqueous medium under sunlight. The earliest description of photodecomposition of organic compounds was reported by Kraeutler and Bard in 1978 [Krautler and Bard, 1978]. Since its infancy, photocatalysis has attracted an increasing interest as attested by the high number of papers present in the literature (Fig. 1.1).

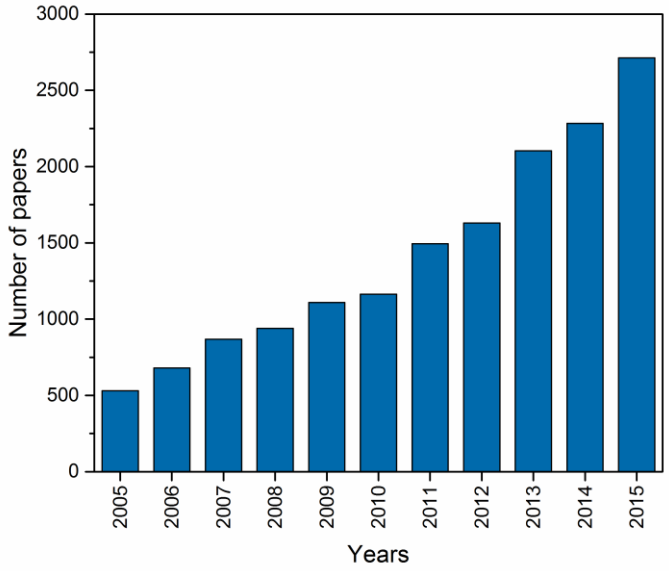

Figure 1.1: Number of publications concerning photocatalysis over the years 2005-2015, based on database of ScienceDirect, with search keywords being "TiO_2 photocatalysis".

Photocatalysis is one of the advanced oxidation processes (AOPs); these processes comprise a class of reactions that use a catalyst activated either by light or chemically [Augugliaro et al., 2006] for the generation of strong reactive radical species such as H_2O_2, $O_2^{\bullet-}$, O_3 and mostly hydroxyl radical ($OH^{\bullet}$) [Pera-Titus et al., 2004], for the mineralization of refractory organic compounds [Wang et al., 2012]. Photocatalysis can be homogeneous or heterogeneous.

The homogeneous photocatalysis methods that are based on the addition of hydrogen peroxide (H_2O_2) to dissolved iron salts can be classified into two types of reaction: Fenton reaction that does not involve any light irradiation and photo-Fenton reaction that reacts up to a light wavelength of 600 nm. In the absence of a light source (Fenton reaction), H_2O_2 will decompose by Fe^{2+} ions present in the aqueous phase, resulting in the formation of hydroxyl radicals, with the following mechanism:

$$Fe^{2+}(aq) + H_2O_2 \longrightarrow Fe^{3+}(aq) + OH^- + HO^{\bullet}$$

When a light source is present (photo-Fenton reaction), the rate of hydroxyl formation enhances compared to dark condition. This is mainly attributed to the regeneration of $Fe^{2+}(aq)$ from the photochemical effect of light [Chong et al., 2010]. Several studies on the photo-Fenton degradation of water pollutants such as chlorophenol, pesticides and phenolic or aromatic compounds have been investigated [Pera-Titus et al., 2004] [Huston et al., 1999] [Gernjak et al., 2007].

The heterogeneous photocatalysis methods instead uses wide-band gap semiconductors in contact with water that, photoexcited by light, are able to produce hydroxyl radicals (this type of photocatalysis will be described in detail in the next paragraph).

Although photo-Fenton photocatalysis has higher reactivity than heterogeneous photocatalysis, its application is complex and expensive due to pH rectification that is required to control the formation of photoactive iron complexes [De Laat et al., 2004]. For these reasons, heterogeneous photocatalysis seems to be the most promising strategy for purification of both air and water streams.

1.1.1 Heterogeneous photocatalysis

Heterogeneous photocatalysis employs inorganic semiconductors, like TiO_2, ZnO, ZnS, ZrO_2, MoS_2, WO_3, SnO_2, Fe_2O_3, CdS, etc, which upon irradiation with light (*hv*) of energy higher than the band gap energy of the material are able to create electron-hole pairs (e^- - h^+). Hence, the electrons are excited from the filled valence band to the empty conduction band to leave a positive hole in the valence band [Gaya and Abdullah, 2008] [Fujishima et al., 2000]. Some electrons and holes can migrate to the surface of the semiconductor without recombination and initiate a series of redox reactions with water, oxygen and other organic or inorganic species adsorbed on the surface of the catalyst, resulting for instance in the degradation of pollutants, as depicted in Fig. 1.2.

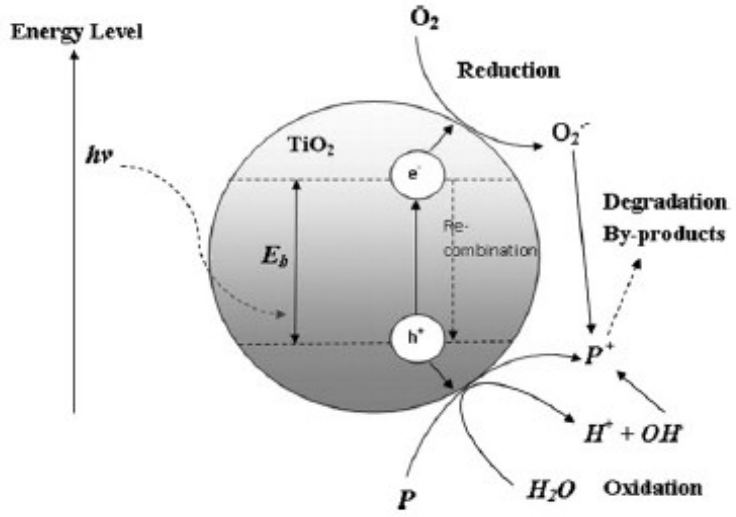

Figure 1.2: Photo-induced formation mechanism of electron-hole pair in a semiconductor with the presence of pollutant (P) [Chong et al., 2010].

Following the usually proposed series of oxidative-reductive reactions that occur at the photon activated surface of the catalyst [Houas et al., 2001]:

- Absorption of efficient photons ($h\nu \geq E_G$) by the inorganic semiconductor catalyst (MO)

  $MO + h\nu \longrightarrow e^-_{CB} + h^+_{VB}$

- Neutralization of OH^- groups of the adsorbed water molecules by the photoholes with production of hydroxyl radical ($OH^\bullet$)

  $(H_2O \rightleftharpoons H^+ + OH^-)_{ads} + h^+_{VB} \longrightarrow H^+ + OH^\bullet$

- Reduction by one electron of the adsorbed oxygen to give superoxide radicals (oxygen's oxidation degree passes from 0 to -1/2)

  $(O_2)_{ads} + e^-_{CB} \longrightarrow O_2^{\bullet -}$

- Protonation of superoxides to give hydroperoxyl radicals

  $O_2^{\bullet -} + H^+ \longrightarrow HO_2^\bullet$

- The formed hydroperoxyl radicals also have scavenging property as O_2 thus doubly prolonging the lifetime of photoholes and forming hydrogen peroxide

  $HO_2^\bullet + e^- \longrightarrow HO_2^-$
  $HO_2^- + H^+ \longrightarrow H_2O_2$

- Reduction of hydrogen peroxide to produce hydroxyl radicals

  $H_2O_2 + e^- \longrightarrow OH^\bullet + OH^-$

- Oxidation of the organic compounds (R) via successive attacks by $OH^\bullet$ radicals

  $R + OH^\bullet \longrightarrow R'' + H_2O \longrightarrow CO_2 + H_2O$

It should be noted that all these photocatalytic events were attributed to the presence of both oxygen and water molecules. Without the presence of water molecules, the highly reactive hydroxyl radicals ($OH^{\bullet}$) could not be formed and impede the photodegradation of dissolved organic compounds. Although the holes have been widely regarded for their ability to oxidize organic species directly, this contribution is negligible [Chong et al., 2010].

From a thermodynamic viewpoint, the photocatalytic reduction and oxidation reactions can be driven by the photo-generated e^- and h^+, respectively, only when their reduction and oxidation potentials lie between the conduction band and the valence band potentials. The energy of the conduction band edge (E_c) corresponds to the potential of the photogenerated electrons, whereas the energy of the valence band (E_v) corresponds to the potential of the holes. If E_c is more negative than the potential of a species present in solution, electrons reaching the surface of the semiconductor can reduce the oxidized form of the redox couple. On the other hand, if the potential of E_v is more positive than that of the redox couple, photoproduced holes can oxidize its reduced form. For this reason, the knowledge of the relative edge positions of the bands and of the energetic levels of the redox couples is essential to establish if thermodynamics allows the occurrence of the reactions with the adsorbed species on the surface of the catalyst, in order to generate free radicals which could then act as reactive species and further degrade the organic pollutants. The potentials for various redox processes for TiO_2, at pH = 7, are given in Fig. 1.3. The band positions for some important semiconductors (at pH = 7 in aqueous solution) and their potential applications are illustrated in Fig. 1.4. In order to correlate the energetic levels of the semiconductor and redox couple, two different scales are used (in eV and V). In fact, in solid-state physics, zero is the level of an electron in vacuum, while in electrochemistry the reference is the potential of the normal hydrogen electron (NHE or SHE). The two scales are correlated using the potential of NHE, which is equal to -4.5 eV and is referred to as that of electron in vacuum [Hu and Apblett, 2014].

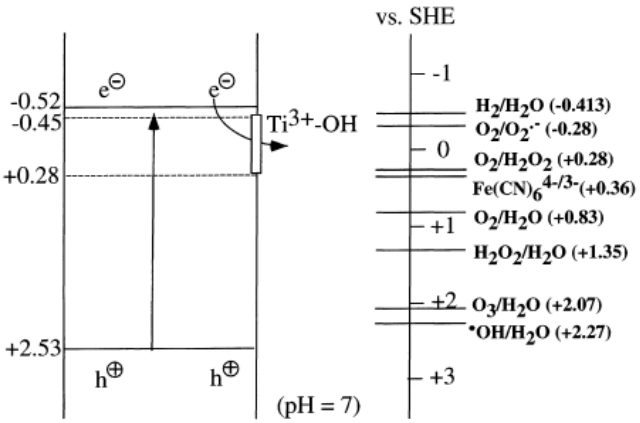

Figure 1.3: Schematic diagram showing the potentials for various redox processes occurring on the TiO_2 surface at pH 7 [Fujishima et al., 2000].

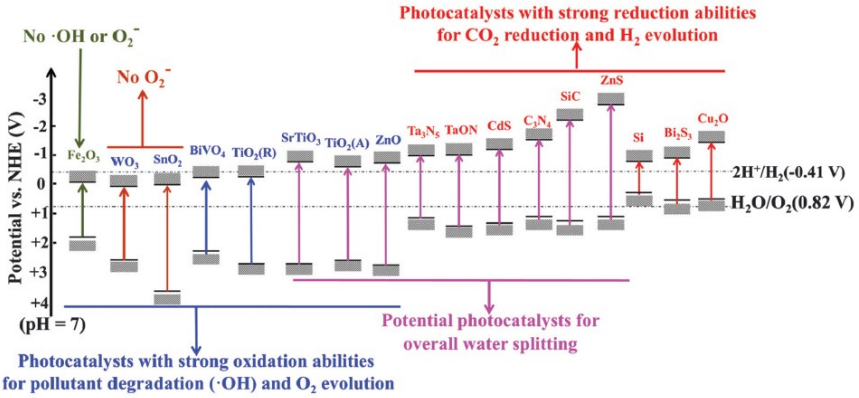

Figure 1.4: Band positions and potential applications of some typical photocatalysts at pH 7 in aqueous solutions [Li et al., 2016].

Thus, the more negative conduction band positions of semiconductors are beneficial for reduction reactions, while the more positive valence band positions of semiconductors are favorable for oxidation reactions. It is clear that the ideal energy band diagram of TiO_2 should ensure the simultaneous formation of holes, $OH^{\bullet}$ radicals, O_2^- and

H_2O_2, all of which have been proven to play an important role for the photocatalytic degradation of organic compounds. Furthermore, TiO_2 is also relative inexpensive, highly stable and readily available, and therefore it is commonly used as the best photocatalytic material.

1.1.2 TiO_2 as photocatalyst

An ideal photocatalyst should be characterized by the following attributes [Gaya and Abdullah, 2008]:

- Photo-stability
- Chemically and biologically inert nature
- Availability and low cost
- Capability to adsorb reactants under efficient photonic activation ($h\nu \geq E_G$).

Among the several semiconductor catalysts, titanium dioxide (TiO_2) has received the greatest attention in the water treatment research including photodegradation of numerous organic pollutants, photoreduction of inorganic contaminants and inactivation of microorganisms, because it satisfies quite well the above mentioned requests.

Titanium dioxide belongs to the family of transition metal oxides. In the beginning of the 20^{th} century, industrial production started with titanium dioxide replacing toxic lead oxides as pigments for white paint. It is used as a white pigment in paints (51% of total production), plastic (19%), and paper (17%), which represent the major end-use sectors of TiO_2. The consumption of TiO_2 as a pigment increased in the last few years in a number of minor end-use sectors such as textiles, food, leather, pharmaceuticals (tablet coatings, toothpastes and as UV absorber in sunscreen cream with high sun protection factors and other cosmetic products) [Carp et al., 2004]. In the photocatalysis field, TiO_2 mediated photocatalytic reactions are gaining nowadays more and more importance and this is reflected in the increasing number of publications that deal with theoretical aspects and practical applications of these reactions.

TiO_2 crystallizes in three major different structures: rutile, anatase and brookite; however, only rutile and anatase play a role in the applications of TiO_2. Their unit cells are shown in Fig. 1.5. In both structures, the basic building block consists of a titanium atom surrounded by six oxygen atoms in a more or less distorted octahedral configuration. In each structure, the two bonds between the titanium and the oxygen atoms at the apices of the octahedron are slightly longer. A sizable deviation from a 90° bond angle is observed in anatase. In rutile, neighboring octahedral share one corner along (110) type directions and are stacked with their long axis alternating by 90°. In anatase the corner-sharing octahedral form (001) planes. They are connected with their edges with the plane of octahedral below [Diebold, 2003].

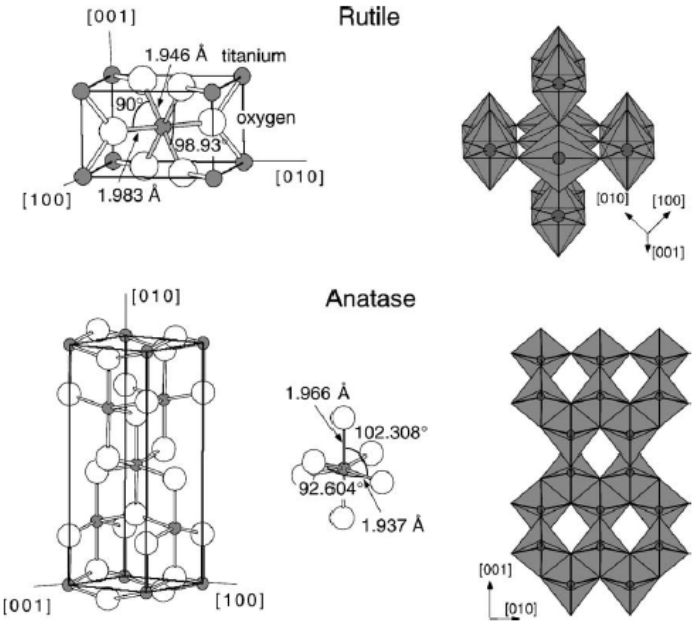

Figure 1.5: Bulk structures of rutile and anatase [Diebold, 2003].

The differences in lattice structures of anatase and rutile TiO_2 cause different densities and electronic band structures, leading to different band gaps, for bulk materials: anatase 3.20 eV and rutile 3.02 eV. Therefore, pure

TiO_2 is primarily active for UV light. Both crystal structures, anatase and rutile, are commonly used as photocatalyst; however, for pure phases it is generally accepted that anatase shows a greater photocatalytic activity for most reactions compared to rutile. It has been suggested that this increased photoreactivity is due to anatase's slightly higher Fermi level, lower capacity to adsorb oxygen and higher degree of hydroxylation (i.e., number of hydroxyl groups on the surface) [Carp et al., 2004]; however, despite the intensive study of TiO_2, there is no generally accepted explanation for the differences of photocatalytic activity of the different forms [Luttrell, 2014]. Furthermore, there are also studies which claim that a mixture of anatase (70-75%) and rutile (30-25%) is more active than pure anatase. Indeed, the most common commercial photocatalyst is the Degussa P-25, a powder consisting of a mixture of anatase and rutile crystallites in an approximate proportion of 80/20, it is for many reactions more active than both the puree crystalline phases. Superior photocatalytic activity of these biphasic TiO_2 results from the effective transfer of photo-generated electrons from the conduction band of anatase to that of rutile, favoring electron-hole separation [Etacheri et al., 2015].

The biocidal action of the TiO_2 photocatalyst is now well recognized; it was first observed in 1985 by Matsunaga et al., who reported that microbial cells could be killed by the contact with a TiO_2-Pt catalyst under illumination with near UV light [Matsunaga et al., 1985]. TiO_2 nanoparticles have been used to successfully inactivate different types of bacteria including *Escherichia coli* [Zimbone et al., 2015], *Pseudomonas aeruginosa, Salmonella typhimurium* and *Enterobacter cloacae* [Ibanez et al., 2003]. According to literature data, the highly reactive oxygen species ($OH^{\bullet}$, $O_2^{\bullet-}$, H_2O_2), formed during the UV activation, are the key species in the photocatalytic disinfection process. In fact, all of three exhibit bactericidal activity, but some studies have emphasized that the hydroxyl radical would be the most important oxidant species responsible for the attack of the bacterial cell wall, leading to modifications of membrane permeability and cell death [Cho et al., 2004].

1.1.3 Operational parameters affecting photo-activity

Some of the main operational parameters affecting the photocatalytic activity are discussed below [Gaya and Abdullah, 2008]:

- *Light intensity*

The photocatalytic reaction rate depends largely on the radiation absorption of the photocatalyst. Some studies revealed an increase in the degradation rate with increasing the light intensity. However, energy loss due to light reflection, transmission and energy loss as heat is inevitable in the photoprocess. The overall quanta of light absorbed by any photocatalyst is given by $\Phi_{overall}$, the quantum yield:

$\Phi_{overall}$= rate of reaction / rate of absorption of radiation

Since metal oxide such as TiO_2 in a heterogeneous regime cannot absorb all the incident radiation due to refraction, it has been experimentally difficult to determine the quantum yield. The light scattering, particularly in solid-liquid regime, is also significant. Another factor limiting photonic efficiency is the thermal recombination between electron and hole. For these reasons, it is argued that the use of quantum yield in heterogeneous system might be misleading. A practical and simple alternative for comparing process efficiencies consists in defining a relative photonic efficiency ζ, defined as the number of reactant molecules transformed divided by the number of incident photons:

$\zeta = N_{mol}$ transformed / N_{ph} incident

- *Nature and concentration of the organic pollutant*

Organic molecules that can adhere more successfully to the surface of the photocatalyst will be more susceptible to direct oxidation. Thus, the photocatalytic degradation of aromatic compounds depends on the substituent group. For instance, it is reported that nitrophenol adsorbs easier

to the photocatalyst surface than phenol and therefore degrades faster [Bhatkhande et al., 2004].

The degradation rate of organic pollutants usually exhibits a saturation behavior, in fact the observed rate constant decreases with increasing the initial organic concentration. Three factors might be responsible for this behavior: 1) at high initial concentration all catalytic sites are occupied, a further increase of the concentration does not affect the actual catalyst surface concentration and therefore this may result in a decrease of the observed first-order rate constant. 2) The generation and migration of photogenerated carriers and their reaction with organic compounds occur in series. At low concentrations, the latter dominates the process and, therefore, the degradation rate increases linearly with concentration. However, at high concentrations, the former will become the governing step and the degradation rate increases slowly with concentration. 3) Intermediates generated during the photocatalytic process also affect the rate constant of their parent compounds. A higher initial concentration will yield a higher concentration of adsorbed intermediates, which will affect the overall rate [Carp et al., 2004].

- *Nature and concentration of the photocatalyst*

There is a direct correlation between organic pollutant and surface coverage of TiO_2 photocatalyst. A very important parameter influencing the performance of photocatalyst in photocatalytic oxidation is the surface morphology, namely the particle size and agglomerate size. Numerous forms of TiO_2 have been synthesized by different methods to obtain a photocatalyst exhibiting desirable physical properties, activity and stability for photocatalytic application. For instance, smaller nano-particle size is reported to give higher conversion in photomineralization of organic compounds.

Generally, decomposition increases with catalyst loading due to a higher surface area of the catalyst that is available for adsorption and degradation. However, an optimum catalyst concentration value is present, while above a certain concentration, the solution opacity increases (due to increased light scattering of the catalyst particles) causing a reduction of light penetration in the solution and a consequent rate decrease. For this reason, in slurry

photoreactors the optimal catalyst dosage or effective optical penetration length, under given conditions, is very important in designing an efficient reactor. If the solution layer thickness exceeds the optical penetration length at any given illumination intensity and catalyst concentration, the photoreactor will be under-utilized. For TiO_2 immobilized systems, there is also an optimal thickness of the catalyst film. The interfacial area is proportional to the thickness of catalyst, as the film is porous. Thus, thick films facilitate catalytic oxidation. On the other hand, the internal mass transfer resistance for both organic species and photogenerated carriers will increase with increasing thickness. This increases the recombination possibility of the electron-hole pair and, as a consequence, the degradation performance is reduced [Carp et al., 2004].

- *pH*

The pH of the solution dictates the surface charge properties of the photocatalyst, its stability and size of aggregates it forms. For instance, Degussa P-25 is reported to have a point of zero charge (pzc) 6.9. Under acidic or alkaline condition, the surface of titania can be protonated or deprotonated, respectively. It is reported that titanium dioxide has a higher oxidizing activity at lower pH, but excess H^+ at very low pH can decrease the reaction rate.

- *Temperature*

Generally, the increase of temperature enhances the recombination of charge carriers and desorption process of adsorbed reactant species, resulting in a decrease of photocatalytic activity. This is in conformity with Arrhenius equation, for which the apparent first order rate constant K_{app} should increase linearly with exp(-1/T).

1.2 Development of visible light active TiO_2 photocatalysts

One of the major drawbacks of pure TiO_2 is the large band gap (~ 3.2 eV for anatase and ~ 3.0 eV for rutile) implying that this material can only be

activated using an irradiation with photons in the UV region ($\lambda \leq 387$ nm). Given that only ~5% of the solar spectrum incident at the earth's surface lies in this spectral region, TiO_2 is inefficient when sunlight is used as light source to drive the photocatalytic reactions. In order to utilize a larger fraction of the solar spectrum for a potential real application in the environmental remediation, designing, fabricating and tailoring the physicochemical and optical properties of TiO_2 is of great importance. For this purpose, TiO_2 has been modified by various strategies such as: metal doping, non-metal doping, dye sensitization, and coupling of a narrow-band gap semiconductor [Pelaez et al., 2012] [Reddy et al., 2016] [Etacheri et al., 2015] [Dong et al., 2015].

1.2.1 Metal deposition

Over the past decades, metal-doped TiO_2 (e.g.,Cu, Co, Ni, Cr, Mn, Fe, Ru, Au, Ag, Pt) photocatalysts have been widely studied for improving the photocatalyitc performance in the degradation of various organic pollutants under visible light irradiation [Anpo, 2000] [Fuerte et al., 2001] [Arabatzis et al., 2003] [Hu et al., 2006] [Zang and Farnood, 2008] [Zaleska, 2008] [Han et al., 2014]. The effect of metal ion dopants on the visible light photoactivity of metal-doped TiO_2 can be explained by a new energy level produced in the band gap of TiO_2, near the conduction band, by the dispersion of metal nanoparticles in the TiO_2 matrix. As shown in Fig. 1.6, electrons can be excited from the TiO_2 valence band to the defect state introduced by the metal.

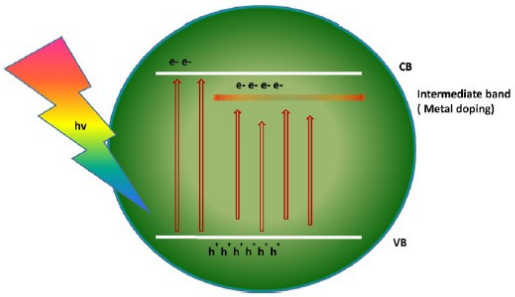

Figure 1.6: Band gap modification in semiconductor photocatalyst by the formation of intermediate band levels through metal doping [Reddy et al., 2016].

In addition, deposition of metal nanoparticles with a large work function, such as Ag, Pt, Au and Pd, onto titanium dioxide surface has been found to efficiently delay the e^- - h^+ recombination acting as an electron trap, because of the Schottky barrier formed at the metal-TiO_2 interface. The decrease of charge carriers recombination results in enhanced photoactivity [Wang et al., 2008].

However, it has been demonstrated that the photocatalytic activity of metal-doped TiO_2 could be influenced by the dopant concentration [Ambrus et al., 2008] [Tong et al., 2008]. A reduced photocatalytic performance was identified above an optimum metal content, which was proven to be resulting from a reduced photon absorption by TiO_2 and from the action of excess metal as electron-hole recombination centres. Moreover, metal doping shows other drawbacks: thermal instability of doped TiO_2 and requirement of expensive ion-implantation facilities. These shortcomings prevent the industrial application of the metal doping methods.

1.2.2 Non-metal doping

Non-metal doping has shown great promise in achieving visible light active photocatalyst. Among all non-metal doped TiO_2 materials, N- and C-doped TiO_2 have been found to exhibit superior photocatalytic activity under visible irradiation. In particular, nitrogen can be easily introduced in the

TiO_2 structure, due to its comparable atomic size with oxygen. There have been a large number of publications that deal with the preparation of N-TiO_2 by physical or chemical methods, including sol-gel, sputtering, ion implantation, mechanochemical and plasma-enhanced chemical vapor deposition method [Impellizzeri et al., 2015] [Zaleska, 2008]. In addition, different conclusions concerning the state of doped nitrogen in the N-TiO_2 lattice and the mechanism of band gap narrowing have been derived (Fig. 1.7). For instance, some studies [Irie et al., 2003] [Lindgren et al., 2003] found that interstitial-type doping of N atoms was related to the photo-threshold energy decrease, which induced localized N 2p states within the band gap just above the top of the valence band, facilitating the production of oxygen vacancies.

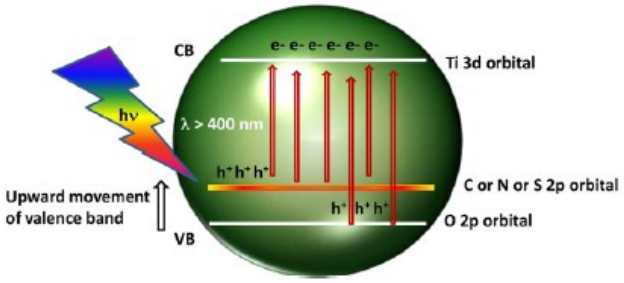

Figure 1.7: The upward movement of valence band in non-metal doping [Reddy et al., 2016].

Despite the visible-light photocatalytic performance of non-metal doped TiO_2, some drawbacks occur with this approach: short term stability; high cost and energy consumption of the preparation method especially due to the required thermal treatment at high temperatures; low efficiency attributed to the fact that the doping of non-metals into the lattice of TiO_2 usually results in the formation of oxygen vacancies in the bulk, acting as massive recombination centers reducing the photocatalytic efficiency.

1.2.3 Dye sensitization

Dye sensitization is now considered to be one of the most effective ways to extend the photoresponse of TiO_2 into the visible region; these types of reactions are already exploited in the dye sensitized solar cells. Visible light-induced dye-sensitized TiO_2 photocatalysts can be readily prepared under a mild condition through interfacial adsorption of dye molecules on TiO_2. Some dyes used as sensitizers include erythrosine B, porphyrins, thionine and phtalocyanine. The mechanism of the dye sensitized photo-degradation of pollutants (Fig. 1.8) is based on the absorption of visible light for exciting an electron from the highest occupied molecular orbital (HOMO) to the lowest unoccupied molecular orbital (LUMO) of the dye. The excited dye molecule subsequently transfers electrons into the conduction band of TiO_2, while the dye itself is converted to its cationic radical. The dye in the excited state has, in general, a lower redox potential then the corresponding ground state. If the redox potential is lower than the conduction band (CB) of TiO_2, an electron may be injected from the excited state into the CB, and consequently the cationic radical and CB electron are formed. The TiO_2 acts only as a mediator for transferring electrons from the sensitizer to the O_2 molecules adsorbed on the TiO_2 surface, being the valence band of TiO_2 unaffected. The injected electrons hop to the surface of titania where they are scavenged by the oxygen to form the reactive radicals for the degradation of the organic pollutants [Pichat, 2013]. Some dyes are even capable of producing electrons by absorbing visible light in the absence of semiconductors. Nevertheless, in the absence of semiconductor charge separators, the photocatalytic activities of these dyes are too low, therefore the presence of TiO_2 is necessary.

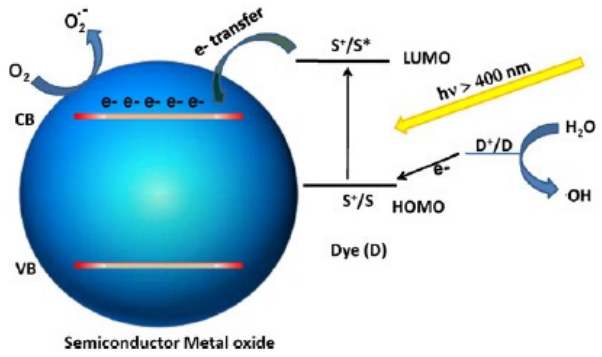

Figure 1.8: Mechanism of dye sensitized semiconductor photocatalysis [Reddy et al., 2016].

One of the main issues in this approach is the degradation of the dye itself. However, this is usually overcome by dye regeneration using sacrificial agents, or redox systems like EDTA and I_3^- /I^- pair [Abe et al., 2002]. Optimum conditions to obtain higher photocatalytic efficiencies are fast electron transfer to the semiconductor and slow recombination. In the case of dye sensitization, electron injections occur in a femtosecond scale compared to the recombination of electron-hole pairs in nanoseconds to milliseconds scale. Advantages of the dye-sensitized reactions are the fast injection of electrons to the semiconductor and slow backward reaction [Etacheri et al., 2015]. The electron transfer from excited dye to TiO_2 usually depends strongly on the adsorption efficiency of the dye molecule. In the case of the dye-sensitized TiO_2 photocatalyst, the dye molecules are only absorbed onto the TiO_2 surface by physical/chemical adsorption, no stable chemical bonds are formed. So the dye molecules tend to partially desorb, which can decrease the photocatalytic activity during the reaction process.

1.2.4 Semiconductor coupling

Coupling of a large band gap semiconductors with a smaller one, which can be activated with visible light, is of great interest for the

degradation of organic pollutants using solar radiation (Fig. 1.9). In addition, blocking trap states in the surface by coating the particles with thin layers of a wide band gap material can lead to a drastic enhancement of the photostability.

The main efforts have been so far devoted to the synthesis of various core-shell nanocrystals. For instance, CdS is a fascinating material with ideal band gap energy for visible light applications (2.4 eV) (see Fig. 1.4). However, CdS is prone to photo-anodic corrosion in aqueous environment. To overcome this stability problem and improve the photoactivity, CdS has been combined with a wide band gap semiconductor, such as ZnO and TiO_2, so improving charge separation of photogenerated electrons and holes [Pelaez et al., 2012]. In addition to the flat band potential of the components, the photocatalytic performance of the coupled semiconductors is also related to the geometry of the particles, the contact surface and the particles size. These parameters strongly depend on the preparation method. The disadvantage of this approach is that the synthesis methods normally require high temperatures, long times, strict inert atmosphere protection and complex multistep reaction process.

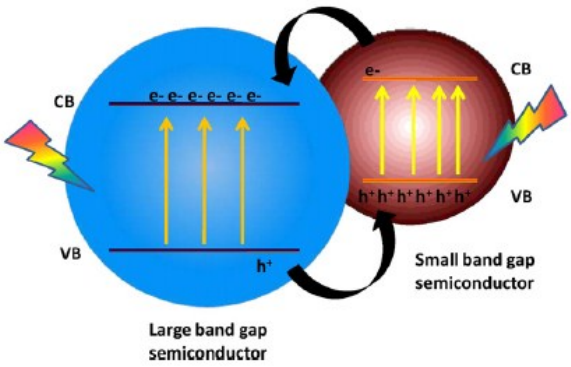

Figure 1.9: Electron transfer process and electron/hole separation in the semiconductor coupled modification [Reddy et al., 2016].

1.3 Nanostructured photocatalysts

One of the most common approach to revolutionize the environmental remediation techniques, such as water treatment, is the use of nanotechnology, which can be defined as a group of emerging technologies that work on nanometer scale, between 1 and 100 nm range, to produce materials, devices and system with fundamentally new properties and functions by controlling the size and the shape of matters [Ibrahim et al., 2016]. The potential applications of nanotechnology are covering many fields: medicine [Kiparissides and Kammona, 2015], food industry [Shanthilal and Bhattacharya, 2014], energy [Hussein, 2015], pollution treatment [Brame et al., 2011].

The good properties of nano TiO_2 are owing to its low dimensionality and quantum size effect. TiO_2 nanomaterials have several advantages over their bulk counterparts in terms of potential applications because of their increased number of delocalized carriers on the surface, improved charge transport and lifetime afforded by their dimensional anisotropy. However, the main advantage for photocatalytic application is the high surface-to-volume ratio that increases dramatically as the size of a material decreases, this property facilitates reaction/interaction between the devices and the adsorbed molecules on the photocatalyst surface. Because of this, it is essential to control the size and shape of the TiO_2 materials. A variety of TiO_2 nanostructures have thus been prepared, such as nanoparticles, nanotubes, nanorods, nanofibers, nanoflowers; these structures can be made through various preparation methods, including sol-gel, chemical vapor deposition, chemical solution decomposition, thermal and hydrothermal method, ultrasonic irradiation, microwave method, reverse micelle method, etc. [Wang et al., 2014].

Although the nanoscale TiO_2 catalysts show considerable improvement in terms of their physical and chemical properties, their size and morphology remains the main problem in a large-scale water treatment process. In fact, to date, the most applied photocatalyst is the Degussa P-25 TiO_2 nanoparticles in a slurry form. This is associated with a high volumetric generation of reactive radicals proportional to the amount of surface active sites on TiO_2

catalyst in suspension. However, with the slurry TiO_2 system, an additional step is needed for the recovery of the catalysts. This separation process can be achieved through conventional sedimentation, cross-flow filtration or various membrane filtrations. All these recovery methods are time and energy consuming, for this reason in this thesis work, we were strongly convinced that immobilization of the nanomaterials in a solid support is the key solution for a real application. This aspect will be illustrated in the next chapter.

1.4 Conclusions

Despite its effectiveness and efficiency for use in large-scale applications still need to be fully validated, heterogeneous photocatalysis is an excellent alternative to the unsatisfactory conventional method for water treatment. It has a wide range of applications for the decontamination of diverse hazardous pollutants in aqueous media. Photocatalysts based on TiO_2, the most used semiconductor in this field, are able to destroy organic and inorganic waste materials under normal temperature and pressure in a few hours without production of harmful secondary products. In addition, promising technological progress has been achieved toward the improvement of the photocatalytic efficiency of TiO_2 by shifting its optical response to the visible range in order to use a large fraction of the solar spectrum. Also the use of TiO_2 nanomaterials provides good opportunities to develop low cost systems for photocatalytic water treatment, that could be used in developing countries and in remote sites.

References

- Abe, R.; Sayama, K.; Arakawa, H. *Chem. Phys. Lett.* **2002**, 362, 441-444
- Ambrus, Z.; Balasz, N.; Alapi, T.; Wittmann, G.; Sipos, P.; Dombi, A.; Mogyorosi, K. *Appl. Catal. B* **2008,** 81, 27-37
- Anpo, M. *Pure Appl. Chem.* **2000,** 72, 1787-1792

- Arabatzis, I.M.; Stergiopoulos, T.; Bernard, M.C.; Labou, D.; Neophytides, S.G.; Falaras, P. *Appl. Catal. B: Environ.* **2003,** 42, 187-201
- Augugliaro, V.; Litter, M.; Palmisano, L.; Soria, J. *J. Photochem. Photobiol. C: Photochem. Rev.* **2006,** 7, 127-144
- Bhatkhande, D.S.; Kamble, S.P.; Sawant, S.B.; Pangarkar, V.G. *Chem. Eng. J.* **2004,** 102, 283
- Brame, J.; Li, Q.; Alvarez, P.J.J. *Trends Food Sci. Technol.* **2011,** 22, 618-624
- Carp, O.; Huisman, C.L.; Reller, A. *Prog. Solid State Chem.* **2004,** 32, 33-177
- Cho, M.; Chung, H.; Choi, W.; Yoon, J. *Water Res.* **2004,** 38, 1069-1077
- Chong, M.N.; Jin, B.; Chow, C.W.K.; Saint, C. *Water Res.* **2010,** 44, 2997-3027
- De Laat, J.; Le, G.T. Legube, B. *Chemosphere* **2004,** 55, 715-723
- Diebold, U. *Surf. Sci. Rep.* **2003,** 48, 53-229
- Dong, H.; Zeng, G.; Tang, L.; Fan, C.; Zhang, C.; He, X.; He, Y. *water Res.* **2015,** 79, 128-146
- Etacheri, V.; Di Valentin, C.; Schneider, J.; Bahnemann, D.; Pillai, S. *J. Photochem. Photobiol. C: Photochem. Rev.* **2015,** 25, 1-29
- Frank, S.N.; Bard, A.J. *J. Phys. Chem.* **1977,** 81, 1484
- Fuerte, M.D.H.A.; Maira, A.J.; Martinez-Arias, A.; Fernandez-Garcia, M.; Conesa, J.C.; Soria, J. *Chem. Commun.* **2001,** 24, 2718-2719
- Fujishima, A.; Honda, K. *Nature* **1972,** 238, 37-38
- Fujishima, A.; Rao, T.N.; Tryk, D.A. *J. Photochem. Photobiol. C: Photochem. Rev.* **2000**, 1, 1-21
- Gaya, U.I.; Abdullah, A.H. *J. Photochem. Photobiol. C: Photochem. Rev.* **2008,** 9, 1-12
- Gernjak, W.; Krutzler, T.; Bauer, R. *J. Sol. Energy Eng.* **2007,** 129, 53-59
- Han, C.; Likodimos, V.; Khan, J.A.; Nadagouda, M.N.; Andersen, J.; Falaras, P.; Rosales-Lombardi, P.; Dionysiou, D.D. *Environ. Sci. Pollut. Res.* **2014,** 21, 11781-11793

- Houas, A.; Lachheb, H.; Ksibi, M.; Elaloui, E.; Guillard, C.; Hermann, J.M. *Appl. Catal. B Environ.* **2001,** 31, 145-157
- Hu, C.; Lan, Y.; Qu, J.; Hu, X.; Wang, A. *J. Phys. Chem. B* **2006**, 110, 4066-4072
- Hu, A.; Apblett, A. *Nanotechnology for water treatment and purification*; Springer International Publishing Switzerland **2014**
- Hussein, A.K. *Renew. Sust. Energ. Rev.* **2015,** 42, 460-476
- Huston, P.L.; Pignatello, J.J. *Water Res.* **1999,** 33, 1238-1246
- Ibanez, J.A.; Litter, M.I.; Pizarro, R.A. *J. Photochem. Photobiol. A Chem.* **2003**, 157, 81-85
- Ibrahim, R.K.; Hayyan, M.; AlSaadi, M.A. Hayyan, A.; Ibrahim, S. *Environ. Sci. Pollut. Res.* **2016**, 23, 13754-13788
- Impellizzeri, G.; Scuderi, V.; Romano, L.; Napolitani, E.; Sanz, R.; Carles, R.; Privitera, V. *J. Appl. Phys.* **2015,** 117, 105308
- Irie, H.; Watanabe, Y.; Hashimoto, K. *J. Phys. Chem. B* **2003,** 107, 5483-5486
- Kiparissides C. and Kammona O. *Nanotechnology advances in diagnostics, drug delivery, and regenerative medicine. The nano-micro interface: bridging the micro and nano worlds* **2015**, 8, 311-340
- Krautler, B.; Bard, A.J. *J. Am. Chem. Soc.* **1978,** 100, 5958
- Li, X.; Yu, J.; Jaroniec, M. *Chem. Soc. Rev.* **2016,** 45, 2603
- Lindgren, T.; Mwabora, J.M.; Avandano, E.; Jonsson, J.; Hoel, A.; Granqvist, C.G.; Lindquist, S.E. *J. Phys. Chem. B* **2003,** 107, 5709-5716
- Luttrell, T. *Scientific Reports* **2014** DOI: 10.1038/srep04043
- Matsunaga, T.; Tomoda, R.; Nakajima, T.; Wake, H. *FEMS Microbiol. Lett.* **1985,** 29, 211
- Pelaez, M.; Nolan, N.T.; Pillai, S.C.; (…); Dionysiou, D.D. *Appl. Catal. B: Environ.* **2012,** 125, 331-349
- Pera-Titus, M.; Garcìa-Molina, V.; Banos, M.A.; Giménez, J.; Esplugas, S. *Appl. Catal. B: Environ.* **2004**, 47, 219-256
- Pichat, P. *Photocatalysis and Water Purification: from fundamentals to recent applications, first edition.* **2013** Wiley-VCH Verlag GmbH & Co.
- Reddy, P.A.K.; Reddy, P.V.L.; Kwon, E.; Kim, K.H.; Akter, T.; Kalagara, S. **2016,** 91, 94-103

- Shanthilal, J.; Bhattacharya, S. *Nanoparticles and nanotechnology in food. In: Conventioanl and advanced food processing technologies.* **2014** Wiley, pp 567-94. doi: 10.1002/9781118406281.ch23
- Tong, T.; Zhang, J.; Tian, B.; Chen, F.; He, D. *J. Hazard. Mater.* **2008,** 155, 572-579
- Wang, W.; Zhang, J.; Chen, F.; He, D.; Anpo, M. *J. Colloid.Interface Sci.* **2008,** 323, 182-186
- Wang, J.L.; Xu, L.J. *Crit. Rev. Environ. Sci. Technol.* **2012,** 42, 251-325
- Wang, Y.; He, Y.; Lai, Q.; Fan, M. *J. Environ. Sci.* **2014,** 26, 2139-2177
- Zaleska, A. *Recent Pat. Eng.* **2008**, 2, 157-164
- Zang, Y.; Farnood, R. *Appl. Catal. B: Environ.* **2008,** 79, 334-340
- Zimbone, M.; Buccheri, M.A.; Cacciato, G.; Sanz,.R.; Rappazzo, G.; Boninelli, S.; Reitano, R.; Romano, L.; Privitera, V.; Grimaldi, M.G.

Chapter 2

Polymer nanocomposites

Nanostructured photocatalysts, especially TiO_2, in various shapes and morphologies, such as nanoparticles, tubes, wires, fibers, etc., are widely studied for the treatment of water contaminated by chemicals (arsenic, iron, manganese, nitrate, heavy metals, etc.), organic pollutants (aliphatic and aromatic hydrocarbons), antibiotics and biological substances, such as viruses, bacteria, parasites. In fact, nanomaterials show a better performance in environmental remediation than other conventional techniques because of their high surface area, due to the high surface-to-volume ratio, and their associated high reactivity. Furthermore, their electronic and optical properties can be tuned by appropriately shaping their size. Many efforts have been done in the fabrication of novel nanoscale materials for the treatment of both drinking water and wastewater. However, although the nanoscale catalysts show considerable improvement in terms of their physical and chemical properties, their size remains the main problem in a large-scale water treatment process because of the need of a post-treatment recovery, necessary to avoid their impact on the environment.

Since the past decade, immobilization of photocatalysts on different substrates has been drawing a significant attention. Considering the various substrates, polymers seem to be very promising due to their several advantages such as flexible nature, low-cost, chemical resistance, mechanical stability, low density, high durability and ease of availability.

In this chapter, an overview of hybrid materials is illustrated, with a particular attention addressed to the polymer nanocomposites. The synthesis methods of this new class of materials are presented, as well as the most recent developments in the application of polymer-TiO_2 nanocomposites for water treatment.

2.1 Hybrid nanocomposites

Recent technological developments and the desire for new functions have generated a huge demand for novel materials. In fact, many of the well-established materials, such as metals, ceramics or plastics, in their pure forms cannot fulfill all technological requirements for the various new applications. Scientists and engineers realized that mixtures of materials can show superior properties compared with their pure counterparts. These hybrid materials are formed by the incorporation of a material into a second substance, the matrix [Kickelbick, 2007]. The term nanocomposites is used for multiphase materials, where at least one of the phases is in a defined size range of 1-100 nm. The nanocomposites research is extremely broad, encompassing areas such as electronics and computing, data storage, communications, aerospace and sporting materials, health and medicine, energy, environment, and transportation [RTO Lecture Series, 2005].

According to their matrix materials, nanocomposites can be classified into three broad types: ceramic matrix, metal matrix and polymer matrix [Cury Camargo et al., 2009]. Despite ceramic materials have a good wear resistance and high thermal and chemical stability, they are typically fragile. This low toughness has blocked their use for many applications; however, ceramic matrix nanocomposites have significantly enhanced mechanical properties that can overcome this problem. By the incorporation of energy-dissipating components such as fibers or particles that can prevent further opening of a crack, the ceramic matrix exhibits increased fracture toughness [Harmer et al., 1992].

Metal matrix nanocomposites consist of a ductile metal or alloy matrix wherein some nanosized reinforcements are implanted. By combining the ductility and toughness of metal with the high strength and modulus of ceramic nanomaterials, nanocomposites with high strength in shear and/or compression processes and for high service temperature applications can be made. These are widely applied in many areas, such as the aerospace and automotive industries and for advanced structural materials [Tjong S.C. etal., 2004].

Polymers are considered good hosting matrices for composite materials because of their ease of production, light weight and ductile nature. Inorganic nanomaterials possess outstanding optical, catalytic, electronic and magnetic properties, which are significantly different from their bulk states. By combining the attractive functionalities of both components, nanocomposites derived from organic polymers and inorganic nanomaterials are expected to display excellent properties. The potential applications of the resultant nanocomposites are various (automotive, aerospace, opto-electronics, etc.), but a little attention has been addressed to their application for photocatalytic water treatment. In this thesis work, we have defined a research strategy based on the application of this class of materials in this field. We will hence describe in detail their realization and performances in the next paragraphs.

2.1.1 Polymer-matrix nanocomposites

In the recent years, polymer nanocomposites have received significant attention, both in the industry and academia. The properties of nanocomposites depend on the type of incorporated nanoparticles, their size and shape, concentration and interactions with the polymer matrix [Hussain et al., 2006] [Jeon and Baek, 2010]. The choice of the polymers is usually guided mainly by their mechanical, thermal, electrical, optical and magnetic behaviors. However, other properties such as hydrophobic/hydrophilic balance, chemical stability, bio-compatibility, opto-electronic properties and chemical functionalities have to be considered in the choice of the polymers. The inorganic nanomaterials not only provide mechanical and thermal stability, but also new functionalities that depend on their chemical nature, structure, size, and crystallinity of the inorganic compounds. Various nanoparticles are incorporated into the polymer matrix for nanocomposite applications. Among them, the nanocomposite with nanoscaled embedded TiO_2 has gained great interests to scientists and researchers around the world because of its unique properties [Li et al., 2006]. A series of nanocomposites with high refractive index, incorporating TiO_2 colloids into several polymers,

with improved optical and electrical properties were reported as well [Kubacka et al., 2007]. Solar cells, based on the nanocomposites of polymers with TiO_2 showed some excellent photovoltaic cell efficiency [Wakabayashi et al., 1905]. TiO_2 was simply used as the filler for the coatings, plastics and rubbers, and the resultant nanocomposites showed improved performance in UV-shielding, dynamic fracture toughness, flame retardant, optical transparency, scratch resistance, and chemical resistance [Dridi et al., 2008].

A simple way to distinguish between various polymeric nanocomposites is based on the possible interactions connecting the inorganic and organic species [Kickelbick, 2007]. Class I hybrid materials are those that show weak interactions between the two phases, such as van der Waals, hydrogen bonding or weak electrostatic interactions. Class II hybrid materials are those that show strong chemical interactions between the components. The different types of polymer-matrix nanocomposites are illustrated in Fig. 2.1. Blends are formed if no strong chemical interactions between the inorganic and organic building blocks exist (Fig. 2.1a). In this case, a material consists of an organic polymer with entrapped discrete inorganic moieties in which, depending on the functionalities of the components, for example weak crosslinking occurs by the entrapped inorganic units through physical interactions or the inorganic components are entrapped in a crosslinked polymer matrix. If inorganic and organic networks interpenetrate each other without strong chemical interactions, so called interpenetrating networks are formed (Fig. 2.1b). Both described materials belong to class I hybrids. Class II hybrids are formed when the discrete inorganic building blocks are covalently bonded to the organic polymers (Fig. 2.1c) or more complex inorganic network and organic polymers are covalently connected each other (Fig. 2.1d).

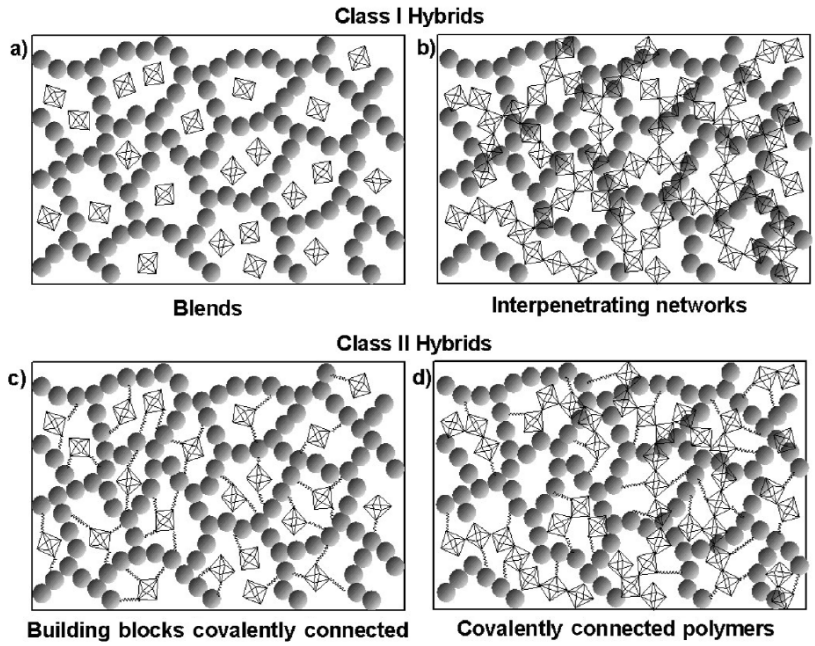

Figure 2.1: The different types of polymer-matrix nanocomposites [Kickelbick, 2007].

The most obvious advantage of inorganic-organic hybrids is that they can favorably combine the often dissimilar properties of organic and inorganic components in one material. Thanks to the many possible combinations this field is very creative, since it provides the opportunity to invent an almost unlimited set of new materials with a large spectrum of known and as yet unknown properties. Another important property of these materials is their processing. Contrary to pure solid-state inorganic materials that often require a high temperature treatment for their processing, hybrid materials show a more polymer-like handling. Hence, these materials can be shaped in any form in bulk and in films by very low-cost methods.

2.2 Polymer nanocomposites synthesis methods

Many approaches have been reported for the preparation of polymer-based inorganic nanoparticles composites [Qiaoyu, 2012] [Hanemann and Szabò, 2010]. In this section, the most important methods are described; they can be mainly distinguished between *ex situ* processes and *in situ* processes.

2.2.1 Ex situ synthesis methods

In these methods, pre-made nanoscale inorganic nanoparticles (NPs) are integrated into the polymer (blending) or monomers, which are then polymerized to fabricate composites (*in situ* polymerization). A schematic illustration of these methods is shown in Fig. 2.2.

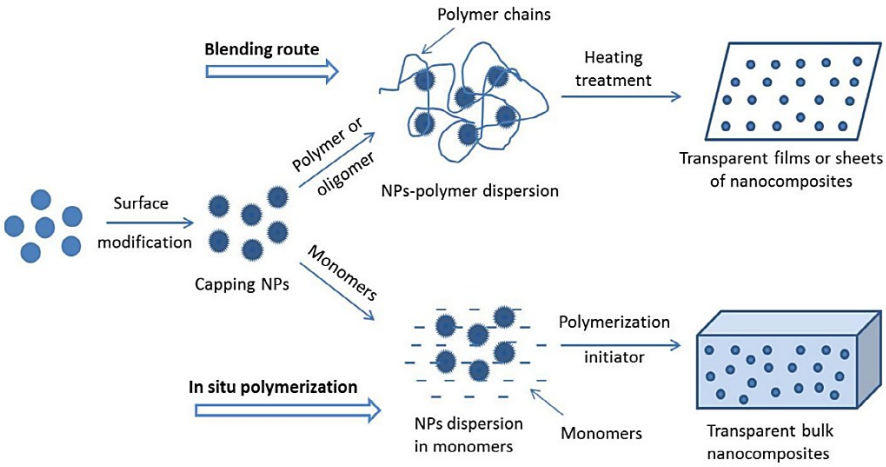

Figure 2.2: Schematic of e*x situ* synthesis of nanocomposites from blending route and *in situ* polymerization process [Lu et al., 2009].

As illustrated in the scheme, the nanoparticles used in this approach are prepared separately, isolated, purified and, if necessary, modified by surface coupling agents before incorporation into the polymer matrix. In this

method, the surface properties of NPs, particle size and size distribution are well controlled, therefore this approach is mostly applied in large-scale industry. Although this is a quite promising route for practical application, the pre-made NPs tend to aggregate. Therefore, the main challenge of this methodology is to prepare NPs with long-term stability against aggregation, and disperse them well into the polymer or monomers. In order to solve this problem, it is important to minimize the interface energies between nanoparticles and the polymer matrix. Generally, in both synthesis methods the nanoparticles are modified by chemi- or physisorption of surfactant molecules onto the surface. The surface modified nanoparticles can hence be dispersed efficiently in the organic medium.

Blending is the simplest approach to prepare nanocomposites. Usually, a solution of polymer or oligomers with dispersed nanoparticles is cast into a container or deposited on a glass or plastic substrate by a spin coating or dip coating process. After the evaporation of the solvent a nanocomposite film is obtained [Hafizah et al., 2014].

In situ polymerization, if compared with other approaches, is particularly suitable to prepare thicker bulk nanocomposites [Khaled et al., 2007] [Demir et al., 2007]. However, it is important to attain stable dispersions of nanoparticles before the subsequent polymerization; otherwise, the low viscosity of particle dispersions in monomers may cause the inorganic particles to precipitate during the long polymerization process. Normally, in order to offer strong interfacial interaction between the monomer molecules and the inorganic particles, the design and tailoring of the surface characteristics of the inorganic particles is necessary.

2.2.2 In situ synthesis methods

The *in situ* method synthesizes, by chemical reactions, inorganic nanoparticles directly within the polymer matrix in order to prepare nanocomposites in one-step. In this route, the particle aggregation caused by handling and mixing processes can be avoided, since the nanoparticles are nucleated and grown inside the polymer matrix. In addition, the polymer

chain functional groups have stabilizing effect on the NPs surface. This effect provides an even spatial distribution in polymer matrices by preventing them from agglomeration, since there is not enough fluid environment in the polymer matrix to allow particles to meet by diffusion. However, the disadvantages of this method is that the unreacted compounds or by-products of the reaction may affect the properties of the final product. The interaction between the inorganic precursor and the polymer matrix is a very important factor for controlling the particle size and polydispersity. Polymers with hydroxyl, mercapto and sulfonic functional groups offer strong interactions between metal elements of inorganic precursors and polymer matrices [Qiaoyu, 2012] [Hanemann and Szabò, 2010]. An illustrative scheme of the *in situ* preparation of polymer nanocomposites is shown in Fig. 2.3. As shown in the figure, the polymer and the metal precursor are first mixed in a solvent, and then the composite can be cast to be a film before or after the introduction of the second precursor, such as the counter-ion S^{2-}, for the synthesis of the inorganic nanoparticles.

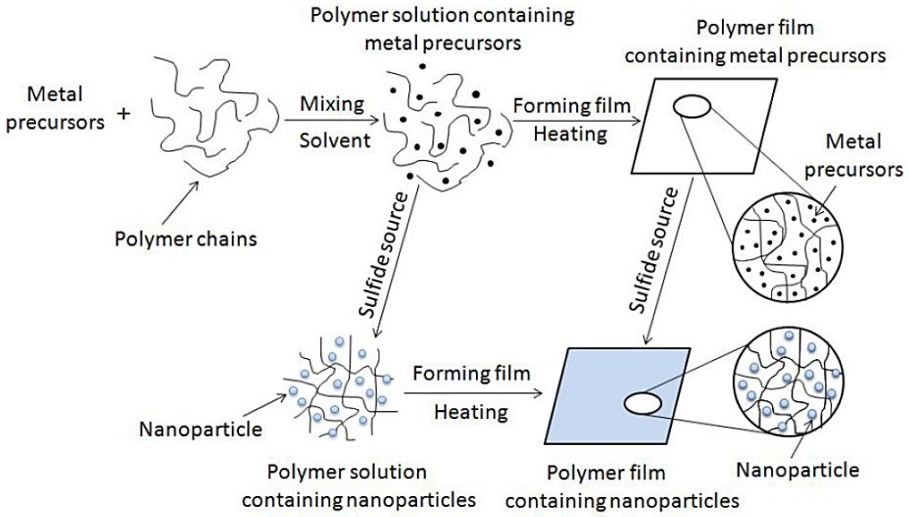

Figure 2.3: Schematic of in *situ* synthesis of nanocomposites [Lu et al., 2009].

The sol-gel reaction is one of the most studied *in situ* processes for the synthesis of polymer nanocomposites, because of its capability to control the miscibility between organic and inorganic components at the molecular level [Chen et al., 1999]. The sol-gel is a process in which molecular precursor, such as metal alkoxides, undergo hydrolysis and condensation reactions to form a three-dimensional network of organic-inorganic hybrid materials. Compared with other techniques, this method requires mild reaction conditions and offers the possibility to produce the inorganic network in the presence of a preformed organic polymer or to carry out the organic polymerization before, during or after the sol-gel process. One of the major challenges in these syntheses is the identification of the right solvent in which the polymers are soluble and which is compatible with the inorganic species present during the sol-gel approach. Phase separation between organic and inorganic components can also be avoided if the polymers contain functional groups that are more compatible with the reaction conditions of the sol-gel process or even undergo an interaction with the inorganic formed material. Despite its advantages, sol-gel technique is not fully scalable, because the raw materials for this process are expensive and since several steps are involved, close monitoring of the process is needed.

2.3 Polymer-supported TiO_2 nanomaterials as photocatalysts

To date, the most used photocatalyst for water treatment is the Degussa P-25 TiO_2 in a slurry form. This type of catalyst consists of fine particles with an average diameter around 50 nm; usually, it is used as a standard reference for comparison of photoactivity with other materials under the same treatment conditions [Serpone et al., 1996]. When TiO_2 is applied as a dispersion, it shows a better efficiency than immobilized catalysts, as illustrated in Fig. 2.4, for example, in the case of TiO_2 fixed on macroscopic β-SiC cellular foam for the treatment of water contaminated by pesticide molecules. The graph reports the concentration variation of pesticide, proportional to the absorbance of the solution according to the Lambert-Beer

law, as a function of time irradiation. The better efficiency is associated with a higher generation rate of reactive radicals thanks to the higher amount of surface active sites of TiO_2 for the catalyst in suspension.

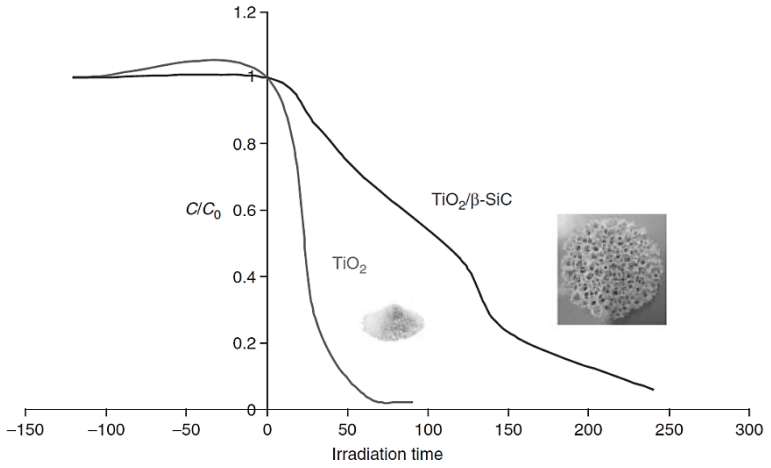

Figure 2.4: Comparison of photocatalytic activity of TiO_2 powder suspension and TiO_2 supported on β-SiC foam (with same loading in TiO_2) for the elimination of a pesticide from water [Kouamé et al., 2011].

However, the slurry TiO_2 system have several drawbacks for industrial scale application, such as separating the catalyst after the treatment, recycling or regenerating it. The post-treatment separation process is crucial to avoid the loss of catalyst particles and their dispersion into the environment. In fact, several unfavorable human health problems are associated with the mobility of the powder form, and there are many recent studies describing the toxicity of nano-sized TiO_2 for aquatic organisms, including algae, invertebrates and fishes [Schultz et al., 2014] [Chavon et al., 2014] [Kwak and An, 2015]. Nonetheless, because of the small size of the TiO_2 particles (less than 0.5 μm for agglomerates and generally 10-100 nm for elementary particles), complete separation is very difficult and expensive. Decantation could be a solution but it needs huge tanks to stock the contaminated and treated water, in addition, this process is very long because the TiO_2 particles decant very slowly [Fernandez-Ibañez et al.,

2003]. Another strategy could be the integration of various membrane filtrations, but several operating issues are associated with this approach, such as pore size and blockage, regeneration and fouling [Lee et al., 2001] [Molinari et al., 2002].

The above mentioned drawbacks can be solved by fixing the photocatalysts on an inert support. With immobilized nanocatalysts the post-treatment recovery is not necessary and the loss of catalysts is minimal. On the other hand, the immobilization of the photocatalysts reduces the surface area available for the reaction and also enlarges the mass transfer limitations. Overall, the advantages of immobilizing TiO_2 nanomaterials outweighs the above said disadvantages and thus, over the recent years, many excellent works have been done in this area [Pichat, 2013]. Several supports have been tried for supporting titania such as glass, silica gel, metal, ceramics, polymer, zeolite, alumina clays, activated carbon, cellulose and others, and a lot of immobilization techniques have been studied [Shan et al., 2010].

A good support for photocatalysis must satisfy the following requirements:

- Strong affinity between the photocatalyst and the support for stable anchoring of the catalyst
- The catalytic activity must not be affected by the attachment method
- Offer a high specific surface area
- Good capacity to adsorb the compounds to be degraded
- Chemically inert
- The photocatalyst-substrate composite must be stable for long term operations
- Strong stability against degradation by strong oxidative radicals generated during the irradiation

Among the several substrates that have been tried, polymers seem to be very promising, because they have some characteristics that make them suitable to be used as a support for TiO_2 photocatalysts [Singh et al., 2013]. The polymers are inexpensive, flexible, readily available and they can be easily processed. Many of them have high UV-resistance and do not undergo oxidation readily [Fabiyi et al., 2000]; they are available in density range

(0.9-2 g cm^{-1}) allowing the development of buoyant photocatalysts. In addition, their hydrophobic nature gives them an added advantage to pre-concentrate the organic pollutants on the surface, so increasing the efficiency of adsorption and subsequent oxidation [Magalhaes et al., 2011]. The choice of the polymeric supports depends on their mechanical and thermal behaviour, hydrophobic/hydrophilic balance, chemical stability, bio-compatibility, optical properties, electronic properties and their chemical functionalities (solvation, wettability, templating effect, etc.) [Kim et al., 2010].

The method selected to immobilize TiO_2 on the polymer substrate could influence the photocatalytic activity of titania and so must be wisely chosen depending on the type of substrate and the pollutant to be degraded. The adopted method should not lead to any reduction in the photocatalytic activity of TiO_2. A wide variety of methods have been reported in the literature; some of them are sol-gel methods [Chen et al., 2008], dip coating [Balasubramanian et al., 2004], hybrid physical chemical vapor deposition, thermal treatment and hydrothermal methods [Fabiyi et al., 2000] [Liu and Chen, 2007], sol-spray methods [Shan et al., 2010] and electrophoretic deposition [Djosic et al., 2006]. However, most of the above mentioned techniques require high temperature, complex procedures and expensive instruments, making them unsuitable for a large-scale application. Until now, it appears that sol-gel has been the main low-temperature deposition techniques for immobilizing titania nanoparticles on various polymeric substrates. Although sol-gel methods are very easy and practical, the photocatalytic activities of TiO_2 films supported on substrates by this technique are restricted. This is attributed to the fact that is very difficult to obtain crystal phase from amorphous sol-gel TiO_2 films, hence a post-deposition thermal treatment at high temperatures (generally 300° C and above) is required. This limits the application of sol-gel method for supporting titania only on those polymeric substrates that have good thermal stability [Langlet et al., 2002].

2.3.1 Overview of some examples of polymer-TiO_2 nanocomposites

In this section, some selected examples of polymer-supported TiO_2 photocatalysts present in the literature will be briefly described and examined.

The first reported study on the use of a polymeric support for TiO_2 photocatalyst was done by Tennakone et al. in the year 1995 [Tennakone et al., 1995]. They supported TiO_2 on polyethene (PE) film by a thermal treatment method for coating. The photocatalytic activity was examined by photomineralization of phenol in terms of outgoing carbon dioxide (CO_2) gas. Experimental results from photomineralization under UV irradiation showed that the experimental value of evolved CO_2 was significantly higher than the expected theoretical value. This may be attributed to either impurities in PE film or the degradation of the polymer. The latter phenomena have to be fully avoided for a real application of the material.

TiO_2 has been reported to be the mostly supported on inorganic substrates as compared to on polymer substrates due to apparent degradation of the polymer during photocatalysis. In order to overcome this limitation, Kasanen et al. applied a protective layer of polyurethane (PU) resin on the substrate surface and fabricated a novel photocatalytic self-cleaning multilayer TiO_2 coating on polymeric substrates by spin-coating method [Kasanen et al., 2009]. The entire process consists of the following steps: coating of the polymeric substrates (PE or polyvinyl chloride) with thermally cured protective PU layer; addition of TiO_2 nanoparticles on PU coating; fixing of titania nanoparticles with a second layer of PU. Finally, to achieve the photocatalytically active surfaces, the samples were etched by reactive oxygen-plasma etching. The main function of the protective PU layer was to prevent the direct contact between substrate and titania, thus preventing the photodegradation of the substrate. Taking their research further, Kasanen et al. found that the compatibility between PE substrate and protective layer was insufficient, which led to poor adherence of PU layer on the polymer. This consequently leads to self-wrinkling and peeling off the PU film when the system was immersed in water.

Fostier et al. [Fostier et al., 2008] adhered TiO_2 on internal surface of polyethylene terephthalate (PET) utilizing the impregnation technique proposed by Meichtry et al. [Meichtry et al., 2007]. They used this approach to obtain low-cost system for the removal of inorganic arsenic (As) from groundwater. The results illustrate that TiO_2 photocatalyst immobilized on readily available, cheap and reusable PET bottles without the use of any expensive precursor, seem to be a good and viable option to be considered for large scale applications for removal of both toxic organic and inorganic contaminations.

Sriwong et al. [Sriwong et al., 2008] demonstrated an economical and simple method of fabricating photocatalytic rubber sheet impregnated with titania powder (commercially available anatase and Degussa P-25). The photocatalytic acivity of the prepared materials is lower than the activity of the disperse P-25 and anatase powder, as expected. Despite this, the ease of recovery and reuse of immobilized titania on rubber sheets make it an obvious choice for being explored and developed further for large scale commercial applications. These last two examples are very interesting and seem promising, but they require further investigation to prove the nanocomposites stability.

A lot of attention has been addressed to the combination of TiO_2 with conductive polymers, such as poly(aniline) (PANI), poly(o-phenylenediamine), poly(thiophene), poly(pyrrole) [Reddy et al., 2015]. This great interest is due to the following properties of the conductive polymers:

- High absorption coefficients in the visible part of the spectrum
- High mobility of charge carriers
- Excellent environmental stability
- Noticeable electrical, optical and photoelectrical properties.

Thanks to these properties, the conductive polymers act not only as inert support for TiO_2, but they operate as sensitizer allowing the realization of photocatalytic activity under visible light. The proposed mechanism of photodegradation of organic pollutants by TiO_2/PANI photocatalysts under both visible and UV light irradiations is illustrated in Fig. 2.5. When the polymer absorbs visible light irradiation, π-π^* transition is induced which transfers the photogenerated electrons to the π^* orbital of the polymer. From

this orbital, the excited electron can efficiently carry out a transition to the more energetically favorable conduction band of TiO_2. Subsequently, these photogenerated electrons can be transferred to the surface of the photocatalyst to react with water and oxygen adsorbed on the surface to form the reactive radicals. Similarly, under UV irradiation, the photogenerated holes in the valence band of TiO_2 can transfer directly to the HOMO of the PANI. These photogenerated holes can easily emigrate to the surface of the photocatalyst and subsequently oxidize the adsorbed organic pollutants. However, this class of polymers is very expensive, and this is the main problem that limits their real application.

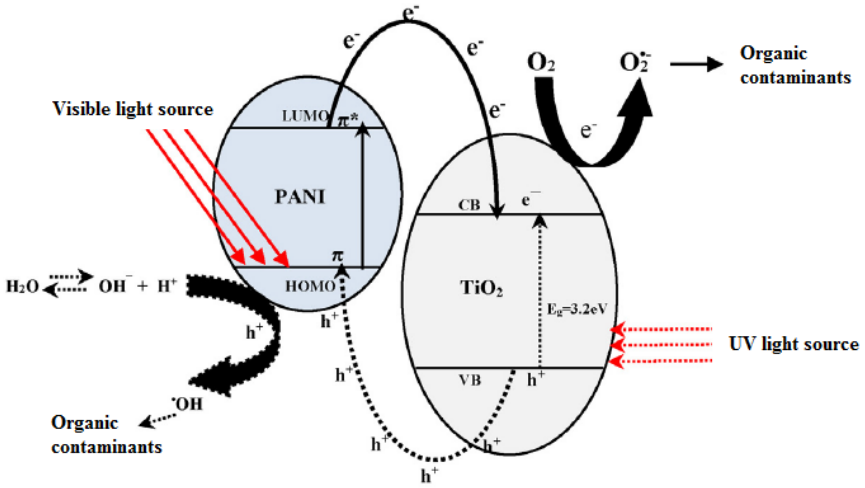

Figure 2.5: Mechanism of photodegradation of organic contaminants by TiO_2/PANI photocatalyst under visible light irradiation (shown by solid lines) and under UV light irradiation (shown by dotted lines). Adapted from [Singh et al., 2013]

2.4 Future research

The potential of nanocomposites in various sectors of research and application, and in particular in the photocatalysis field attracts increasing

interest in many parts of the world. However, there are some challenges that need to be solve in order to progress further in this promising area:

- The low thermal stability of polymeric substrate precludes the use of many of the physical and chemical methods that need high sintering temperature for adherence of titania on the polymer surface. This calls for development of novel, low-temperature and economical methods for fabrication of polymer supported titania photocatalysts.
- The photocatalytic degradation of the polymeric support due to the strong oxidative radicals generated by TiO_2 during the irradiation, needs to be further explored.
- Nanomaterials aggregation that prevent their homogeneous dispersion in the polymer matrices, still need to be overcome.
- Recyclability without loss of efficiency is an important parameter that is always considered for successful and economical large-scale application. Therefore, simple and low-cost based techniques to maintain the efficiency of polymer- supported TiO_2 photocatalysts after several successive reuses need to be developed.
- The practical application of nanocomposite membranes for water treatment is still in its infancy, there are many laboratory-based studies on the application of nanocomposite, but very few reports exist on the large-scale production and industrial application.

In this thesis work, we realized polymer nanocomposites by solution casting of a mixture consisting of pre-made TiO_2 nanoparticles and polymer solution. We are really convinced that this simple and low-cost method is easily scalable. The polymer matrix selected for supporting titania is poly(methyl methacrylate) (PMMA). This choice relies on its transparency to visible light and high resistance to UV light, its mechanical properties and environmental stability, its cheapness. This polymer is hydrophobic and suitable to contact with food and beverages. PMMA is an excellent host for functional inorganic particles, in fact various types of metal oxide fillers have been introduced to further improve its properties, such as glass transition and thermal stability of the composites [Demir et al., 2006] [Demir

et al., 2007]. This nanocomposite has not been deeply studied yet and very few examples exist concerning the applications of the PMMA-TiO_2 nanocomposites for water treatment [Elfeky and Al-Sherbini, 2011].

References

- Balasubramanian, G.; Dionysiou, D.D.; Suidan, M.T.; Baudin, I.; Laine, J.M. *Appl. Catal. B: Environ.* **2004,** 47, 73-84
- Chen, W.C.; Lee, S.J.; Lee, L.H.; Lin, J.L. *J. Mater. Chem.* **1999,** 9, 2999-3004
- Chen, Y.; stathatos, E.; Dionysiou, D.D. *Surf. Coat. Technol.* **2008,** 202, 1944-1950
- Cury Camargo, P.H.; Gundappa Satyanarayana, K.; Wypych, F. *Mat. Res.* **2009,** 12(1), 1-39
- Demir, M.M.; Memesa, M. Castignolles, P.; Wegner, G. *Macromol. Rapid Commun.* **2006,** 10, 763-770
- Demir, M.M.; Castignolles, P.; Akbey, U.; Wegner, G. *Macromolecules* **2007,** 40, 4190-4198
- Djosic, M.S.; Miskovic-Stankovic, V.B.; Janackovic, D.T., Kacarevic-Popovic, Z.M.; Petrovic, R.D. *Colloids Surf. A* **2006,** 274, 185-191
- Dridi, C.; Barlier, V.; Chaabane, H.; Davenas, J.; Ben Ouada, H. *Nanotechnology* **2008,** 19, 375201
- Elfeky, S.A.; Al-Sherbini, A.A. *Kinet. Catal.* **2011,** 52, 391-396
- Fabiyi, M.E.; Skelton, R.L. *J. Photochem. Photobiol. A* **2000**, 132, 121-128
- Fernandez-Ibanez, P.; Blanco, J.; Malato, S.; De Las Nieves, F.J. *Water Res.* **2003,** 37, 3180-3188
- Fostier, A.H.; Pereira, M.D.S.S.; Rath, S.; Guimaraes, J.R. *Chemosphere* **2008,** 72, 319-324
- Hafizah, N.N.; Mamat, M.H.; Abidin, M.H.; Said, C.M.S.; Rusop, M. *Adv. Mater. Res.* **2014,** 832, 700-705
- Hanemann, T.; Szabò, D.V. *Materials* **2010,** 3, 3468-3517

- Harmer, M.P.; Chan, H.M.; Miller, G.A. *J. Am. Ceram. Soc.* **1992,** 75, 1715-1728
- Hussain, F.; hojjati, M.; Okamoto, M.; Gorga, R.E. *J. Compos. Mater.* **2006,** 40, 1511-1575
- Jeon, I.Y.; Baek, J.B. *Materials* **2010,** 3, 3654-3674
- Kasanen, J.; Suvanto, M.; Pakkanen, T.T. *J. Appl. Polym. Sci.* **2009,** 111, 2597-2606
- Khaled, S.M.; Sui, R.; Charpentier, P.A.; Rizkalla, A.S. *Langmuir* **2007,** 23, 3988-3995
- Kickelbick, G. *Hybrid Materials. Synthesis, Characterization, and Applications.* **2007,** Wiley-VCH Verlag GmbH & Co. KGaA, Weinheim ISBN: 978-3-527-31299-3
- Kim, H.; Hong, H.J.; Jung, J.; Kim, S.H.; Yang, J.W. *J. Hazard. Mater.* **2010,** 176, 1038-1043
- Kouamé, N.A.; Robert, D.; Keller, V.; Pham, C.; Nguyen, P. *Catal. Today* **2011**, 161, 3-7
- Kubacka, A.; Serrano, C.; Ferrer, M.; Lunsdorf, H.; Bielecki, P.; Cerrada, M.L.; Fernandez-Garcia, M.; fernandez-Garcia, M. *Nano Lett.* **2007,** 7, 2529-2534
- Kwak, J.I.; An, Y.J. *Int. J. Environ. Sci. Technol.* **2015,** 12, 1163-1172
- Langlet, M.; Kim, A.; Audier, M.; Hermann, J.M. *J. Sol-Gel Sci. Technol.* **2002,** 25, 223-234
- Lee, S.A.; Choo, K.H.; Lee, C.H.; Lee, H.I.; Hyeon, T.; Choi, W.; Kwon, H.H. *Ind. Eng. Chem. Res.* **2001,** 40, 1712-1719
- Li, F.; Zhou, S.; You, B.; Wu, L. *J. Appl. Polym. Sci.* **2006,** 99, 3281-3287
- Liu, A.; Chen, X. *J. Chem. Technol. Biotechnol.* **2007,** 82, 453-459
- Lu, C.; Yang, B. *J. Mater. Chem.* **2009,** 19, 2884-2901
- Magalhaes, F.; Moura, F.C.C.; Lago, R.M. *Desalination* **2011,** 276, 266-271
- Meichtry, J.M.; Lin, H.J.; de la Fuente, L.; Levy, I.K.; Gautier, E.A.; Blesa, M.A.; Litter, M.I. *J. Sol. Energy Eng.* **2007,** 129, 119-126
- Molinari, R.; Palmisano, L.; Drioli, E.; Schiavello, M. *J. Memb. Sci.* **2002,** 206, 399-415

- Qiaoyu, L. *"Synthesis of PDMS-metal oxide hybrid nanocomposites using an in situ sol-gel route"* Dissertation, Michigan Technological University, **2012**
- Pichat, P. *Photocatalysis and Water Purification: From Fundamentals to Recent Applications, First Edition.* **2013** Wiley-VCH Verlag GmbH & Co
- Reddy, K.R.; Hassan, M.; Gomes, V.G. *Appl. Catal. A* **2015,** 489, 1-16
- RTO Lecture Series, EN-AVT-129, May **2005**
- Schultz, A.G.; Boyle, D.; Chamot, D.; Ong, K.J.; Wilkinson, K.J.; McGeer, J.C.; Sunahara, G.; Goss, G.G. *Environ. Chem.* **2014,** 11, 207-226
- Serpone, N.; Sauvé, G.; Koch, R.; tahiri, H.; Pichat, P.; Piccinini, P.; Pelizzetti, E.; Hidaka, H. *J. Photochem. Photobiol. A: Chem.* **1996,** 94, 1999111-203
- Shan, A.Y.; Ghazi, T.I.M.; Rashid, S.A. *Appl. Catal A* **2010,** 389, 1-8
- Singh, S.; Mahalingam, H.; Singh, P.K. *Appl. Catal A* **2013,** 462, 178-195
- Sriwong, C.; Wongnawa, S.; Patarapaiboolchai, O. *Catal. Commun.* **2008,** 9, 213-218
- Tennakone, K.; Tilakaratne, C.T.K.; Kottegoda, I.R.M. *J. Photochem. Photobiol. A* **1995,** 87, 177-179
- Tjong, S.C.; Wang, G. *Mater. Sci. Eng. A* **2004,** 386, 48-53
- Wakabayashi K.; Uchida, T.; Yamazaki, S.; Kimura, K. *Macromolecules* **2008,** 41, 4607-4614
- Walters, C.; Pool, E.J.; Somerset, V.S. *J. Environ. Sci. Health. Part A* **2014,** 49, 1588-1601

Chapter 3

Immobilization of TiO_2-based nanomaterials in PMMA

In the two previous chapters, the excellent properties of the TiO_2 nanomaterials as photocatalysts for water treatment and the necessity of their immobilization into a solid substrate, such as a polymer matrix, for a safe and real application have been widely illustrated. Taking into account this analysis, in the present chapter we describe the main topic of this dissertation: the immobilization of nanostructured TiO_2 into a matrix of poly (methyl methacrylate) (PMMA). We realized, through a simple and low-cost method of solution casting, polymer nanocomposites made of PMMA/TiO_2 nanoparticles or nanotubes with high photocatalytic and antibacterial activity under UV irradiation. Furthermore, we combined titanium dioxide nanoparticles with single walled carbon nanotubes (SWCNTs), as acceptor system, and obtained a significantly higher photocatalytic efficiency under UV irradiation, compared to the systems with TiO_2 only. Photoactive materials even under visible light were synthesized thanks to the functionalization of the TiO_2 nanoparticle surface with *meso*-tetraphenylporphyrin-4,4′,4″,4‴-tetracarboxylic acid (TCPP) as dye sensitizer. The adopted synthesis procedure allowed us to obtain films in freestanding form. Their morphology, photocatalytic activity, stability and antibacterial activity have been extensively studied and here reported.

3.1 Experimental section

In this section, the methods used to synthesize the TiO_2 based nanocomposites with PMMA are described. Furthermore, the adopted photocatalytic and antibacterial test used to evaluate the efficiency of such nanocomposites are illustrated.

3.1.1 Synthesis method

Commercial titanium dioxide nanoparticles (TiO_2 NPs) (mixture of rutile and anatase, <100 nm particle size, by Sigma-Aldrich) were used in this work.

Titanium dioxide nanotubes (TNTs) were instead grown by electrochemical anodization in our laboratory in electrolytes consisting of ethylene glycol/NH_4F/H_2O as reported by Roy et al. [Roy et al., 2001]. After annealing, the Ti substrate covered by the grown TNTs was immersed in acetone and sonicated for two hours. This sonication produces the separation of the TNTs from the Ti substrate and their dispersion in the solvent.

The PMMA/TiO_2 nanocomposites were prepared according to the method of sonication and solution casting at different weight percent of TiO_2 nanomaterials [Hafizah et al., 2013]. In this procedure a dispersion of nanomaterials is mixed by sonication with a PMMA (M_w ~120,000 Da, supplied by Sigma Aldrich) solution. After that, the resulting mixture was cast into a Petri dish and was dried overnight to produce a nanocomposite film that was peeled off from the Petri dish and used in freestanding form for characterization, photocatalytic tests and antibacterial tests. The several steps involved in the preparation of these nanocomposites are illustrated in the Fig. 3.1.

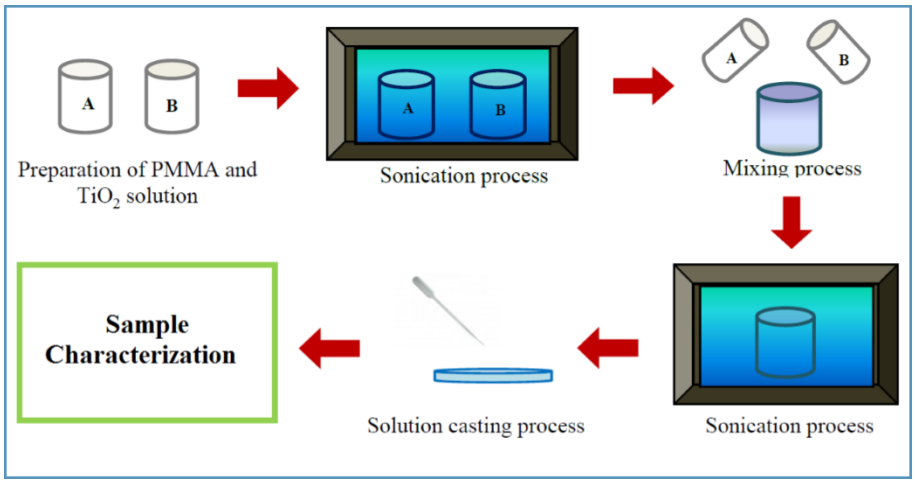

Figure 3.1: Schematic representation of the several steps for the preparation of PMMA/TiO_2 nanocomposites. Adapted from [Hafizah et al., 2013]

Commercial single-walled carbon nanotubes (SWCNTs, carboxylic acid functionalized) and *meso*-tetraphenylporphyrin-4,4′,4″,4‴-tetracarboxylic acid (TCPP), used to increase the photocatalytic efficiency and to modify the photoresponse of the TiO_2 nanoparticles, respectively, were mixed to the TiO_2 nanomaterials before blending with the polymer solution.

3.1.2 Photocatalytic activity tests

The photocatalytic activity of the surface of the samples was evaluated by adapting the methodology with the current ISO 10678:2010 test [Mills et al., 2012] [Fine ceramics, 2010], by degradation of dyes and phenol (C_6H_5OH, ≥ 99.5%) in aqueous medium under irradiation. The dyes, used in this work, were: methylene blue (MB, 0.05 wt% in H_2O), methyl orange (MO, 0.1%), rhodamine B (RhB, 0.2% in isopropanol). The molecular structures of these dyes are reported in Fig. 3.2.

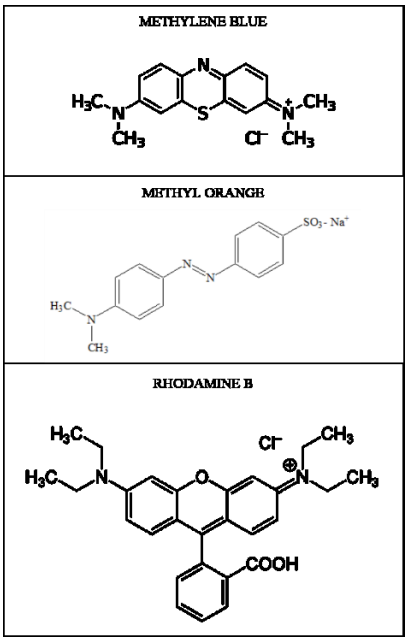

Figure 3.2: Molecular structures of methylene blue, methyl orange and rhodamine B.

The first step of the photocatalytic test consists in a preconditioning procedure: 1 cm^2 of the sample to be tested was immersed in 2 mL of the dye (or phenol) aqueous solution (~ 10^{-5} M) and left for 18 h in the dark to allow the physical adsorption reach the equilibrium. After this step, the solution was removed and replaced by 2 mL of a fresh solution. Then, the system was covered with a quartz glass, to avoid the evaporation of the solution during the experiment, and irradiated with a UV light (TL 8 W BLB 1FM, Philips) at 368 nm (full width at half maximum, FWHM, lower than 10 nm) with a measured irradiance of 2 mW/cm^2 at the surface of the tested samples. The schematic representation of the adopted irradiation set up for the photocatalytic tests is illustrated in Fig. 3.3. The variation of concentration of the dye solution as a function of the irradiation time was measured spectrophotometrically (using a PerkinElmer Lambda 45 UV-vis spectrophotometer) via the solution absorbance at 664 nm for the MB, at 464 nm for the MO and at 554 nm for the RhB. The irradiation process was

carried out for 240 min; the dye photodegradation without any sample in contact with the solution was conducted in the same conditions in all the experiments as control reference. Fig. 3.4 represents a typical absorbance behaviour of the MB solution in contact with an active sample, obtained by varying the time of irradiation under UV light. The variation of concentration of the phenol solution, under UV irradiation in the presence of our samples, was measured spectrophotometrically (Hach DR 3900 spectrophotometer), by using an established protocol involving the use of other reagents (Hach, LCK345 cuvette tests).

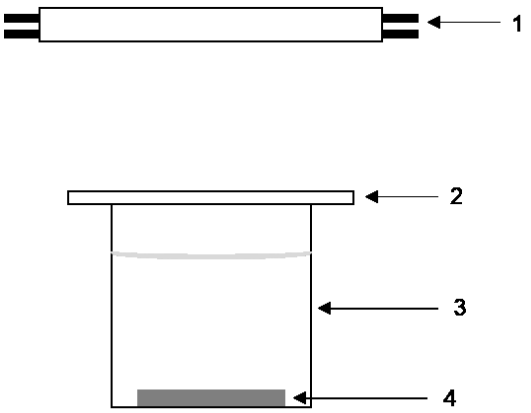

Figure 3.3: Schematic irradiation set up for the photocatalytic test, comprising: (1) light source, (2) quartz glass, (3) testing cylinder and (4) sample under test. Adapted from [Mills et al., 2012]

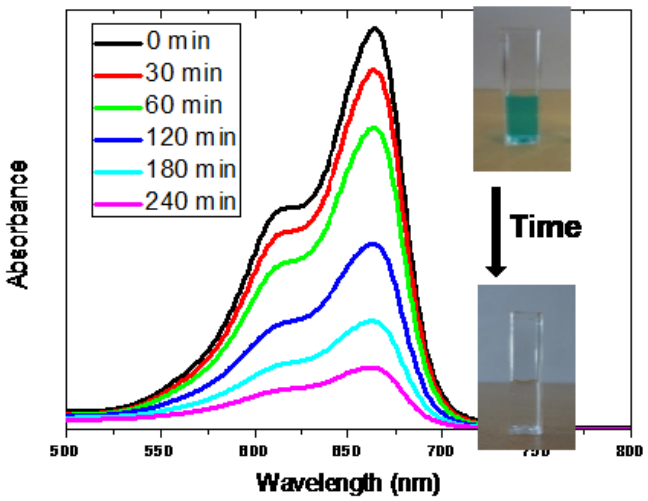

Figure 3.4: Typical absorbance spectra of the MB solution in contact with an active sample, for different irradiation time under UV light. Inset: MB aqueous solution in a cuvette at the beginning and at the end of the photocatalytic test.

For the samples with porphyrin, the experiments were conducted by using a visible light source (Osram DULUX S BL 9 W/71 lamp) emitting at around 453 nm (FWHM ~40 nm), with an irradiance of ~1.5 mW/cm^2 at the surface of the sample and with a 420 nm cutoff filter (Schott Glass) placed between the lamp and the beaker, containing the samples in the solution, in order to absorb the UV tail of the lamp spectrum.

Fig. 3.5 summarizes the relative positions of the absorbance spectra of the dyes and phenol, the absorbance spectrum of the porphyrin (TCPP), and the emission of the light sources used for the experiments.

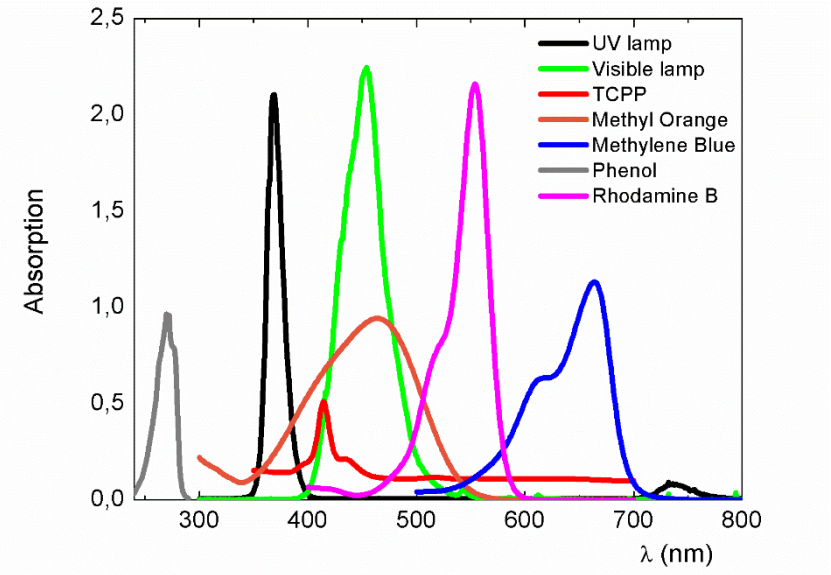

Figure 3.5: Absorbance spectra of TCPP, MO, MB, phenol and RhB and emission spectra of the light sources used for the experiments. Adapted from [Cantarella et al., 2016a]

3.1.3 Antibacterial activity tests

The antibacterial activity was tested on *Escherichia coli* ATCC 25922. The strain was routinely maintained in McConkey Agar. In order to run tests, a single colony was inoculated in 50 ml of Luria-Bertani (LB) broth and grown overnight at 37°C by constant agitation at 180 rpm under aerobic conditions. The following day, the bacterial growth was measured by optical density at 600 nm. Bacteria were diluted up to 10^5 CFU/ml in phosphate buffer saline (PBS) and 100 µl were added onto the nanocomposite samples. The wavelength of the UV light source was 368 nm (FWHM lower than 10 nm) and UV irradiance was 2 mW/cm^2 as in the photocatalytic test. Untreated and exposed to UV bacteria, but in the absence of nanocomposite samples, were treated in parallel as control samples. Aliquots were collected at 15 and 60 minutes respectively, conveniently

diluted by serial dilutions 1:10 and plated in LB Agar Petri dishes. Plates were incubated overnight at 37°C. CFU were counted the following day. For the samples with porphyrin, the experiments were run with the same procedures, but using a visible light source at 460 nm.

3.2 PMMA/TiO_2 composites

This section is dedicated to the discussion of the results obtained with the PMMA/TiO_2 nanoparticles (NPs) composites, in terms of morphological characterization, photocatalytic properties, antibacterial properties and stability. In the last part of this section, the results relative to the PMMA/TiO_2 nanotubes (TNTs) will be described.

3.2.1 Preparation of PMMA/TiO_2 NPs nanocomposites and characterization

Following the method of sonication and solution casting, 800 mg of PMMA were dissolved in 4 mL of tetrahydrofuran (THF). In a separate vial, a dispersion in THF of TiO_2 NPs (5 wt%, 10 wt%, 15 wt% or 20 wt% with respect to the polymer) was prepared. Both, solution and dispersion were sonicated for about 45 min. Then, the polymeric solution was mixed with the dispersion and sonicated again for 1 h. After that, the mixture was cast into a Petri dish (6 cm diameter) and was dried overnight to produce a nanocomposite film. The pictures of a PMMA film and of a PMMA film with 15 wt% TiO_2 nanoparticles are shown in Fig. 3.6. After the evaporation of the solvent, each prepared film was peeled off from the Petri dish.

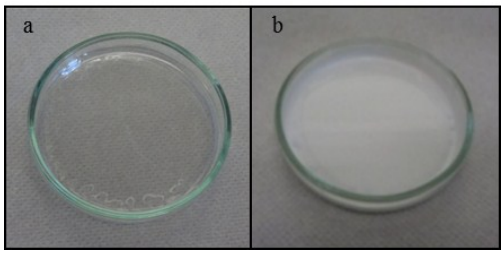

Figure 3.6: (a) PMMA film without nanostructures in the Petri dish; (b) PMMA/TiO_2 film with 15 wt% NPs in the Petri dish.

Before performing the photocatalytic and antibacterial activity, the obtained nanocomposites were characterized by scanning electron microscopy (SEM, using a Zeiss FEG-SEM Supra 25 Microscope operating at 2-3 kV) and by atomic force microscopy (AFM, using a Veeco-Innova microscope operating in high amplitude mode with an ultra-sharpened Si tip). All of these characterizations have been conducted in order to investigate the distribution of the nanostructures into the polymer matrix and the entity of their aggregation. More details concerning the theoretical aspects of the above-mentioned characterization techniques are reported in the appendix of this dissertation.

Fig. 3.7a shows the SEM plan-view of a PMMA film without nanostructures, Fig. 3.7b and c report the SEM images of PMMA/TiO_2 film with 15 wt% NPs. The SEM images reveal that the NPs are distributed homogeneously in the film forming small aggregates with an average diameter of 300 nm. The cross section micrographs of the same film are presented in Fig. 3.7d-f. The complete cross section image (Fig. 3.7d) shows that the NPs are indeed distributed along the whole thickness of the film (~200 μm). However, a higher concentration of NPs is located in the proximity of the back surface (Fig. 3.7e) of the film (the surface in contact with the Petri dish during the preparation of the films). This higher concentration is not observed in the front surface of the film (Fig. 3.7f). This effect is most probably due to the sedimentation of the nanostructures during the evaporation of the solvent.

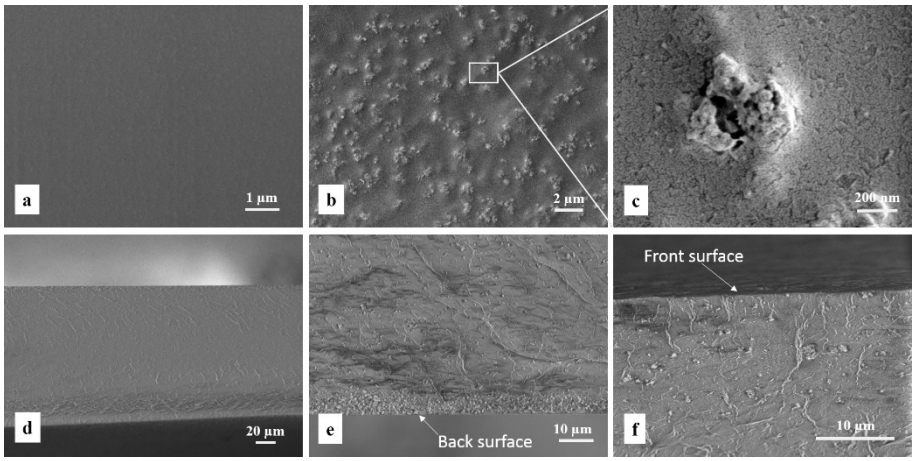

Figure 3.7: (a) SEM plan view of a PMMA film without nanostructures; (b and c) SEM plan views of the PMMA/TiO_2 film with 15 wt% NPs; (d) SEM cross section of the PMMA/TiO_2 film with 15 wt% NPs; (e) SEM magnification of the cross section in proximity of the back surface of the film; (f) SEM magnification of the cross section in proximity of the front surface of the film [Cantarella et al., 2016a].

The topography results are presented in Fig. 3.8. Fig. 3.8a, shows the bare PMMA (without NPs) film surface and Fig. 3.8b (front side) and Fig. 3.8c (back side) show the AFM images of both sides of the PMMA film with 15 wt% NPs. The roughness of the front side of the PMMA/TiO_2 film is 14.2 nm, the average height of the nanostructures exposed is 55.7 ± 23 nm and the density of the nanostructures in the surface is ~35/100 μm^2. For the back side: the roughness is 24.1 nm, the average height of the nanostructures exposed is 76.3 ± 30.2 nm with a density of ~50/100 μm^2. This analysis confirms the results obtained by SEM and provides further information on the exposed part of the NPs.

The SEM analyses (not reported) of the films with the other percentage to be investigated exhibit a distribution of the nanostructures comparable to the distribution of the NPs showed in Fig. 3.7.

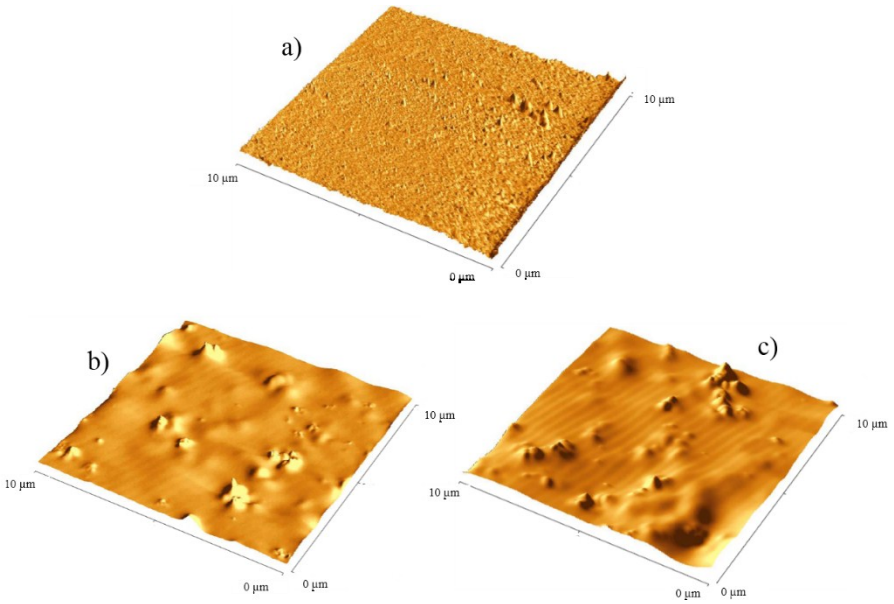

Figure 3.8: (a) AFM image of the PMMA film without nanostructures; (b) AFM image of the front side of the PMMA/TiO_2 film with 15 wt% NPs; (c) AFM image of the back side of the PMMA/TiO_2 film with 15 wt% NPs [Cantarella et al., 2016a].

The surface wettability of a PMMA film without nanostructures and of a PMMA/TiO_2 film with 15 wt% NPs was characterized by measuring the contact angles using a DATAPHYSICS-OCA 15 PRO contact angle measurement device. The used liquid is water. The mean value of five measurements, in five different areas of each sample, is reported in Fig. 3.9. For both films, the measured contact angles are similar within the experimental error (63° and 60° ± 6° respectively), so demonstrating that the presence of the TiO_2 NPs does not affect the wettability properties of the polymer.

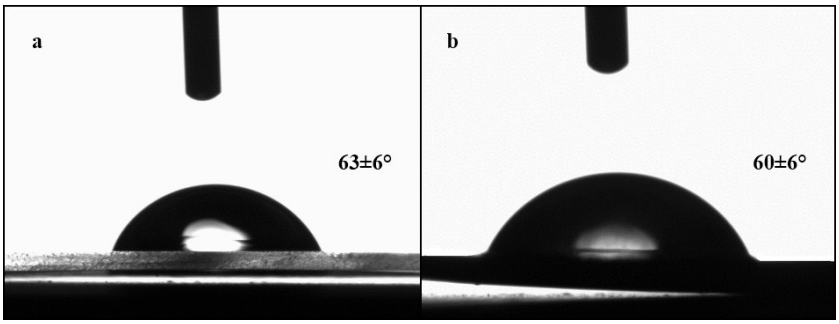

Figure 3.9: Contact angle measurement on: (a) PMMA film without nanostructures and (b) PMMA/TiO_2 film with 15 wt% NPs.

3.2.2 Photocatalytic activity: results and discussion

The photocatalytic activity of all the synthesized polymeric nanocomposites were evaluated by means of the discoloration of methylene blue (MB) dye. Using the absorption at 664 nm as a marker of MB concentration, we plotted the concentration variation of MB, proportional to the absorbance of the solution according to the Lambert-Beer law, as a function of time of irradiation. For all the tested samples, a pseudo-first order discoloration rate constant was extracted from steady state photocatalytic regimes, and the photonic efficiency was calculated following the method ascribed in ISO 10678:2010 [Fine ceramics, 2010]. The decrease of pure MB under illumination is always reported for comparison. Some experiments have been repeated five times, obtaining a high repeatability with a calculated standard deviation within 4% related to measurement sensitivity. Fig. 3.10 shows the photocatalytic activity of 1 cm^2 (back side) of the films PMMA/TiO_2 NPs with different contents of nanomaterials: 5 wt%, 10 wt%, 15 wt% and 20 wt%. The graph includes the period preceding the UV exposition, given in negative values and denoted as dark in the graph, which reports the initial adsorption of MB onto the films. Despite the nanostructures are embedded in the polymer and only a fraction of them is in contact with water, the samples exhibit a considerable photocatalytic

activity. In particular, for the samples with 15 wt% and 20 wt% of NPs the discoloration rates are $(4.6\pm0.2)\cdot10^{-3}$ min^{-1} and $(5\pm0.2)\cdot10^{-3}$ min^{-1}, and the photonic efficiencies are 0.027 ± 0.004 % and 0.027 ± 0.009 %, respectively. In fact, the initially blue solution became almost colorless after 240 min under UV-A light, indicating the significant degradation of MB. From experimental observations, we can argue that increasing the TiO_2 concentration over 15 wt% does not significantly improve the photocatalytic performance of the polymeric nanocomposites. This saturation effect is presumably due to a limitation of the amount of NPs reaching the surface during the sample preparation. However, in general we have to consider that the degradation process is limited by the reaction between the free carriers and H_2O or O_2 molecules at the sample surface. This reaction process might induce some saturation effect. In the literature, a comparable activity was observed using 50 μg/ml of TiO_2 NPs in dispersion form [Zimbone et al., 2015]. In order to verify that the polymer does not release any nanomaterials into the solution, after 240 min we removed the samples from the solution and we continued the irradiation with the UV-A lamp, but no reduction of MB concentration was observed after 60 min, so demonstrating that no appreciable release of NPs occurred in the MB solution, capable of inducing detectable photodegradation.

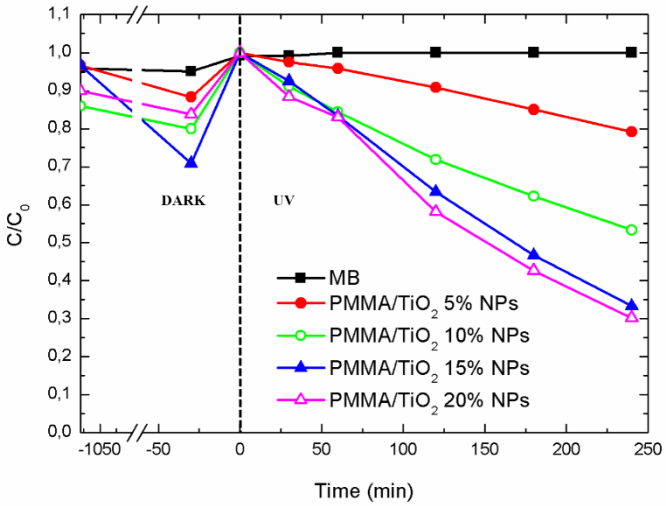

Figure 3.10: Photocatalytic activity of the PMMA/TiO_2 films with 5 wt% NPs (full dots), with 10 wt% NPs (open dots), with 15 wt% NPs (full triangles) and with 20 wt% NPs (open triangles) compared to the discoloration of pure MB under UV illumination (squares) (lines are to guide the eye). Adapted from [Cantarella et al., 2016a]

To confirm that such nanocomposites are broadly active for the degradation of organic compounds, other dyes have been used as model pollutants. In particular, the photocatalytic activity of the PMMA/TiO_2 film with 15 wt% NPs was evaluated also by measuring the decomposition rate of methyl orange (MO) and rhodamine B (RhB) in water under the same conditions used for the test with MB. Fig. 3.11 reports the removed percentage of these dyes in the presence of the photocatalyst after 240 min under UV irradiation. The obtained results reveal that the nanocomposite was able to destroy 35% of MO and more than 50% of RhB. The lower efficiency towards MO, compared to the degradation rate of MB and RhB, is due to an electrostatic repulsion between MO, negatively charged (Fig. 3.2), and the surface of the sample, where a negatively charge density exists because of the presence of ester groups. This repulsion does not facilitate the initial adsorption of the dye onto the photocatalyst surface, making slower

the dye degradation. However, as reported in many papers [Rochkind et al., 2015], the use of methylene blue and any other dye that behaves similarly might be inadequate for testing photocatalytic activity. In fact, the dye photobleaching can also occur via a dye photosensitized process in which the electronically excited state of the dye injects an electron into the conduction band of the semiconductor to produce an oxidized dye radical which is unstable and able to decompose subsequently to bleached products. The presence of this second mechanism, sensitization, reduces the generality required for a model contaminant used for testing a photocatalyst. Hence, in order to demonstrate that these materials are indeed active for the degradation of particularly dangerous organic pollutants, and to exclude any possible artefact, the photocatalytic properties of the PMMA/TiO_2 film with 15 wt% NPs was also tested for the degradation of another contaminant, phenol, which is toxic and potentially responsible of genetic alteration, used in many industrial processes. As reported in Fig. 3.11, after 240 min under UV light, the nanocomposite was able to remove 45% of phenol present in the solution. Both for the dyes and for the phenol, a reference solution without any photocatalyst immersed, irradiated under UV light for the same time is also reported in Fig. 3.11, not showing any significant reduction of the concentration (the estimated error was 4% according to our analysis, p.59).

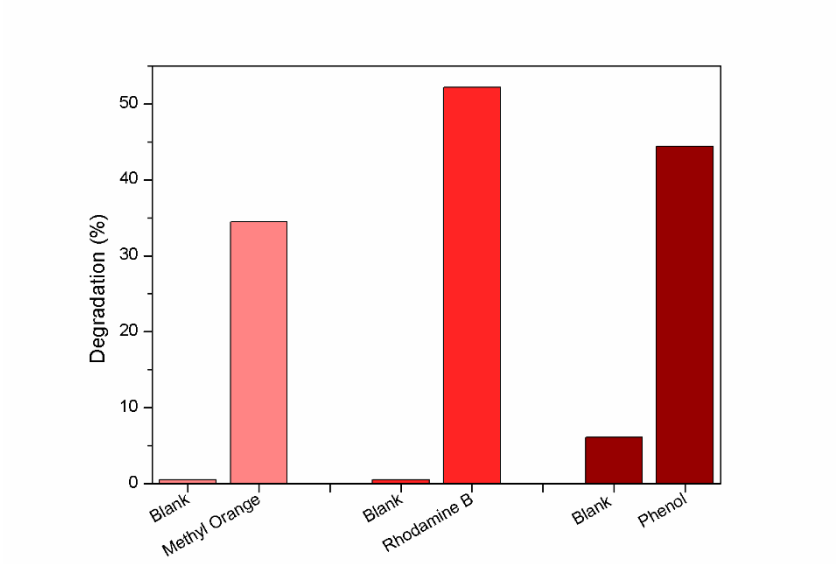

Figure 3.11: Photocatalytic degradation of MO, RhB and phenol by 1 cm^2 PMMA/TiO_2 film with 15 wt% NPs after 240 min under UV irradiation; for each model pollutant, the photodegradation without any sample in contact with the solution is reported as blank control.

The 8 W UV lamp used in this work has an irradiance comparable to the UV component of the solar spectrum reaching the earth's surface, in accordance with the up to date ISO 10678:2010 test. The photocatalytic efficiency increases significantly with increasing the lamp power, suggesting a potential engineering option when the possibility of using artificial light source, such as a LED, exists. To demonstrate the influence of the lamp on the activity of the materials, we performed a photocatalytic test with an 18 W UV lamp. The obtained results are reported in Fig. 3.12, in which we can see an increment of the activity: in particular, the discoloration rate for the film with 15 wt% of NPs is $(8\pm0.4)\cdot10^{-3}$ min^{-1} almost twice as that measured in the experiment with the 8 W lamp. This graph shows only the reduction of MB concentration ascribed to the photocatalytic activity, not including the period preceding the light exposition (18 hours) in which the MB reduction, due to the physical adsorption, is comparable to that showed before.

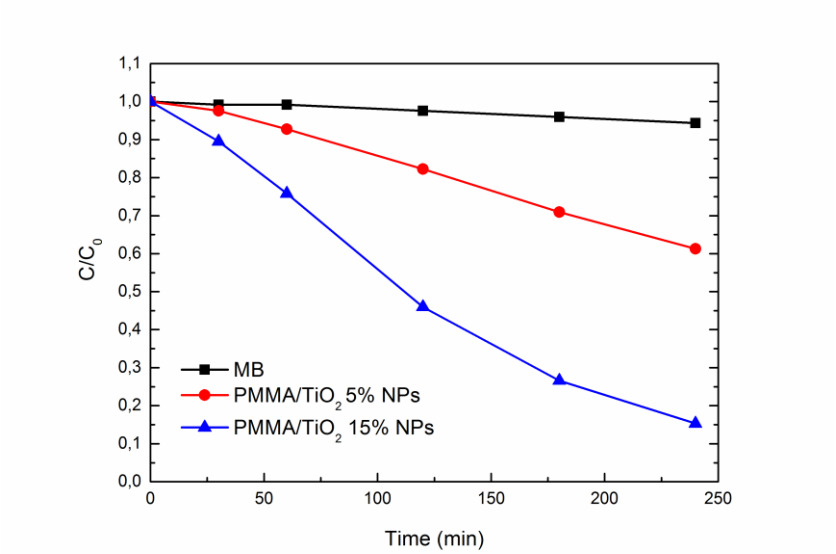

Figure 3.12: Photocatalytic activity, using an 18 W UV lamp, of the PMMA/TiO_2 film with 5 wt% NPs (dots) and with 15 wt% NPs (triangles) compared to the discoloration of pure MB under UV illumination (squares) (lines are to guide the eye) [Cantarella et al., 2016a].

3.2.3 Antibacterial activity: results and discussion

Antibacterial activity of the PMMA/TiO_2 film with 15_{wt}% NPs was tested by measuring the survival rate of *Escherichia coli* after exposure to UV activated samples. *E. coli* is a well-known Gram-negative bacterium, it is a representative of coliforms and it is considered as an indicator of fecal contamination. International regulations on wastewater treatment fix an upper limit of *E. coli* concentration in drinkable water. In our study, *E. coli* ATCC25922 was chosen as the model organism. The ATCC25922 strain is mostly used in tests aimed to testing food safety. Thus, it is not genetically modified for molecular biology purposes, so that the possible resistance mechanisms were not weakened. Hence, *E. coli* ATCC25922 looked as a proper model organism for the photocatalytic test. The best results, showed in Fig. 3.13, were obtained after 1h exposure to the PMMA/TiO_2 sample and UV; the *E. coli* survival rate has been reduced up to ~30% whereas in the

same time frame, the survival ofbacteria exposed to PMMA and UV was above 98%. Indicating the key role of the TiO_2 nanomaterials in the significant decrease of bacteria survival. Literature data indicate that antibacterial activity of photocatalytic titania nanomaterials is related to the production of reactive oxygen species (ROS). It is generally accepted that the hydroxyl radical ($OH\cdot$) is the major responsible for bacterial inactivation [Cho et al., 2004]. In fact, the latter is able to react with membrane phospholipids triggering a reaction of lipid peroxidation, which, in turn, generates an extensive membrane damage.

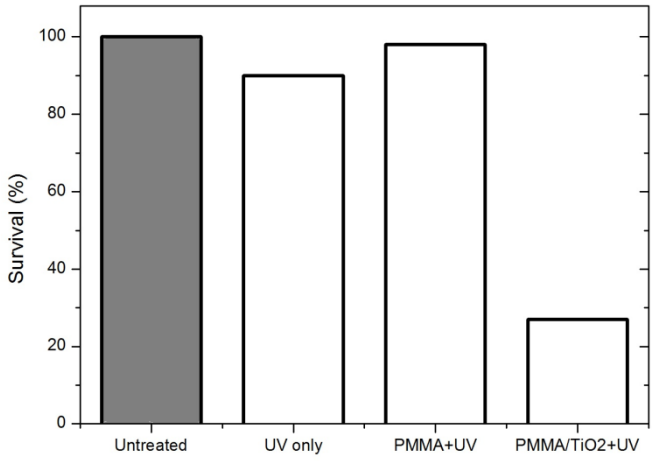

Figure 3.13: *E. coli* survival rate for CFU count after 60 min exposure to PMMA/TiO_2 film with 15 wt% NPs and to PMMA film. Untreated control and UV control were run in parallel [Cantarella et al., 2016].

3.2.4 Stability of the PMMA/TiO_2 NPs photocatalysts

The stability of the polymers, against degradation by oxidative radicals generated during the irradiation process, is one of the main issues

associated to the use of polymers as substrates for photocatalysts. In order to evaluate the stability of the synthesized polymer nanococomposites, we re-used the same fragment of PMMA/TiO_2 film with 15 wt% NPs for the degradation of MB and checked its efficiency after several cycles. The relative results are shown in Fig. 3.14. We found that the photocatalytic activity does not significantly change even after eight cycles, suggesting that PMMA nanocomposites can be efficiently recycled and reused for repeated cycles without loss of efficiency. The variability of the results is slightly larger (~10%) than the measurement repeatability we estimated (~4%), probably due to a non perfect reproducibility of the conditions of the sample surface after every cycle. However, such a difference is rather negligible. No NPs were released from the material as attested by the absence of any photocatalytic activity when the sample was extracted from the solution. In addition, no modification of the absorbance spectra was observed, that instead would occur in the case that NPs are present in the solution. This is indeed a sufficient test for a Technology Readiness Level (TRL) of the material not above 5 (technology validated in relevant environment); for demonstrating a higher TRL, longer term exposure effects on the matrix should be evaluated, this being out of the scope of the thesis work.

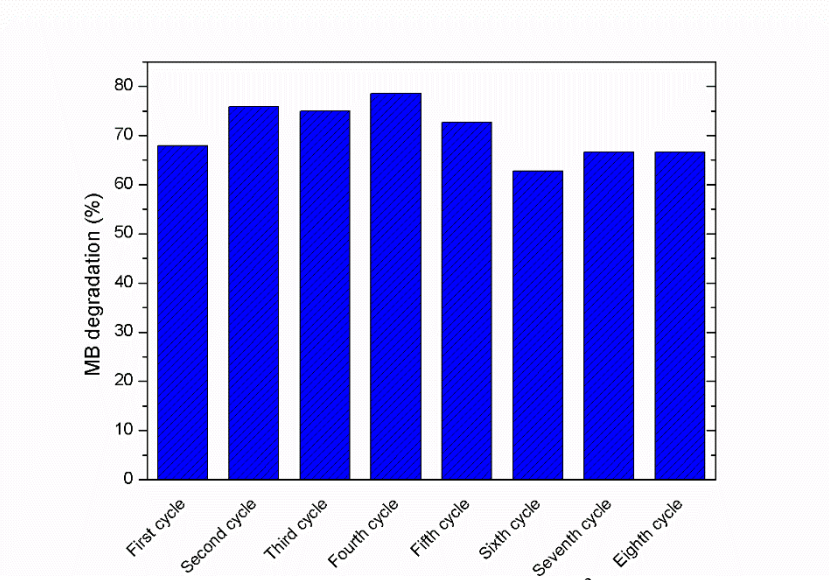

Figure 3.14: Photocatalytic degradation of MB by 1 cm^2 of the PMMA/TiO_2 film with 15 wt% NPs after up to eight cycles measured after UV light irradiation of duration 240 min [Cantarella et al., 2016a].

As said, apart from the stability test, the polymer is susceptible anyway of degradation by the photocatalytic environment, as attested by the SEM analysis (Fig. 3.15a) of a film of PMMA/TiO_2 with 15 wt% NPs after several photocatalytic cycles. In this image, the consumption of the polymer in proximity of the titania is clearly visible. However, we have found that the addition of an antioxidant to the polymer matrix represents a viable solution to improve the response of the polymer to the oxidation process. Fig. 3.15b shows the SEM image of a sample of PMMA/TiO_2 with 15 wt% NPs and 2 wt% of pentaerythritol tetrakis(3,5-di-tert-butyl-4-hydroxyhydrocinnamate (PTBHC) used as antioxidant (molecular structure reported in Fig. 3.16). After the same number of photocatalytic cycles, the PMMA matrix in the sample with the antioxidant was not damaged. In Fig. 3.17 the photocatalytic activity of a sample with PTBHC is compared to the activity of a sample with the same quantity of TiO_2 NPs but without antioxidant. The two discoloration rates are comparable $(5.4\pm0.02)\cdot10^{-3}$ min^{-1} and $(4.6\pm0.2)\cdot10^{-3}$

min^{-1}, respectively, so demonstrating that the presence of the antioxidant does not affect the photocatalytic efficiency of the material.

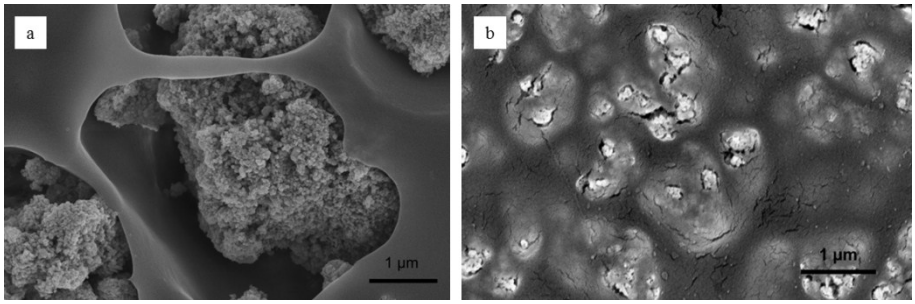

Figure 3.15: SEM plan views of PMMA/TiO_2 films with 15 wt% NPs without PTBHC (a) and with 2 wt% of PTBHC (b) after the same number of photocatalytic cycles.

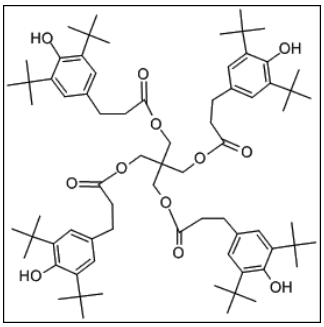

Figure 3.16: Molecular structure of the antioxidant PTBHC.

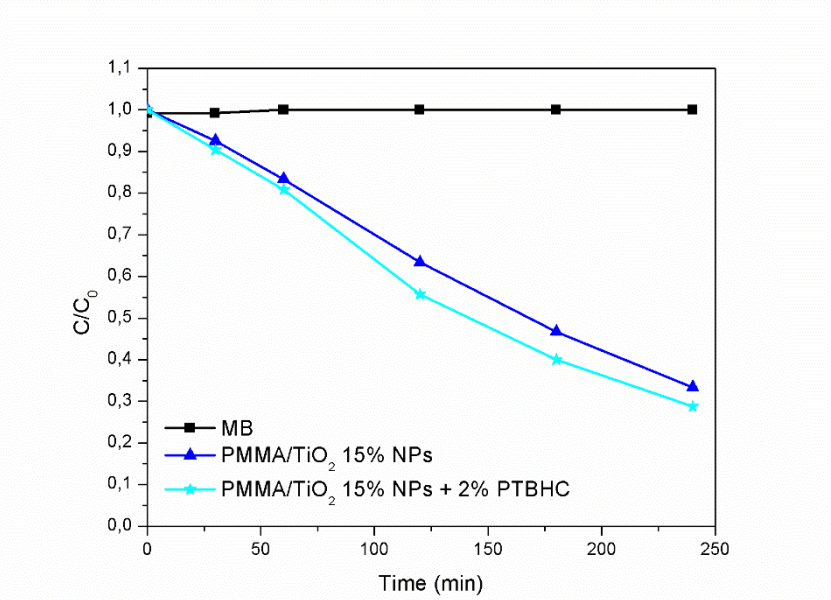

Figure 3.17: Photocatalytic activity of the PMMA/TiO_2 films with 15 wt% NPs without PTBHC (triangles) and with 2 wt% of PTBHC (stars) compared to the discoloration of pure MB under UV illumination (squares) (lines are to guide the eye).

3.2.5 PMMA/TiO_2 nanotubes composites

As mentioned in section 3.1.1, titanium dioxide nanotubes (TNTs) were grown on Ti foils by electrochemical anodization in our laboratory, in order to test an alternative TiO_2 based nanomaterial with respect to the commercially available nanoparticles. Fig. 3.18 shows two SEM images of the obtained nanotubes. After annealing, the TNTs were detached from the substrate by sonication and used for the preparation of the PMMA nanocomposites, following the above reported procedure of sonication and solution casting, with two different contents of TNTs: 5 wt% and 15 wt% with respect to the polymer.

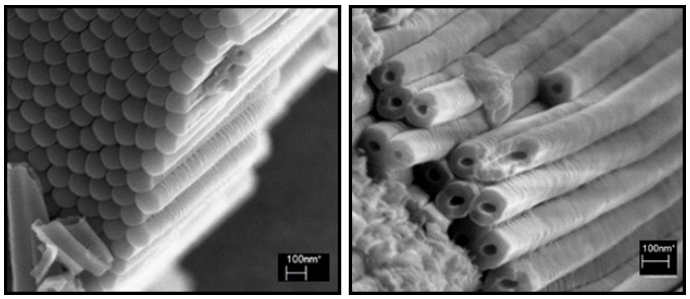

Figure 3.18: SEM images of TNTs obtained by electrochemical anodization on Ti foils.

Fig. 3.19a and b show SEM plan views of the back surface (the surface in contact with the Petri dish during the preparation of the films) of the PMMA/TNTs film with 5 wt% of nanotubes at low and high magnification, respectively. The SEM images indicate that the nanotubes form large aggregates, as "island" with different extension, distributed in the back surface of the film quite homogeneously. The cross section micrograph of the same film in the region of one aggregate is reported in Fig. 3.19c; the aggregated nanotubes arrange only in proximity of the back surface of the nanocomposite film and are aligned along the normal to the surface, while no nanostructures are visible in other regions of the film. This distribution is probably due to a significant sedimentation of the nanostructures during the evaporation of the solvent, occurring for the much longer size of these agglomerates with respect to the NPs.

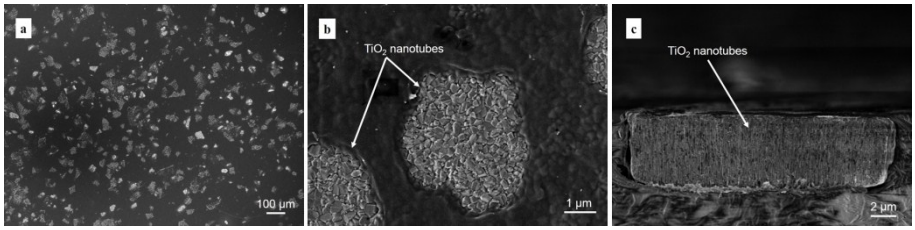

Figure 3.19: (a) SEM plan view of the back surface of the PMMA/TNTs film with 5 wt% nanotubes at low magnification; (b) SEM plan view of the back surface of the PMMA/TNTs film with 5 wt% nanotubes at high magnification; (c) SEM cross section magnification in proximity of the back surface of the film showing the vertical aligned nanotubes [Cantarella et al., 2016b].

The photocatalytic activity of the synthesized PMMA/TNTs composites was evaluated by means of the bleaching of MB dye. In Fig. 3.20 we show the photocatalytic activity of 1 cm^2 of back side of the PMMA/TNTs films with two different contents of nanotubes, 5 wt% and 15 wt%. The graph reports only the reduction of MB concentration ascribed to the photocatalytic activity, not including the period preceding the light exposition (18 h) in which the MB reduction, due to the physical adsorption, is less than 3%. In the graph, the decrease of pure MB under UV irradiation is also reported for comparison. Each experiment has been performed five times, obtaining a high repeatability with a calculated standard deviation within 4% related to measurement sensitivity. Despite the nanotubes are agglomerated and embedded in the polymer and only a fraction of their surface is in contact with water, the samples exhibit a considerable activity, because a large surface of TiO_2 is anyway in contact with water. In particular, the discoloration rate for the sample with 15 wt% of TNTs is $(3.0\pm0.1)\cdot10^{-3}$ min^{-1} and the photonic efficiency, calculated following the method described in ISO 10678:2010, is 0.047 ± 0.007 %.

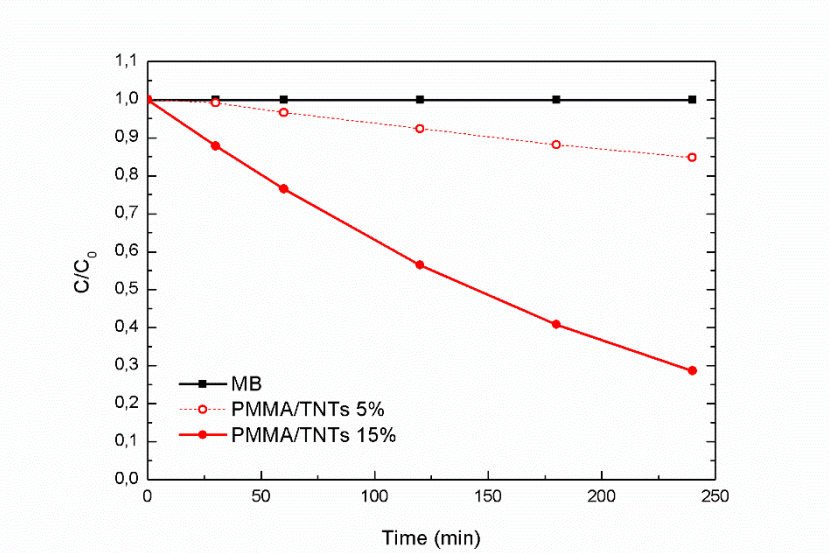

Figure 3.20: Photocatalytic activity of the PMMA/TNTs film with 5 wt% nanotubes (open dots) and with 15 wt% nanotubes (full dots) compared to the discoloration of pure MB (squares)under UV illumination (lines are to guide the eye). Adapted from [Cantarella et al., 2016b].

The antibacterial activity of the PMMA/TNTs films was tested by measuring the survival rate of *Escherichia coli* after exposure to UV activated samples. The PMMA/TNTs film with 5 wt% nanotubes does not show a significant antibacterial activity. In fact, after 1h exposure, bacteria survival remains at 93%, as shown in Fig.3.21. Longer exposures do not improve the results. On the other hand, the PMMA/TNTs film with 15 wt% NPs displays a huge antibacterial activity. The best results, shown in Fig. 3.21, were obtained after 1h exposure to the PMMA/TNTs sample; *E. coli* survival rate has been reduced up to ~ 15%. In the same time frame, bacteria exposed to PMMA only and to UV light survived quite well. The experimental error is around 5%. These results indicate that titanium dioxide nanomaterials have a key role in the decrease of the survival of bacteria. However, our results suggest that a certain percentage of nanotubes is needed in order to confer antibacterial properties to the composite film. In our experiments, it may be reasoned that the inclusion of 5% titania

nanotubes does not allow the generation of an hydroxyl radical amount sufficient to significantly damage the bacterial membrane.

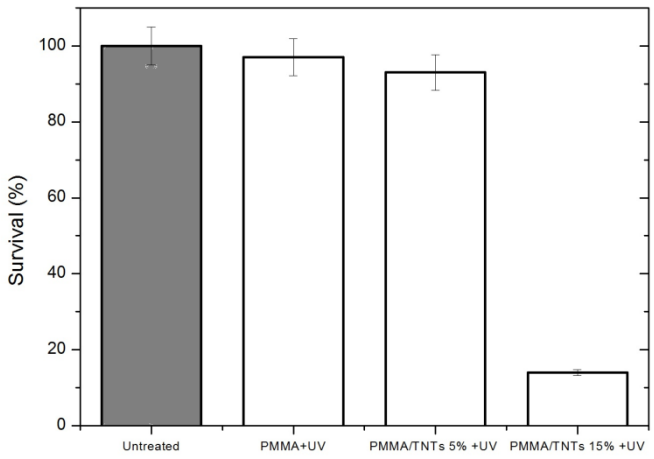

Figure 3.21: *E. coli* survival rate for CFU count after 60 min exposure to PMMA film, PMMA/TNTs film with 5 wt% nanotubes and PMMA/TNTs film with 15 wt% nanotubes. Untreated control was run in parallel [Cantarella et al., 2016b].

3.3 PMMA/TiO_2 NPs/ SWCNTs composites

A limitation of TiO_2 can be attributed to the recombination phenomena affecting the free carriers generated by light irradiation, having a negative impact on the decomposition of the pollutants. Photo-generated electron-hole pairs have indeed a recombination time on the order of 10^{-9} s, while the chemical interaction with adsorbed pollutant species has a time scale of 10^{-8}-10^{-3} s [Hoffmann et al., 1995].

In this section, we present our approach to reduce this problem based on the coupling of TiO_2 with carbon nanotubes (CNTs). It is known that all

closed cage carbon structures, including fullerenes and carbon nanotubes, are natural electron acceptors. Proof of this can be obtained mathematically even by qualitative molecular orbital theory. The argument starts from isolated C_2 fragments that are brought together from infinite distance. Each fragment has a π and a π^* orbital. As they are brought together to form the nanotube, the two degenerate sets of π and π^* orbitals mix prevalently between themselves and spread in energy. The low-lying end of the π^* orbitals is very stable and readily accept electrons. Upon receiving the charge, the transport along the axis of the nanometers-long carbon structure can contribute to a reduced probability of back transfer to the oxidized donor [Guldi et al., 2005]. Combining titania with CNTs, the strong interaction between metal oxide and nanotube results in a close contact to form a junction which offers an effective route of reducing electron-hole recombination by promoting the injection of electrons into the nanotube. Therefore, CNTs act as photo-generated electrons acceptor while TiO_2 is the electron donor under irradiation. The adsorbed oxygen molecules on the nanotubes react with the electrons forming very reactive oxygen radicals that oxidize the contaminants. On the other side, the holes remain on the TiO_2 to take part in redox reactions. A schematic of this mechanism is shown in Fig. 3.22 [Tawfik, 2013] [Woan et al., 2009] [Chen et al., 2015]. This property of the nanotubes allows to obtain potential efficient photocatalytic systems for water purification. In the literature, there are some examples of the application of such nanomaterials in dispersed forms into water. This approach sets several issues concerning the disposal of the TiO_2 nanoparticles and CNTs into the environment, that need to be recovered before the water is available for potabilization purposes. Our method, based on the immobilization of these nanomaterials into the polymer matrix, overcomes this limitation.

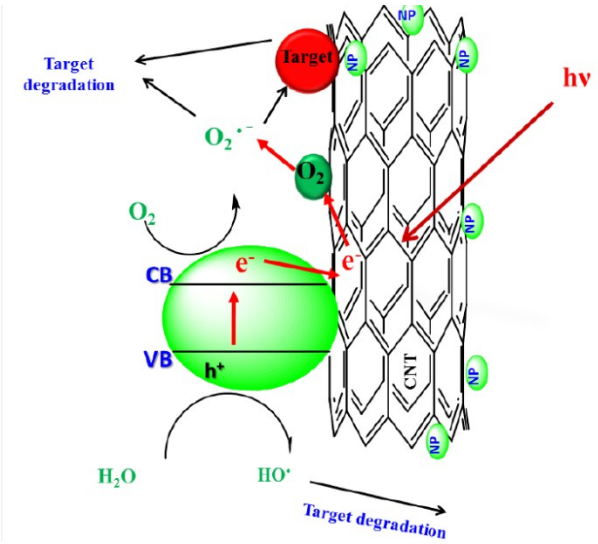

Figure 3.22: Schematic diagram of the proposed mechanism of photodegradation over TiO_2/CNTs composite. Adapted from [Tawfik, 2013].

3.3.1 Results and discussion

The PMMA/TiO_2 NPs/SWCNTs composites were prepared using the same procedure of sonication and solution casting described in section 3.2.1, adding a dispersion of single-walled carbon nanotubes (SWCNTs, carboxylic acid functionalized) in acetone to the polymer solution before the sonication process. The percentage of TiO_2 NPs in the prepared nanocomposites was 5 wt%, 10 wt% and 15 wt%, with respect to the polymer. The weight ratio between TiO_2 NPs and SWCNTs was 4:1 for all samples. The SEM analyses (not reported) of these films exhibit a distribution of the nanostructures comparable to the distribution of the NPs showed in Fig. 3.7.

Fig. 3.23 shows the photocatalytic activity of the films realized combining titania with SWCNTs in PMMA matrix; for comparison in the graph, we report also the photocatalytic activity of the samples with the same quantity of TiO_2 NPs, but without SWCNTs. The photocatalytic activity for the sample with 5 wt% TiO_2 NPs and SWCNTs resulted in a higher reaction

rate $(2.4 \pm 0.2) \times 10^{-3}$ min^{-1} (photonic efficiency $0.016 \pm 0.007\%$), compared to that of the sample with only TiO_2 NPs in the same quantity $(9.7 \pm 0.5) \times 10^{-4}$ min^{-1} (photonic efficiency $0.006 \pm 0.001\%$). This observed increase in the photoactivity may be ascribed to a reduction in the electron-hole recombination rate by inclusion of SWCNTs. In these nanocomposites, the strong interaction between the TiO_2 and the SWCNTs offers an effective route of reducing electron-hole recombination. However, we observed that this effect is especially clear for the samples with 5 wt% TiO_2 NPs, while with increasing the TiO_2 concentration the effect becomes less significant. For a clear reading of this saturation effect, we report in Fig. 3.24 the percentage of MB degraded after 240 min under UV light in the presence of our nanocomposite films.

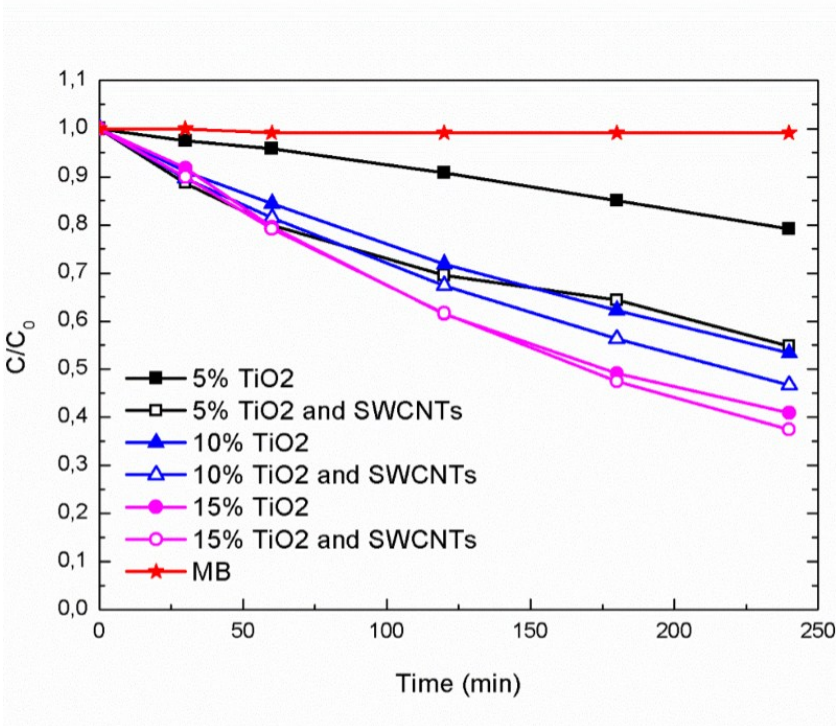

Figure 3.23: Photocatalytic activity of the PMMA/TiO_2 films with three different contents of NPs (5 wt%, 10 wt% and 15 wt%) and of the PMMA films with the same quantities of TiO_2 NPs and SWCNTs compared to the discoloration of pure MB (stars) under UV illumination (lines are to guide the eye). Adapted from [Cantarella et al., 2016a].

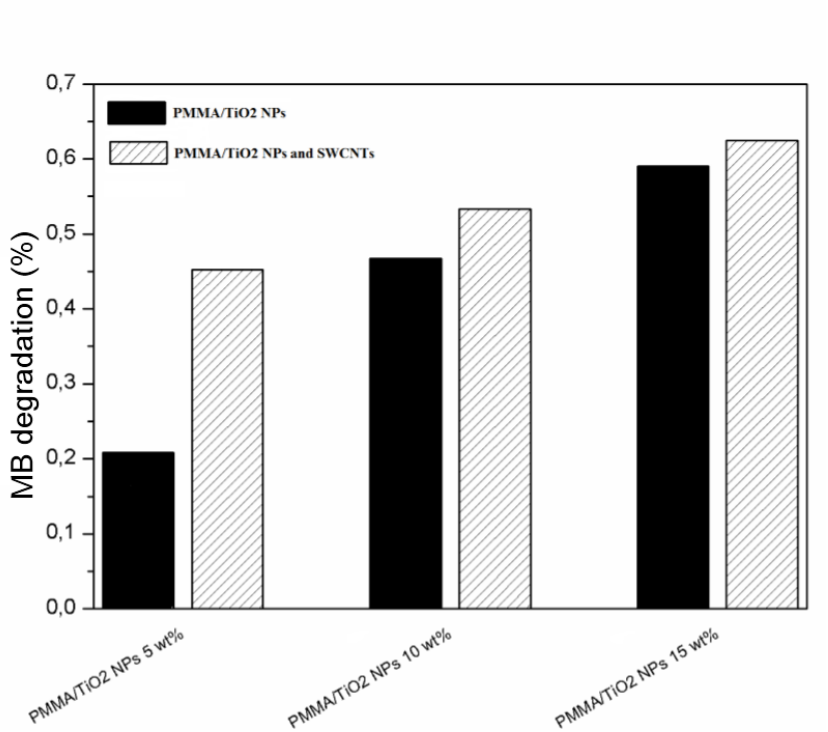

Figure 3.24: Percentage of MB degraded after 240 min under UV light in presence of the PMMA/TiO_2 films with three different contents of NPs (5 wt%, 10 wt% and 15 wt%) and of the PMMA films with the same quantities of TiO_2 NPs and SWCNTs. Adapted from [Cantarella et al., 2016a].

The saturation effect for 15 wt% TiO_2 NPs is presumably due to the higher nanoparticles aggregation that occurs with increasing the titania concentration. Such higher agglomeration prevents the injection increase of electrons from TiO_2 to the CNTs, because of a limitation of the surface to volume ratio of the NPs. Due to such a limitation in the increase of the exposed surface of the NPs, induced by their agglomeration, we do not observe any significant improvement of the photocatalytic performance of the polymeric nanocomposites for such NPs concentration.

3.4 PMMA/TiO_2-TCPP nanocomposites

The main drawback of TiO_2 limiting its application is the value of its band gap (~3.2 eV), allowing an absorption only in the ultraviolet range ($\lambda <$ 387 nm). For this reason, diverse methods have been proposed to extend the light absorption of TiO_2 into the visible region (see chapter 1, section 1.2).

Dye sensitization has been used in photovoltaics as a strategy to modify the photoresponse of solar cells, and porphyrins are recognized as valid candidate for sensitization process [Wang et al., 2007] [Youngblood et al., 2009] [Pellegrino et al., 2011] [Zhou et al., 2012] [Wang et al., 2010] [Cherian and Wamser, 2000]. We have transferred this approach to the case of photocatalysis and water treatment by functionalizing the PMMA/TiO_2 NPs with a porphyrin, namely *meso*-tetraphenylporphyrin-4,4′,4″,4‴-tetracarboxylic acid (TCPP).

The working principle of a sensitized material is based on the absorption of visible light for exciting an electron from the highest occupied molecular orbital (HOMO) to the lowest unoccupied molecular orbital (LUMO) of the sensitizer, such as a porphyrin. The excited molecule subsequently transfers electrons into the conduction band of TiO_2, while the sensitizer itself is converted to its cationic radical. The ability of the excited state porphyrins to inject their electrons into the conduction band of TiO_2 is determined by the energy difference between the conduction band of TiO_2 and oxidation potential of the excited state porphyrins. In Fig. 3.25, the energy level diagram of the conduction and valence bands of TiO_2 is illustrated together with the electron-donating energy levels of three different porphyrins: TCPP, *meso*-tetrakis(4-sulfonatophenyl)porphyrin (TSPP) and *meso*-tetrakis(4-metoxyphenyl)porphyrin (TMeOPP). These differences suggest that electronic transfer from excited state porphyrin to the conduction band of TiO_2 is energetically favorable [Kathiravan and Renganathan, 2009]. Subsequently the injected electrons reach the surface of titania where reduce the O_2 molecules adsorbed on the surface to $O_2^{\bullet -}$, which can further

transform into H_2O_2 and $OH^{\bullet}$, resulting in the oxidation of the pollutants. The proposed mechanism is illustrated in Fig. 3.26.

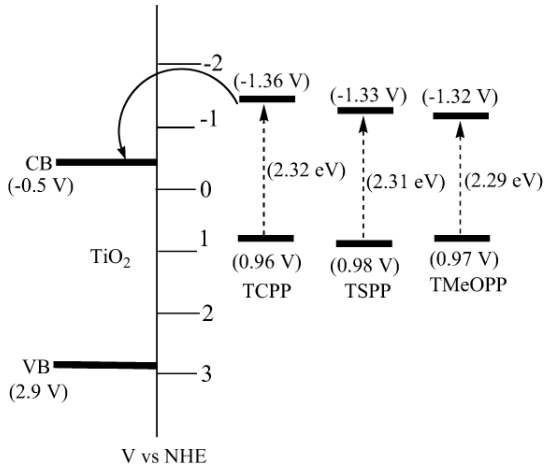

Figure 3.25: Energy level diagram describing the conduction and valence bands of TiO_2 and the electron-donating energy levels of porphyrins [Kathiravan and Renganathan, 2009].

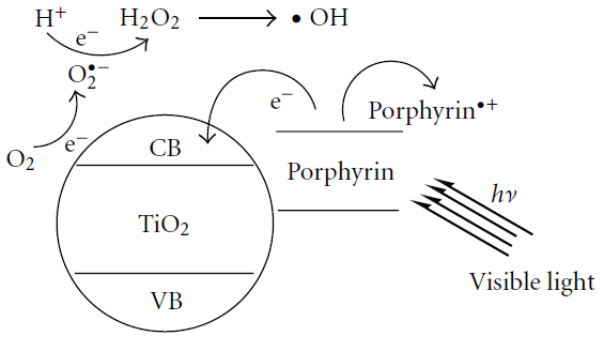

Figure 3.26: Mechanism of pollutants photooxidation on the surface of TiO_2-TCPP NPs [Cai et al., 2012].

3.4.1 Results and discussion

The PMMA/TiO_2-TCPP nanocomposites were prepared by impregnating the TiO_2 NPs with 60 μmol/g of the sensitizer TCPP: the porphyrin was dissolved in THF and the TiO_2 NPs were added to this solution. The resulting suspension was magnetically stirred for 6 h, and then it was added to the PMMA solution for the already described sonication and solution casting method. The percentage of the TiO_2, used in these nanocomposites, was 15 wt% with respect to the polymer. The TCPP was chosen as TiO_2 sensitizer due to the presence of anchoring groups (-COO^-) in its molecular structure (Fig. 3.27), that facilitate a strong adsorption on the TiO_2 surface. The resulting nanocomposite film is showed in Fig. 3.28.

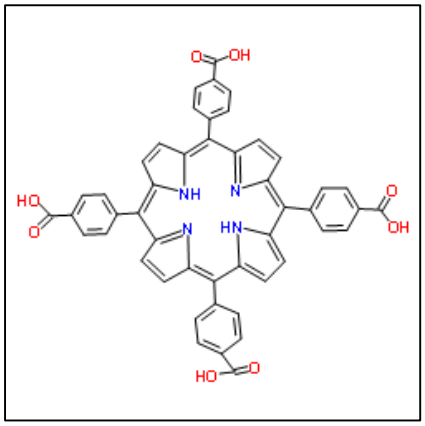

Figure 3.27: Molecular structure of the porphyrin TCPP.

Figure 3.28: PMMA/TiO_2 film with 15 wt% NPs impregnated with TCPP in the Petri dish.

The photocatalytic degradation of MB under visible light irradiation using 1 cm^2 of the PMMA/TiO_2 film with 15 wt% NPs impregnated with TCPP is reported in Fig. 3.29. As observed, the efficiency of degradation of MB under visible light in contact with the sample is comparable to the efficiency obtained with the film of PMMA/TiO_2 with 15 wt% NPs, but under UV light (Fig. 3.10). In fact, in 240 min the discoloration rates are similar for the two samples: $(4.3\pm0.1)\cdot10^{-3}$ min^{-1} under visible irradiation for the PMMA/TiO_2 sample with TCPP and $(4.6\pm0.2)\cdot10^{-3}$ min^{-1} under UV irradiation for the sample without porphyrin. For comparison, blank experiments were done, in which the photodegradation of MB was measured, using visible light, in the presence of the film PMMA/TiO_2 15 wt% NPs and a film PMMA/TCPP. No significant photocatalytic activity is obtained, being the slow decrease of the absorbance due to the slight MB degradation for the direct effect of the used visible wavelength.

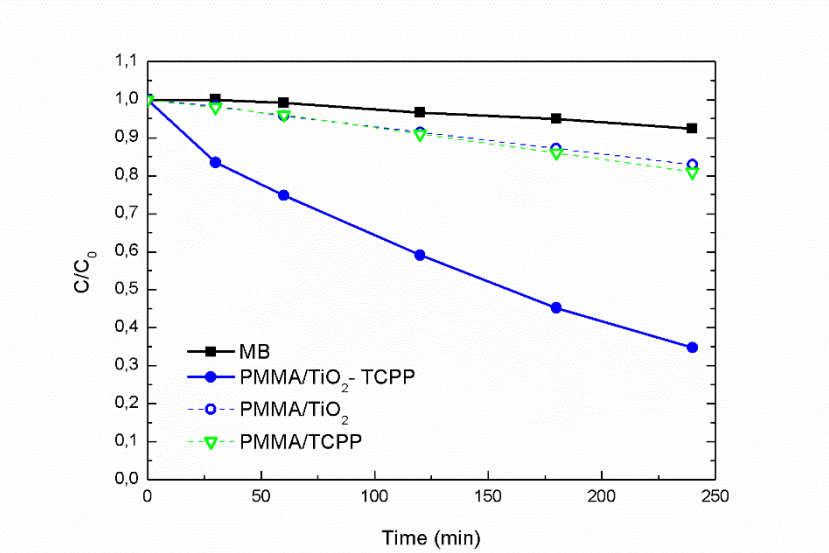

Figure 3.29: Photocatalytic activity of the PMMA/TiO_2 films with 15 wt% NPs impregnated with TCPP 60 µmol/g (full dots); of the PMMA/TiO_2 film with 15 wt% (open dots); of the PMMA/TCPP film (open triangles); compared to the discoloration of pure MB under visible illumination (squares) (lines are to guide the eye). Adapted from [Cantarella et al., 2016a].

The photocatalytic activity of the sample with the porphyrin was evaluated also by measuring the decomposition rate of RhB in water under the same conditions used for the tests with MB. The obtained results, reported in Fig. 3.30, reveal that the degradation rate in this case is $(2.2 \pm 0.2) \times 10^{-3}$ min^{-1}. This value is lower than the degradation rate obtained with MB, however, it is significant and it confirms the effective activity of these nanocomposites under visible light. The difference of the two cases lies in the different reaction kinetics taking place for the oxidation and degradation of the two different polluting molecules.

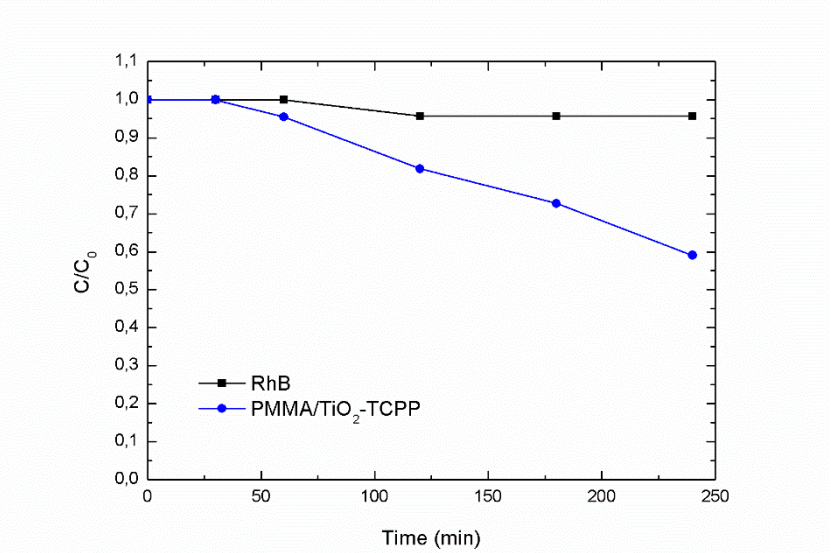

Figure 3.30: Photocatalytic activity in RhB aqueous solution of the PMMA/TiO_2 films with 15 wt% NPs impregnated with TCPP 60 µmol/g (full dots) compared to the discoloration of pure RhB under visible illumination (squares) (lines are to guide the eye).

The stability of these films was evaluated by re-using the same fragment of PMMA/TiO_2 film with 15 wt% NPs impregnated with TCPP for the degradation of MB checked its efficiency after several cycles, as well as for the film without the porphyrin. The obtained results are shown in Fig. 3.31. We found that the activity does not significantly change after up to eight photocatalytic cycles. Despite we did not add sacrificial agents into the nanocomposites to reduce the degradation of the dye (see chapter 1, section 1.2.3), the results demonstrate the stability both of the polymer matrix and of the dye itself. The variability between every cycle is due to a non perfect reproducibility of the surface, similarly to the situation with the samples active under UV light.

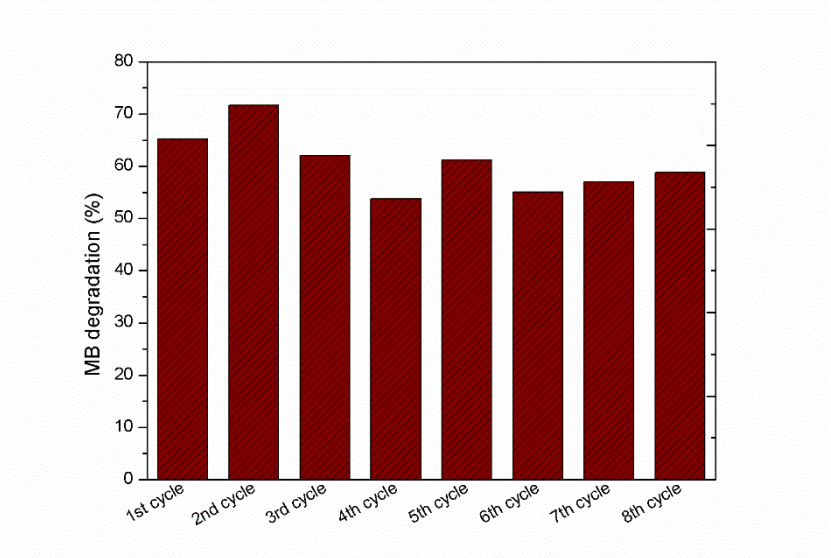

Figure 3.31: Photocatalytic degradation of MB by 1 cm^2 of the PMMA/TiO_2 film with 15 wt% NPs impregnated with TCPP 60 µmol/g after up to eight cycles measured after visible light irradiation of duration 240 min.

We also tested the antibacterial activity of the PMMA/TiO_2 film with 15_{wt}% NPs impregnated of TCPP. In this case, the light used was a visible light source at 460 nm. Again, the best results were obtained after 1 h exposure (see Fig. 3.32). Visible light promotes bacterial growth, in fact bacteria exposed to visible light only and to PMMA and visible light were able to nearly double after 1 h exposure, if compared to the untreated sample. It is worth to notice, in the presence of PMMA/TiO_2-TCPP film, that the *E. coli* survival rate has been reduced up to ~60%, suggesting that the combination of TiO_2 and TCPP displays antibacterial activity even in the presence of favorable conditions for bacterial growth. In both tests, the experimental error is around 5%.

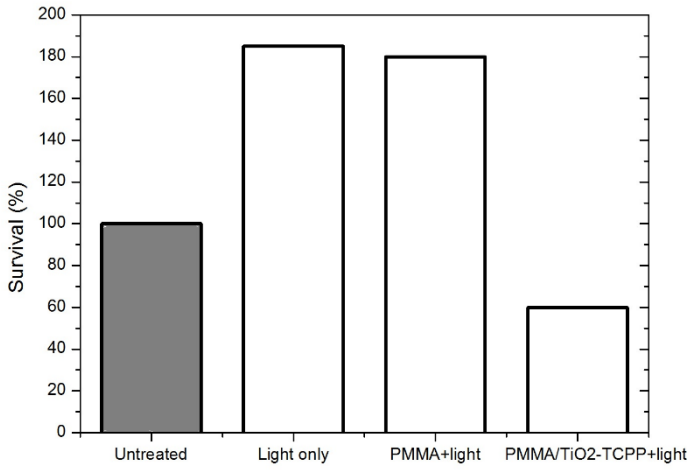

Figure 3.32: *E. coli* survival rate for CFU count after 60 min exposure to PMMA/TiO_2 film with 15 wt% NPs impregnated with TCPP 60 µmol/g and to PMMA film. Untreated control and visible light control were run in parallel [Cantarella et al., 2016a].

3.5 Conclusions

In this chapter it has been demonstrated that efficient polymeric nanocomposites with high photocatalytic and antibacterial activity were synthesized. These materials overcome many of the current issues that prevent the real application of the nanomaterials for water treatment, such as their dispersion in water. In addition, we realized both systems with a very high photocatalytic efficiency under UV light for the activation of the degradation process, and materials having the same high efficiency using visible light. These composites with PMMA are stable, harmless, cheap and can be realized with simple methods, allowing potential industrial tools for removal of organic and bacterial contaminants from water.

References

- Cai, J.H.; Huang, J.W.; Yu, H.C.; Ji, L.N. *Int. J. Photoenergy* **2012,** 348292
- Cantarella, M.; Sanz, R.; Buccheri, M.A.; Ruffino, F.; Rappazzo, G.; Scalese, S.; Impellizzeri, G.; Romano, L.; Privitera, V. *J. Photochem. Photobiol. A* **2016,** 321, 1-11
- Cantarella, M.; Sanz, R.; Buccheri, M.A.; Romano, L.; Privitera, V. *Mater. Sci. Semicond. Process.* **2016,** 42, 58-61
- Chen, J.; Qiu, F.; Xu, W.; Cao, S.; Zhu, H. *Appl. Catal. A* **2015,** 495, 131-140
- Cherian, S.; Wamser, C.C. *J. Phys. Chem. B* **2000,** 104, 3624-3629
- Cho, M.; Chung, H.; Choi, W.; Yoon, J. *Water Res.* **2004,** 38, 1069-1077
- Fine ceramics (advanced ceramics, advanced technical ceramics) – Determination of photocatalytic activity of surfaces in an aqueous medium by degradation of methylene blue. ISO 10678:2010(E). International Organization for Standardization, Switzerland, **2010**
- Guldi, D.M.; Rahman, G.M.A.; Zerbetto, F.; Prato, M. *Acc. Chem. Res.* **2005,** 38, 871-878
- Hafizah, N.N.; Mamat, M.H.; Said, C.M.S.; Abidin, M.H.; Rusop, M. *IOP Conf. Ser. Mater. Sci. Eng.* **2013,** 46, 012045
- Hoffmann, M.R.; Martin, S.T.; Choi, W.; Bahnemann, D.W. *Chem. Rev.* **1995,** 95, 69-96
- Kathiravan, A.; Renganathan, R. *J. Colloid. Interface Sci.* **2009,** 331, 401-407
- Mills, A.; Hill, C.; Robertson, P.K.J. *J. Photochem. Photobiol. A* **2012,** 237, 7-23
- Pellegrino, G.; Condorelli, G.G.; Privitera, V.; Cafra, B.; Di Marco, S.; Alberti, A. *J. Phys. Chem. C* **2011,** 115, 7760-7767
- Rochking, M.; Pasternak, S.; Paz, Y. *Molecules* **2015,** 20, 88-110
- Roy, P.; Berger, S.; Schmuki, P. *Angew. Chem. Int. Ed.* **2011,** 50, 2904-2939

- Saleh, T.A. (**2013**). The Role of Carbon Nanotubes in Enhancement of Photocatalysis, Syntheses and Applications of Carbon Nanotubes and Their Composites, Dr. Satoru Suzuki (Ed.), InTech, DOI: 10.5772/51050
- Wang, C.; Li, J.; Mele, G.; Yang, G.M.; Zhang, F.X.; Palmisano, L.; Vasapollo, G. *Appl. Catal. B* **2007,** 76, 218-226
- Wang, C.; Li, J.; Mele, G.; Duan, M.Y.; Lu, X.F.; Palmisano, L.; Vasapollo, G.; Zhang, F.X. *Dyes Pigm.* **2010,** 84, 183-189
- Woan, K.; Pyrgiotakis, G.; Sigmund, W. *Adv. Mater.* **2009,** 21, 2233-2239
- Youngblood, W.J.; Anna Lee, S.H.; Maeda, K.; Mallouk, T.E. *Acc. Chem. Res.* **2009,** 42, 1966-1973
- Zhou, X.T.; Ji, H.B.; Huang, X.J. *Molecules* **2012,** 17, 1149-1158
- Zimbone, M.; Buccheri, M.A.; Cacciato, G.; Sanz, R.; Rappazzo, G.; Boninelli, S.; Reitano, R.; Romano, L.; Privitera, V.; Grimaldi, M.G. *Appl. Catal. B* **2015,** 165, 487-494

Chapter 4

Future perspectives: molecularly imprinted polymers

In the recent years there has been an increasing interest on the environmental risks related to the so called "emerging contaminants" (ECs) in wastewaters, as the traditional methods are not able to remove them. These ECs are ubiquitous in the aquatic environment and they originate from a variety of product types, the most common ones being the highly prescribed non-steroidal anti-inflammatory drugs (NSAIDs). We propose molecularly imprinted polymers (MIPs) as valid tools for the selective removal from water of these drugs. MIPs are synthesized by copolymerization of cross-linking and functional monomers in the presence of a target analyte, which acts as a molecular template. Following the polymerization, the template is removed to leave cavities with selectivity for the analyte, allowing the polymer to rebind the analyte with a very high specificity.

In this last chapter, we describe the basic principle of the molecular imprinting of polymers, the obtained preliminary results and our future perspectives in this field.

4.1 Emerging contaminants in water

Recently, a growing interest is directed to a large number of substances that have been detected in the environment, but which are currently not included in routine monitoring programs at EU level and whose fate, behaviour and (eco)toxicological effects are not well understood. Such substances are identified as emerging contaminants (ECs), they have been detected in a wide range of environmental compartments including surface waters, groundwaters, and drinking waters. ECs originate from a variety of product types including human pharmaceuticals, veterinary medicines, nanomaterials, personal care products, paints and coatings [Boxall, 2012]. The increasing concern over the risks of ECs is reflected by a rapid rise in the numbers of scientific publications exploring the environmental impacts of ECs over the past decade (Fig. 4.1).

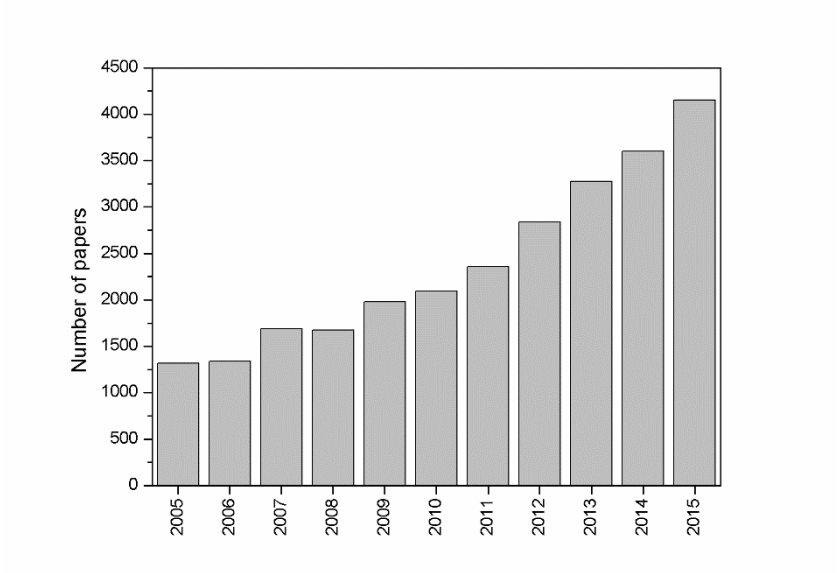

Figure 4.1: Number of publications concerning emerging contaminants over the years 2005-2015, based on database of ScienceDirect, with search keywords being "emerging contaminants".

Numerous studies have been performed to explore the effects of a range of ECs on the biochemistry, cell structure, growth, reproduction and mortality of organisms in the environment. Many data indicates that various ECs could affect negatively on the human and environmental health. For example, the diclofenac, which is a human drug used as an anti-inflammatory treatment, was found to be responsible for the massive decline in populations of vulture species in certain areas of Asia [Oaks et al., 2004]; the veterinary drug ivermectin, which is used to treat parasitic infections in livestock, has been shown to affect the growth of aquatic invertebrates at concentration lower than expected to occur in the aquatic environment [Garric et al., 2007]; ethinylestradiol, one of the active ingredients in the contraceptive pill, has been associated with endocrine disruption of fish population [Lange et al., 2001]; finally there is a concern regarding long-term exposure to antibiotic pharmaceuticals, used in human and veterinary medicine, that may be contributing to the selection of resistant bacteria in the environment with significant implications for human health [Boxall et al., 2003].

There are a number of EC types of potential concern, including:

- Naturally produced compounds such as toxins produced by fungi, bacteria and plants;
- Bio-terrorism/sabotage agents;
- Human personal care products such as essential oils, herbal medicines, antibacterials and fragrances;
- Emerging persistent organic pollutants such as flame retardants and dioxin-like compounds;
- Veterinary medicines such as antibiotics and antiparasitic agents;
- Hormones such as synthetic and natural estrogens and androgens;
- Nanomaterials;
- Human medicines;
- Metabolites and transformation products of synthetic chemicals that are produced from biological, chemical and physical breakdown reactions.

The presence of ECs in the environment is mainly attributed to the discharge of treated wastewater from conventional secondary water treatment processes, such as activated sludge and trickling filters. These processes are not indeed designed to remove ECs resulting in their release to receiving surface waters including rivers, lakes and coastal waters. In addition, the simultaneous presence of these chemicals in the environment is more dangerous, considering that they do not appear individually, but as a complex mixture, which could lead to unwanted synergistic effects.

Among the several EC types, we have pointed our attention to the pharmaceutical products used to cure human and animal health. The worldwide average per capita consumption of pharmaceuticals per year is estimated to be about 15 g; in industrialized countries the usage is even as high as 50 to 150 g [Alder et al., 2006]. Usually, drugs are developed with an intention of having a beneficial biological effect on the organism to which they are administered, though many such compounds will often pass into the environment where they may apply an unwanted biological effect. Among pharmaceutical products, NSAIDs are widely used throughout the world and detected in different aquatic environments at concentrations ranging from ng L^{-1} to mg L^{-1} [Lonappan et al., 2016]. Table 4.1 reports the amount of prescription of four common NSAIDs (paracetamol, diclofenac, ibuprofen and naproxen) in UK in 2012 and their detected quantity in the surface water. The observations of the UK data set are typical of EC research reported throughout the rest of Europe [Hughes et al., 2013] [Loos t al., 2013].

Table 4.1: NSAIDs contaminant information in the UK. Adapted from [Petrie et al., 2015].

EMERGING CONTAMINANT	**PRESCRIPTION 2012 IN UK (kg)**	**SURFACE WATER (ng l^{-1})**
PARACETAMOL	>2,000,000	2,382
DICLOFENAC	10,652	568
IBUPROFEN	108,435	5,044
NAPROXEN	126,258	146

The conventional treatment systems cannot fully remove these compounds from water. Additionally, the traditional techniques are generally designed to remove various pollutants simultaneously, but cannot effectively remove specific pollutants in wastewater. For these reasons, there is an urgent need of new methods that are both effective and selective to remove this class of pollutants. For this purpose, here we propose molecularly imprinted polymers (MIPs) as potential solution to this problem.

4.2 Molecular imprinting

The history of molecular imprinting technology starts in 1940, when Pauling put forward the idea about molecular imprinting that involved a protein antibody self-assembly with an antigen acting as template [Pauling, 1940]. Later, Dickey synthesized a type of substrate selective adsorbents via the precipitation of a mixture of silica gel and a template dye; after removal of the "patterning" dyes, the silica gel exhibited an increased affinity to the target dye [Dickey, 1955]. In 1972, Wulff et al. first demonstrated molecular imprinting in organic polymers by constructing a synthetic receptor using reversible chemical bonds between a template and functional monomers [Wulff et al., 1972]. In 1981, Mosbach and co-workers first prepared MIPs using non-covalent molecular interactions (such as hydrogen bonds, van der Waals forces, ionic interactions and hydrophobic effects) [Arshady and Mosbach, 1981]. Based on these pioneering studies, molecular imprinting technology started to grow rapidly [Alexander et al., 2006] [Whitcombe et al., 2014].

Molecular imprinting is a synthesis method used to create molecular recognition sites that are chemically and sterically complementary to the target of interest in a synthetic polymer. In this process, monomers with appropriate functional groups are co-polymerized with cross-linker monomers in the presence of the target analyte, which acts as a molecular template. The schematic representation of the imprinting process is shown in

Fig. 4.2. The functional monomers initially form a complex with the template, and after it polymerizes (by thermal or photo initiation) with the cross-linker. Subsequent removal of the template from the polymer matrix, by physical or chemical methods, reveals binding sites that are complementary in size and shape to the analyte. In this way, a molecular memory is introduced into the polymer, which becomes able to rebinding the analyte with a very high specificity [Haupt and Mosbach, 2000].

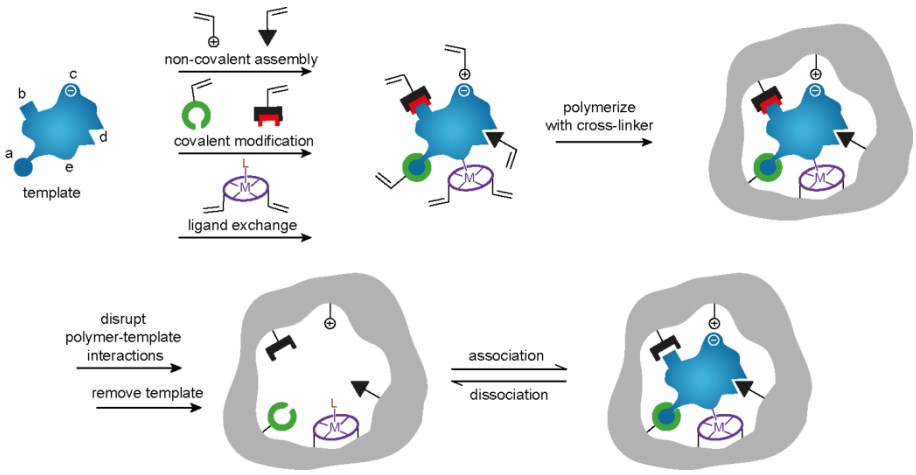

Figure 4.2: Schematic representation of the imprinting process showing some of the possible template-monomer interactions [Alexander et al., 2006].

Generally, there are two distinct approaches to molecular imprinting: covalent and non-covalent. The covalent approach involves the formation of reversible covalent bonds between template and monomers prior to polymerization. The advantage of this technique is that binding sites are more homogeneous and the template-monomer interaction is more stable [Martín-Esteban, 2013]. However, the interactions between template and monomers are so strong that it is difficult to remove thoroughly the template. Alternatively, non-covalent approach combines template and monomer by

non-covalent interactions such as electrostatic forces, hydrogen binding, or van der Waal forces. The drawback of this procedure is the low-electivity binding sites. However, due do the weak interaction, it is rather simple and it is more flexible concerning the choice of functional monomers and target molecules [Malitesta et al., 2012]. Moreover, it is more similar to natural processes in the sense that most biomolecular interactions are non-covalent in nature.

To satisfy the different application purposes, MIPs materials have been synthesized by several polymerization techniques [Huang et al., 2015].

Traditionally, MIPs have been prepared by bulk polymerization. In this method, functional monomers, template, cross-linker and initiator are dissolved by suitable solvent. Subsequently, the mixture is purged with nitrogen to remove oxygen and it is sealed in vacuum. Finally, the obtained bulk monoliths are downsized by grinding and sieving, which result in irregularly shaped particles. Bulk polymerization is by far the most widely used method for the preparation of MIPs due to its simplicity [He et al., 2007]. However, it is time-consuming and produces poor yields [Zheng et al., 2013].

Suspension polymerization is one of the simplest and most common approaches for the production of the MIP particles. In this polymerization, all the components involved in the polymerization process are dispersed in water in the presence of stabilizer and surfactant. However, the use of water as a dispersing agent reduces the binding site number and strength between the functional monomer and template [Mayes and Mosbach, 1996].

In the precipitation polymerization the functional monomers, cross-linker, template and initiator are dissolved in a large amount of porogen. Nevertheless, as the polymerization proceeds, the growing polymer chains become insoluble in the porogen and tend to precipitate. The advantage of this method includes the absence of surfactant and a control on a micron size range of MIPs by the polymerization conditions [Yan et al., 2007].

Two-step or multiple swelling polymerization is another common method for preparing MIP beads, but it is also one of the more laborious procedures. In this technique, preformed uniformed-sized seed particles are suspended in water, and after several additions of suitable organic solvents,

the initial particles swell to a final size with desirable performance [Hu et al., 2007].

Surface imprinting technique has attracted significant interest as a new alternative for improving the performance of MIPs. In this strategy, the imprinted binding sites are located at the surface of the polymer, overcoming the problem of limited mass transfer and incomplete template removal, which is often associated with materials obtained by the previous molecular imprinting methods. Surface imprinting polymers were usually prepared by either synthesizing a thin polymer film using similar approaches to those in bulk imprinting or by attaching the template on the surface of a substrate with polymerization [Gao et al., 2008].

One interesting feature of the molecular imprinting method is that it can be applied to a wide range of analytes. MIPs have been synthesized indeed with specific recognition ability for both chemical and biological molecules, such as drugs [Puoci et al., 2007], pollutants [Bhaskarapillai et al., 2009], food ingredients [Gholivand et al., 2012], amino acids and proteins [Ivanova-Mitsev et al., 2012], various nucleotides and their derivatives [Spivak and Shea, 1998]. Therefore, MIPs have been widely used in many areas such as chromatograph separation [Byun et al., 2010], chemical analysis and detection [Apodaca et al., 2011], catalysis [Abbate et al., 2011], drug delivery [da Silva et al., 2011], as well as acting as plastic antibodies and receptors [Hoshino et al., 2010]. Recently, the molecular imprinting technique has been applied also for the determination and removal of pollutants from wastewater and drink water [Huang et al., 2015] [Shen et al., 2013].

4.2.1 MIPs for water treatment

Because of their outstanding properties, MIPs have become increasingly attractive in environmental chemistry. In particular, several researchers have begun to study the use of MIPs for wastewater treatment. In contrast to the conventional methods, MIPs are advantageous for treatment of trace contaminants because they can be specifically designed to remove

one or a group of target pollutants with low cost, low energy consumption and low environmental impact.

Due to the advantages of high selectivity and strong affinity, MIPs can become efficient methods for selective recognition, separation, determination and purification of pollutants in contaminated water [Huang et al., 2015].

Adsorption has been widely applied to remove chemical pollutants from water. This process is a phenomenon in which the adsorbates are attracted to the surface of solid adsorbent and form attachments via physical or chemical bonds. To date, various materials including activated carbon, graphene-based materials, etc., have been applied to removal of pollutants from water. Among these available adsorbents, it seems that MIPs are the most promising ones for pollutant removal, possessing high selectivity and considerable capacity to attract organic pollutants. Currently, a lot of experiments have been undertaken to examine the removal efficiency of organic pollutants by using MIPs, particularly for the treatment of trace contaminants in large-volume water samples [Dai et al., 2011] [Jing et al., 2014]. Another outstanding property of MIPs is the possibility to regenerate and subsequent reuse the polymers without significant loss in loading capacity for a large number of cycles so reducing the overall costs of treatment [Meng et al., 2012].

Further, MIP-based catalyst are attractive thanks to the advantages of MIPs to withstand aggressive conditions, including high temperature and pressure, extreme pH and organic solvent. In addition, MIP catalysts are able to mimic the active center of enzymes which are generally utilized as catalysts in several reactions and have high selectivity toward substrates. For these reasons, MIPs can be employed to develop tailored catalysts for special substrates. The MIP catalysts are mainly prepared by two approaches. The first one involves introduction of suitable catalytic groups in the active sites of the polymer [Liu and Wulff, 2008]. The second approach is based on the immobilization in MIPs of metal or metal oxide, such as TiO_2, exhibiting catalytic properties. The prepared MIP-coated photocatalysts not only enhanced the activity toward the photodegradation of target pollutants but also showed great selectivity compared to the conventional TiO_2 [Shen et al., 2008].

Although considerable progresses have been achieved , the real use of MIPs for water treatment is still in its infancy. Thus, there are many aspects that need further improvements. Firstly, some targets are still difficult to be used as templates; to overcome this problem it is important to study the fundamental mechanisms underlying the MIP formation, with particular attention on the stability and strength of the monomer template complex prior to polymerization. Therefore, a better understanding of the mechanism behind the molecular imprinting process is necessary for a successful preparation of MIPs. Secondly, the imprinting technologies to synthesis water-compatible MIPs are still required. The traditional polymers are often synthesized in organic solvent and display a different swelling effect when they are used in an aqueous system. In addition, water molecules compete with the template, making weaker or destroying the binding between template and functional monomer. A possible solution to synthesize water compatible MIPs is represented by the introduction of hydrophilic properties into the polymer [Pan et al., 2011]. Lastly, the potential risk for leakage of the residual template molecules, remained in the polymer matrix after the template-washing step, during the adsorption process is still a challenge.

Aim of this part of the thesis work was the synthesis of water-compatible MIPs, able to recognize and remove NSAIDs, such as diclofenac, from water. This specific activity was carried out during an internship at Linnaeus University in Kalmar (Sweden).

4.3 Experimental section

In this section, the chemicals and the procedure used to synthesize a molecular imprinted polymer able to recognize diclofenac will be described. In addition, the method adopted to verify the polymer's affinity toward the drug will be illustrated.

4.3.1 MIP film synthesis

MIP thin films were prepared by electrochemical polymerization under cyclic voltammetric conditions using a Reference 600 potentiostat/galvanostat (Gamry instruments, Warminster, PA, USA). The software, Gamry framework, provided by the manufacturer was used to control the instrument. Ag/AgCl electrode and Pt wire were used as counter and reference electrodes, respectively. 10 MHz quartz resonators (Attana AB, Stockholm, Sweden) of 8 mm diameter, sputtered on both the sides with 140 nm gold (adhered with a 10 nm Ti or Cr underlying layer), were used as working electrode and as substrates for the deposition of the polymeric films.

Before the electropolymerization, each gold coated quartz resonator was washed by piranha solution (H_2O_2:H_2SO_4, 1:3 v/v) for less than a minute, rinsed extensively with Milli-Q grade water and sonicated in Milli-Q water for ten minutes. After sonication, it was dried with air and then placed in the specially designed working electrode-holder for the electrochemical polymerization. This holder consists of a well-shaped groove carved into the plastic cover of it to provide a volume of 5 mm diameter and 2.5 mm depth above the gold surface. Next, it was electrically connected to the working electrode terminal of the Gamry potentiostat. A drop (~ 100 μL) of the pre-polymerization solution was then placed over the Au/quartz substrate. The counter and reference electrodes were carefully dipped into the solution close to the gold surface, though without making contact with the Au surface, or between the electrodes. The experimental set-up adopted during the electrochemical synthesis and a gold coated quartz resonator after the polymerization are showed in Fig. 4.3.

Pre-polymerization reaction mixtures were prepared by mixing diclofenac sodium salt (template), 3-aminophenylboronic acid hydrochloride (3-APBA) (functional monomer) and *p*-phenylenediamine (p-PD) (cross linker) in the ratio 1:5:25 and dissolved in Milli-Q water containing 0.2 M of Na_2SO_4 as supporting electrolyte [Suriyanarayanan et al., 2014]. The molecular structures of the above mentioned chemicals are reported in Fig. 4.4.

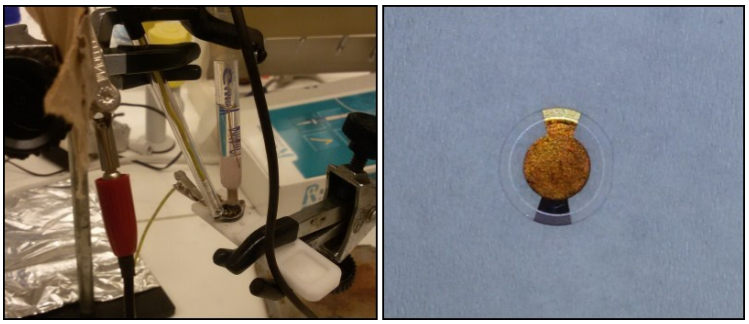

Figure 4.3: Experimental set-up for the electrochemical synthesis (on the left); and a gold coated quartz resonator with the MIP thin film on the top after the electropolymerization (on the right).

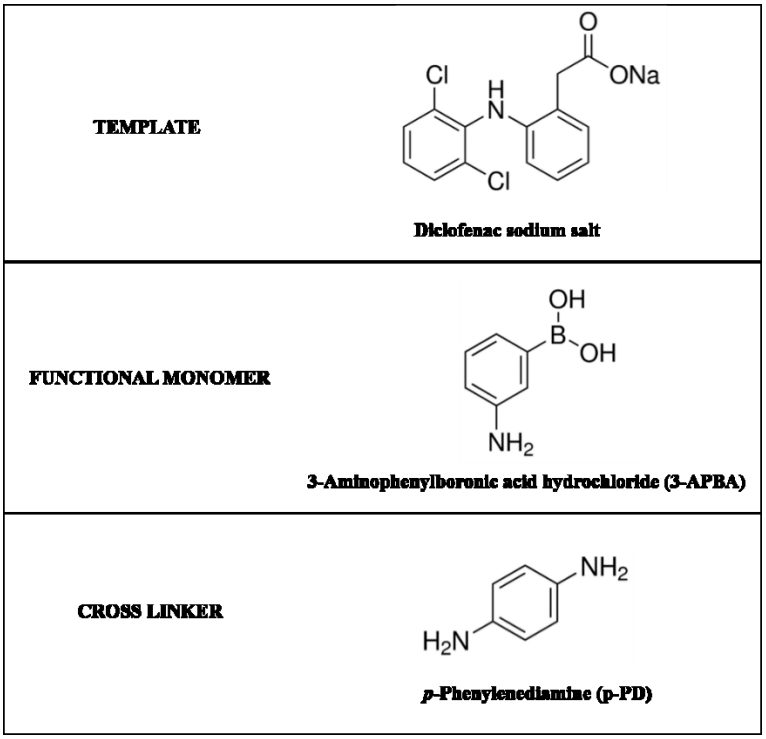

Figure 4.4: Molecular structures of template, functional monomer and cross linker, respectively.

The MIP films were deposited on the Au/quartz resonators by scanning the potential of the working electrode from -0.5 to 1.5 V at 50mV/s for 30 cycles. The growth of the polymer was governed by the number of cycles. Afterwards, the obtained polymer film was rinsed with water to remove the physisorbed species. The diclofenac template was extracted from the MIP films by washing them with 5 mM NaOH for 1 h.

A reference film was prepared by an identical procedure to that described above, but in the absence of the template diclofenac.

All chemicals used in this work were purchased from Sigma Aldrich and used as received.

4.3.2 Quartz Crystal Microbalance analysis

The difference in the recognition properties of the prepared polymeric films was studied by using a quartz crystal microbalance (QCM) system (Attana A100 and A200, Attana AB, Stockholm, Sweden) configured for flow injection analysis (FIA). The evaluation was made by measuring the variation in the resonant frequency of gold coated quartz resonators overlaid with the prepared films due to the binding of the analyte to the film. The QCM is a simple, cost effective, high-resolution mass sensing technique based upon the piezoelectric effect, major details about the working principles of this technique will be illustrated in the appendix of this dissertation.

Our substrates, overlaid with the MIP and the reference films, were mounted in the flow cell holders of the instruments. A mixture of EtOH:H_2O 40:60 v/v was used as the carrier buffer. A dual piston peristaltic pump, present within the QCM instrument, was used to pump the carrier buffer solution over the polymer film on the substrates. The buffer solution was allowed to equilibrate with polymer film at this condition to have minimum change (± 0.5 Hz) in the resonant frequency for over 400 s. The affinity of the synthesized MIP films towards the diclofenac was evaluated by injection in the flow cell using a 6-point injection valve of aliquots of this drug diluted with the carrier buffer. To investigate the specificity of the binding, the

answer of the MIP films was tested injecting in the QCM instrument solutions in EtOH:H_2O 40:60 v/v of other three different NSAIDs: naproxen, acetylsalicylic acid and ibuprofen. All of these drugs were purchased from Sigma Aldrich and used as received.

4.4 Results and discussion

Molecular imprinting can be achieved with a number of different methods including thermal initiated, electrochemical and photo-chemical polymerization. In this work, the electrochemical polymerization method has been preferred to prepare recognition film, as the polymer can be imprinted on the sensor surface without any initiator, easily and with a low toxicity process. The functional and cross linker monomers used in this study were selected on the basis of a previous work, as well as the experimental conditions adopted for the electropolymerization [Suriyanarayanan et al., 2014]. The functional monomer is the key player for the binding interaction with the template; the cross linker is important to control the polymer morphology, the durability of the binding sites and to improve the mechanical stability of the MIP.

During cyclic voltammetric conditions, the functional monomer is oxidized to form radical cations with delocalized electron of 3-APBA (Fig. 4.5). In the second step, which is named as chain propagation step, radical cations combine with other monomer of 3-APBA to form dimmer radical. Repeated activation and deactivation, which imply oxidation and reduction, propagate the polymer chain. In termination step, radicals combine to form a polymer network. Contemporary, the p-PD polymerizes with the same mechanism (Fig. 4.6) through the formation of radical cations. The reactions between different radical cations of 3-APBA and p-PD produce the copolymer film deposited on the electrode surface. At the end of the process, a uniformly brown thin layer on the Au/quartz resonator is obtained (Fig.

4.3). Non-imprinted polymer (REF) was prepared under the same conditions, but without the presence of diclofenac.

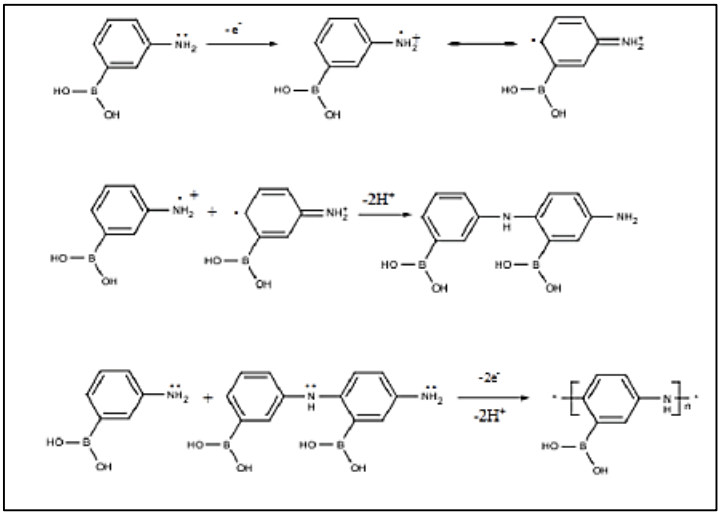

Figure 4.5: Mechanism of 3-APBA polymerization.

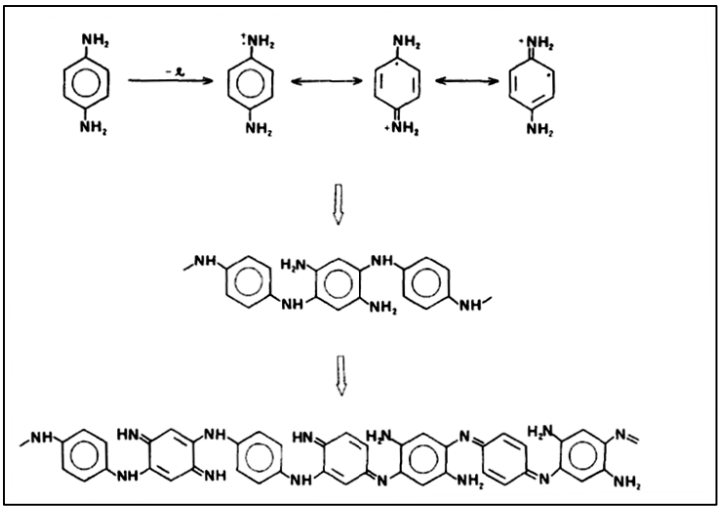

Figure 4.6: Mechanism of p-PD polymerization [Cataldo, 1996].

After electropolymerization, repeated rinsing of the imprinted polymer film with 5 mM NaOH solution for one hour carried out the extraction of the diclofenac template. This is a crucial step since it generates molecular cavities that carry the memory of the template and can recognize diclofenac under FIA condition.

Subsequent to the template extraction, the polymer's capacity to rebind diclofenac was examined by QCM under FIA conditions. With this technique, it is possible to detect small variations in mass of the Au/quartz resonators overlaid with the polymer films due to the binding between the injected analyte and the film. The variation in the mass of the resonator produces a change in its resonant frequency and a signal is observed. If there is not a binding event, no signals are visible in the QCM curve. The intensity of this variation is proportional to the strength of the binding. Fig. 4.7 reports the variation in the resonant frequency for both MIP and REF films, as a function of diclofenac concentration. The detected variations are significantly higher for the MIP film if compared to the variations obtained with the REF film. This result is confirmed by the relative sensitivities values calculated from the slopes of the plots and reported in Table 4.2. The value for the MIP film is considerably greater than the corresponding value for the REF film. The relative sensitivity values reflect the affinity between the polymer and the analyte.

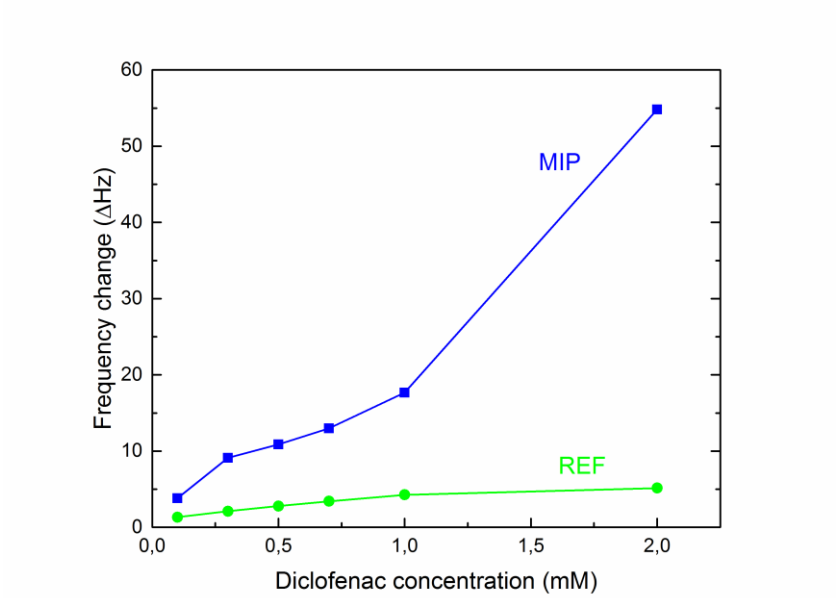

Figure 4.7: Variation in the resonant frequency of gold-coated quartz resonators overlaid with MIP and REF films versus diclofenac concentrations.

Table 4.2: Relative sensitivities of MIP and REF films toward diclofenac.

POLYMER FILM	RELATIVE SENSITIVITY (Hz/mM)
MIP	26.44 ± 3.18
REF	1.94 ± 0.34

In order to investigate the specificity of the binding, the answer of the MIP film was tested using four different NSAIDs: diclofenac, naproxen, acetylsalicylic acid and ibuprofen. The obtained variations in the resonant frequency as a function of each drug concentration are showed in Fig. 4.8, and the calculated relative sensitivity values are reported in Table 4.3. As evidenced by the results, the MIP film shows a higher affinity for the

diclofenac, the drug used as template during the electropolymerization. The frequency changes are indeed higher injecting diclofenac, this effect being clearly illustrated in Fig. 4.9, which reports the frequency change for the 2 mM concentration, and it is confirmed by the relative sensitivity value significantly higher using the diclofenac.

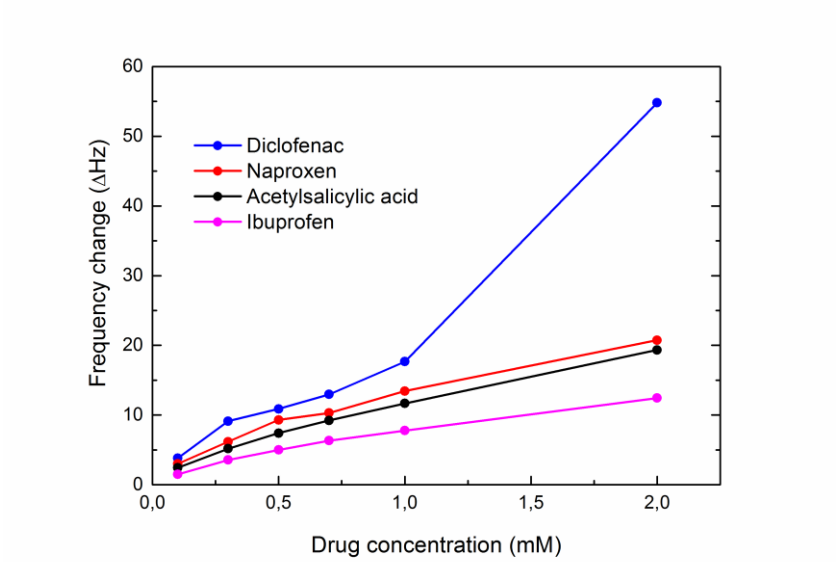

Figure 4.8: Relative response of the MIP film to four different NSAIDs at different concentrations.

Table 4.3: Relative sensitivities of MIP film toward four different NSAIDs.

ANALYTE	RELATIVE SENSITIVITY (Hz/mM)
Diclofenac	26.44 ± 3.18
Naproxen	8.93 ± 0.76
Acetylsalicylic acid	8.62 ± 0.48
Ibuprofen	5.5 ± 0.43

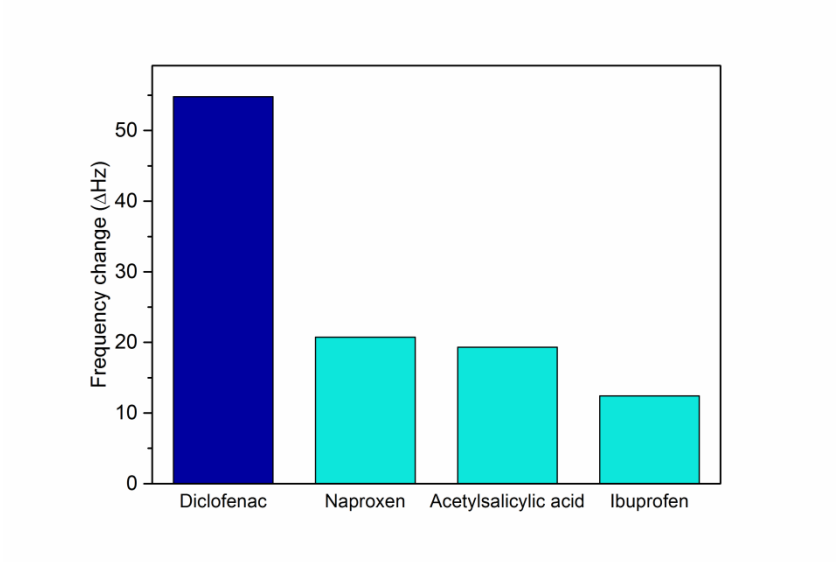

Figure 4.9: Relative response of the MIP film to four different NSAIDs with a concentration of 2 mM in EtOH:H_2O 40:60 v/v.

4.5 Conclusions and future perspectives

In this chapter, molecularly imprinted polymers have been proposed as valid solutions to recognize and remove ECs from water, that are representing a dramatic issue for the environment. In particular, we have synthesized by electropolymerization a MIP film able to recognize with a very high selectivity a non-steroidal anti-inflammatory drug, the diclofenac, which is one of the most alarming ECs.

These preliminary results are strongly promising and encourage to develop and improve the synthesis procedures to prepare polymer films with particular affinity for other NSAIDs. In addition, with the QCM we were able to study the recognition properties of the synthesized film; however, the stability of the binding between the polymer film and the analyte, needs also to be studied in more details.

References

- Abbate, V.; Bassindale, A.R.; Brandstadt, K.F.; Taylor, P.G. *J. Catal.* **2011,** 284, 68-76
- Alder, A.C. **2006** *Consumption and occurrence. In: T.A., T., A., J. (Eds), Human Pharmaceuticals, Hormones and Fragrances. The challenge of Micropollutants in Urban Water Management.* IWA Publishing
- Alexander, C.; Andersson, H.S.; Andersson, L.I.; Ansell, R.J.; Kirsch, N.; Nicholls, I.A.; O'Mahony, J.; Whitcombe, M.J. *J. Mol. Recognit.* **2006,** 19, 106-180
- Apodaca, D.C.; Pernites, R.B.; Ponnapati, R.; Del Mundo, F.R.; Advincula, R.C. *Macromolecules* **2011,** 44, 6669-6682
- Arshady, R.; Mosbach, K. *Macromol. Chem. Phys.* **1981,** 182, 687-692
- Bhaskarapillai A.; Sevilimedu, N.V.; Sellergren, B. *Ind. Eng. Chem. Res.* **2009,** 48, 3730-3737
- Boxall, A.B.A.; Kolpin, D.W.; Halling-Sorensen, B.; Tolls, J. *Environ. Sci. Technol.* **2003,** 37, 286A-294A
- Boxall, A.B.A.; *New and Emerging Water Pollutants arising from Agriculture; Environment Department, University of York, United Kingdom, OECD* **2012**
- Byun, H.S.; Youn, Y.N.; Yun, Y.H.; Yoon, S.D. *sep. Purif. Technolog.* **2010,** 74, 144-153
- Cataldo, F. *Eur. Polym. J.* **1996,** 32, 43-50
- Dai, C.M.; Geissen, S.U.; Zhang, Y.L.; Zhang, Y.J.; Zhou, X.F. *Environ. Pollut.* **2011,** 159, 1660-1666
- da Silva, M.S.; Viveiros, R.; Morgada, P.I.; Aguiar-Ricardo, A.; Correia, I.J.; Casimiro, T. *Int. J. Pharm.* **2011,** 416, 61-68
- Dickey, F.H. *J. Phys. Chem.* **1955,** 59, 695-707
- Gao, B.; Wang, J.; An, F.; Liu, Q. *Polymer* **2008,** 49, 1230-1238
- Garric, J.; Vollat, B.; Duis, K.; Péry, A.; Junker, T.; Ramil, M.; Fink, G.; Ternes, T.A. *Chemosphere* **2007,** 69, 903-910
- Gholivand, M.B.; Torkashvand, M.; Malekzadeh, G. *Anal. Cim. Acta* **2012,** 713, 36-44

- Haupt, K.; Mosbach, K. *Chem. Rev.* **2000,** 100, 2495-2504
- He, C.Y.; Long, Y.Y.; Pan, J.L. *J. Biochem. Bioph. Meth.* **2007,** 70, 133-150
- Hoshino, Y.; Koide, H.; Urakami, T.; Kanazawa, H.; Kodama, T.; Oku, N.; Shea, K.J. *J. Am. Chem. Soc.* **2010,** 19, 644-6645
- Hu, X.; Hu, Y.; Li, G. *J. Chromatogr. A* **2007,** 1147, 1-9
- Huang, D.L.; Wang, R.Z.; Liu, Y.G.; Zeng, G.M.; Lai, P.; Lu, B.A.; Xu, J.J.; Wang, C.; Huang, C. *Environ. Sci. Pollut. Res.* **2015,** 22, 963-977
- Hughes, S.R.; Kay, P.; Brown, L.E. *Environ. Sci. Technol.* **2013,** 47, 661-677
- Ivanova-Mitsev, P.K.; Guerreiro, A.; Piletska, E.V.; Whitcombe, M.J.; Zhou, Z.; Mitsev, P.A.; Davis, F.; Piletsky, S.A. *Angew. Chem., Int. Ed.* **2012,** 51, 5196-5199
- Jing, T.; Wang, J.; Liu, M.; Zhou, Y.; Zhou, Y.; Mei, S. *Environ. Sci. Pollut. R.* **2014,** 21, 1153-1162
- Lange, R.; Hutchinson, T.H.; Croudace, C.P.; Siegmund, F.; Schweinfurth, H.; Hampe, P.; panter, G.H.; Sumpter, J.P. *Environ. Toxicol. Chem.* **2001,** 20, 1216-1227
- Liu, J.; Wulff, G. *J. Am. Chem. Soc.* **2008,** 130, 8044-8054
- Lonappan, L.; Brar, S.K; Das, R.K.; Verma, M.; Surampalli, R.Y. *Environ. Int.* **2016,** 96, 127-138
- Loos, R.; Carvalho, R.; Antonio, D.C.; Comero, S.; Locoro, G.; Tavazzi, S.; Paracchini, B.; Ghiani, M.; Lettieri, T.; Blaha, L.; Jarosova, B.; Voorspoels, S.; Servaes, K.; Haglund, P.; Fick, J.; Lindberg, R.H.; Schwesig, D.; Gawlik, B.M. *Water Res.* **2013,** 47, 6475-6487
- Malitesta, C.; Mazzotta, E.; Picca, R.A.; Poma, A.; Chianella, I.; Piletsky, S.A. *Anal. Bioanal. Chem.* **2012,** 402, 1827-1846
- Martín-Esteban, A. *Trac-Trends Anal. Chem.* **2013**, 45, 169-181
- Mayes, A.G.; Mosbach, K. *Anal. Chem.* **1996,** 68, 3769-3774
- Meng, Z.; Zhang, Q.; Xue, M.; Wang, D.; Wang, A. *Propellants Explos. Pyrotech.* **2012,** 37, 100-106
- Oaks, J.L.; Gilbert, M.; Virani, M.Z.; Watson, R.T.; Meteyer, C.U.; Rideout, B.A.; Shivaprasad, H.L.; Ahmed, S.; Chaudhry, M.J.I.; Arshad, M.; Mahmood, S.; Ali, A.; Khan, A.A. *Nature* **2004,** 427, 630-633

- Pan, G.Q.; Zhang, Y.; Ma, Y.; Li, C.X.; Zhang, H.Q. *Angew. Chem., Int. Ed.,* **2011,** 50, 11731-11734
- Pauling, L.; *J. Am. Chem. Soc.* **1940,** 62, 2643-2657
- Petrie, B.; Barden, R.; Kasprzyk-Horden, B. *water Res.* **2015,** 72, 3-27
- Puoci, F.; Iemma, F.; Cirillo, G.; Picci, N.; Matricardi, P.; Alhaique, F. *Molecules* **2007,** 12, 805-814
- Shen, X.; Zhu, L.; Liu, G.; Yu, H.; Tang, H. *Environ. Sci. Technol.* **2008,** 42, 1687-1692
- Shen, X.; Xu, C.; Ye, L. I*nd. Eng. Chem. Res.* **2013,** 52, 13890-13899
- Spivak, D.A.; Shea, K.J. *Macromolecules* **1998,** 31, 2160-2165
- Suriyanarayanan, S.; Nawaz, H.; Ndizeye, N.; Nicholls, I.A. *Biosensors* **2014,** 4, 90-110
- Whitcombe, M.J.; Kirsch, N.; Nicholls, I.A. *J. Mol. Recognit.* **2014,** 27, 297-401
- Wulff, G.; Sarhan, A. *Angew. Chem., Int. Ed.* **1972,** 11, 341-344
- Yan, S.L.; Gao, Z.X.; Fang, Y.J.; Cheng, Y.Y.; Zhou, H.Y.; Wang, H.Y. *Dyes Pigm.* **2007,** 74, 572-577
- Zheng, C.; Huang, Y.P.; Liu, Z.S. *Anal. Bioanal. Chem.* **2013,** 405, 2147-2161

Conclusion

Water is a fundamental natural resource upon which all the economic activities and ecosystems depend. Universal access to safe drinking water and in general to water resources is an imperative that concerns a great number of internationally agreed development objectives. Sufficient water supply, of good quality, is a key ingredient in the health and well-being of humans and ecosystems and for socio-economic development. For too long time water was taken as granted until increasing pollution and diminishment of potable water supplies delineated a need to protect our water provisions and develop new technologies to purify water. The starting point of this thesis originated from these observations. Aim of this work was the development of new tools that overcome the limits of the traditional water treatment methods. Our goal was to realize active materials able to remove organic pollutants with low cost, low energy consumption and low environmental impact.

One of the most promising approach to revolutionize the water treatment techniques is the use of nanostructured photocatalysts, especially TiO_2 nanomaterials. The main advantage of these materials is represented by the high surface-to-volume ratio that increases enormously as the size of a material decreases. This property facilitates the reactions on the photocatalyst surface that are responsible for the degradation of organic contaminants in water. To date, the most applied photocatalyst is the Degussa P-25, formed by TiO_2 nanoparticles in a slurry form. However, with the slurry TiO_2 system, an additional step is needed for the recovery of the catalysts to avoid their impact on the environment. All the potential recovery methods are time and energy consuming, and for this reason we established at the beginning of the thesis work, after a deep investigation of the methodologies present in the literature, that immobilization of the nanomaterials in a solid support, such as a polymer, is the key solution for their use in large-scale applications. We hence took this decision and, during our work, tried to affirm our position in the water purification scenario.

Our general approach consisted in the realization of polymer nanocomposites based on solution casting of a mixture consisting of pre-made TiO_2 nanomaterials and polymer solution. This simple and low-cost method is easily scalable. The polymer matrix selected for supporting titania is poly(methyl methacrylate) (PMMA). This choice relies on its transparency to visible light and high resistance to UV light, its mechanical properties and environmental stability, its cheapness. The adopted synthesis procedure allowed us to obtain highly stable films in freestanding form. We realized polymer nanocomposites made of PMMA/TiO_2 nanomaterials with high photocatalytic and antibacterial activity under UV irradiation. Furthermore, we combined titanium dioxide nanoparticles with carbon nanomaterials, as acceptor system, and obtained a significantly higher photocatalytic efficiency under UV irradiation, compared to the systems with TiO_2 only. Photoactive materials even under visible light were synthesized thanks to the functionalization of TiO_2 with dye sensitizer.

In the last part of this thesis, our attention has been addressed to the emerging dangerous contaminants present in traces in wastewater. Emerging contaminants are defined as chemicals that are not currently regulated and about which some concerns exist regarding their impact on human or ecological health. We propose molecularly imprinted polymers (MIPs) as valid tools to remove these contaminants from water and solve this dramatic issue for the environment. We have synthesized by electropolymerization MIPs able to recognize with a very high selectivity non-steroidal anti-inflammatory drugs, such as diclofenac, one of the most alarming emerging contaminants. The obtained results are strongly promising and encourage to further study these polymer material in this field.

The materials studied and realized in this work overcome many of the current issues of the traditional methods for water purification and provide good opportunities to develop low cost systems for water treatment, with a particular impact for developing countries and remote sites.

Appendix: Characterization techniques

Appendix A: Scanning Electron Microscopy

A scanning electron microscope (SEM) uses a high-energy beam of electrons to obtain images of a surface with a very high resolution. Values on the order of 2 to 5 nm (20-50 Å) are now usually quoted for commercial instruments, while advanced research instruments are available that have achieved resolutions of better than 1 nm (10 Å). The reason for such a high resolution lies in the probe size, i.e. the beam, and in the reduced interaction volume obtained at low energy of the beam. The electrons interact with the atoms of the sample producing signals that contain information about the sample surface topography and composition.

The resolution is the finest detail that can be distinguished in an image. The way to improve the resolution is to use an incident beam with short wavelengths and media with large indices of refraction. The SEM exploits these principles by using extremely short wavelengths of accelerated electrons to form high-resolution images. In addition, due to the very narrow electron beam, SEM micrographs have a large depth of field yielding a characteristic three-dimensional appearance useful for understanding the surface structure of a sample (see Fig. A.1).

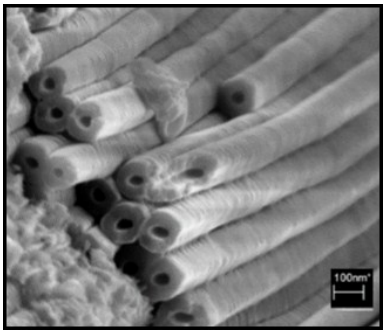

Figure A.1: SEM image of TiO_2 nanotubes obtained by electrochemical anodization on Ti foils.

Fig. A.2 shows the fundamental components of a scanning electron microscope. The electron beam is produced at the top of the microscope by an electron gun. Electron guns are typically of two types: thermionic guns, which are the most common type, apply thermal energy to a filament (usually made of tungsten, which has a high melting point, or LaB_6) to emit electrons toward the specimen under examination; field emission guns (FEG), on the other hand, create a strong electrical field to pull electrons away. The thermionic sources have the disadvantages of relatively low brightness, evaporation of the cathode material and thermal drift during operation. The way of generating electrons in a FEG is instead free from these disadvantages; the SEM instrument used in this work has a FEG as electron source. The produced electrons are accelerated towards the anode with an energy ranging from 0.2 KeV to 40 KeV. The electron beam is focused by one or more lenses to a spot about 0.4 nm to 5 nm in diameter. The beam passes through pairs of scanning coils or pairs of deflector plates in the electron column, typically in the final lens, which deflect the beam in the x and y axes so that it scans in a raster fashion over a rectangular area of the sample surface. Conventional SEM requires samples to be imaged under vacuum (10^{-6} mbar), because a gas atmosphere rapidly spreads and attenuates electron beams.

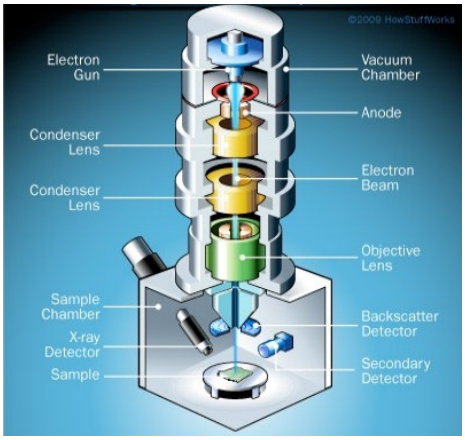

Figure A.2: Design of a scanning electron microscope.

When the primary electron beam interacts with the sample, the electrons lose energy by repeated random scattering and absorption within a teardrop-shaped volume of the specimen known as the interaction volume, which extends from less than 100 nm to approximately 5 µm into the surface. The size of the interaction volume depends on the electron's landing energy, the atomic number of the specimen and the specimen's density. The energy exchange between the electron beam and the sample results in the reflection of high-energy electrons by elastic scattering, emission of secondary electrons by inelastic scattering and the emission of electromagnetic radiation, each of which can be detected by specialized detectors. In the scanning electron microscope imaging, the signals of greatest interest are the secondary and backscattered electrons, since these vary according to differences in surface topography as the electron beam sweeps across the specimen. The secondary-electron emission is confined to a volume near the beam impact area, sloping surface will tend to produce increased emission, somewhat explaining the sensitivity of the SEM to surface topography. This also contributes to the "optical" appearance of an SEM micrograph. Edges and steps also tend to produce increased emission, due to bleeding of secondaries from neighboring surfaces.

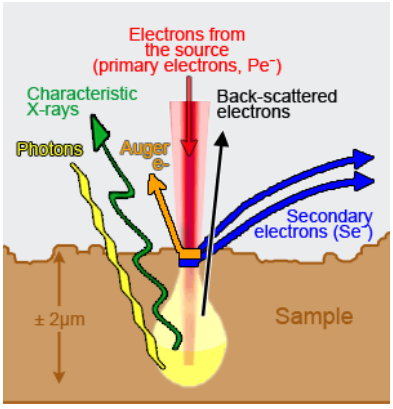

Figure A.3: Signals emitted from the interaction between the primary electron beam and the sample.

As the SEM utilizes vacuum conditions and uses electrons to form an image, special preparations must be done to the sample. All water must be removed from the samples because the water would vaporize in the vacuum. All metals are conductive and require no preparation before being used. All non-metals need to be made conductive by covering the sample with a thin layer of conductive material.

The SEM images, showed in this thesis, have been acquired using a Gemini Field Emission SEM – Zeiss SUPRA 25 operating at 2-3 kV. For the SEM analysis, the samples to be analyzed were coated, by sputter deposition, with 3 nm of gold in order to prevent the electron beam charging of the insulating polymer.

References

- Egerton, R.F. *"Physical Principles of Electron Microscopy"* Springer, **2005**
- Goldstein, J. et al. *"Scanning Electron Microscopy and X-Ray Microanalysis"* Springer, **1992**

Appendix B: Atomic Force Microscopy

Atomic force microscopy (AFM) is a technique used to produce quantitative topographic images of surfaces at a magnification of up to 10^7. The underlying principle is surface scanning using a sharp tip or stylus and the measurement of atomic forces between the stylus and the specimen. The stylus on an atomic force microscope is sensitive to both attractive and repulsive surface forces, but in practice the repulsive forces are the most stable, and these are the most widely used to obtain images. Scanning can be carried out in vacuum, but a major advantage of AFM over scanning electron microscopy (SEM) is that AFM can be performed in air or with the sample immersed in a liquid. Also, in contrast to SEM, no pretreatment of insulating samples, such as gold coating, is required. The resulting data also provide a true three-dimensional profile (see Fig. B.1), not a two-dimensional image of a surface, as obtained by SEM.

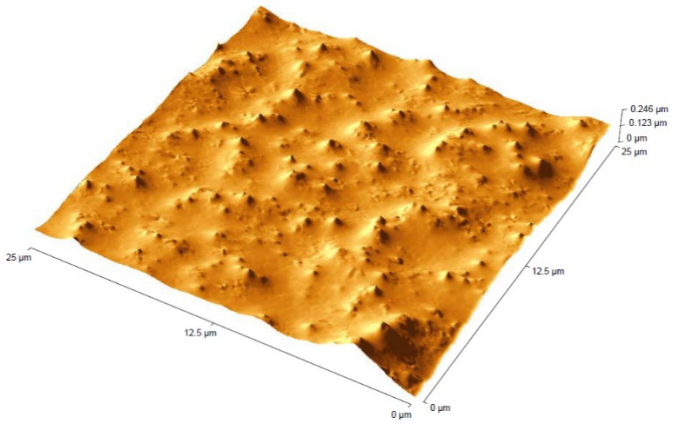

Figure B.1: AFM image of the surface of a polymeric film with embedded TiO_2 nanoparticles.

AFM is based on a related technique called scanning tunneling microscopy (STM). The main difference between AFM and STM is that the latter requires a conducting surface that can sustain a stable tunneling current, making it unsuitable for most applications. Since AFM works also on non conducting surfaces, it is suitable for the analysis of polymeric materials, cells, membranes, protein complexes, individual proteins, and nucleic acids.

A typical AFM setup is shown in Fig. B.2. At the heart of the AFM is a force sensor, a micro-cantilever that has a sharp tip at its free end. The atoms on the tip of the cantilever and the atoms on the surface of sample exert a force on each other. These forces are typically in the piconewton range and qualitatively have the characteristics of an attractive nature for large separations and sharp repulsive nature at short ranges. A good qualitative model for the interatomic forces is the Lennard–Jones potential, where the force F between the atoms is given by $F(r) = -A/r^7 + B/r^{13}$, where r represents the separation between the atoms. The cantilever deflection is sensed by a laser beam that reflects from the cantilever surface into a split photodiode. The sample is positioned using a piezoelectric scanners that provide motion of the cantilever tip with respect to all three directions; the two lateral x and y directions as well as the vertical z direction.

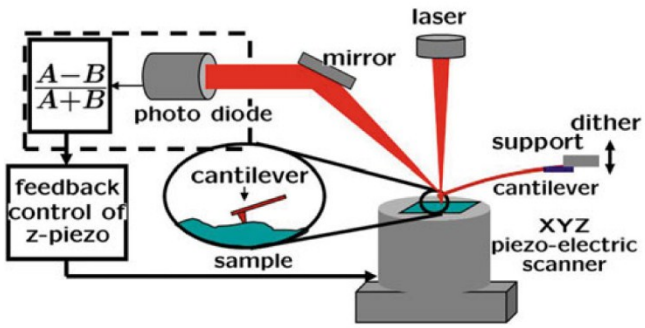

Figure B.2: An atomic force microscope schematic illustration.

Two operation mode are distinguished: contact mode and tapping mode. The so-called contact mode operation uses the cantilever deflection as the feedback signal. In other words, the AFM probe traces the surface corrugation with keeping the deflection signal constant, commonly in the repulsive region by moving the sample up and down using a piezoelectric scanner. In this method, since the AFM probe is scanned over a sample surface in contact, it makes the existence of frictional force inevitable. The damage by the frictional force is sometimes very serious. The tapping mode has been indeed developed to overcome problems seen in contact mode; the AFM cantilever is now vibrated at a certain frequency near its resonant frequency. When its probe starts to touch the sample surface intermittently, the oscillation amplitude decreases. Tapping mode operation uses this amplitude signal for feedback control. As indicated by the naming of "tapping", the contact between the probe and the sample is limited to a very short period during a vibration cycle, and many problems occurring in contact mode can be improved. The contact force exerted to the sample can be minimized and the effect of frictional interaction becomes negligible even when harder cantilevers are used.

The AFM images, showed in this thesis, have been acquired using a Veeco-Innova microscope operating in contact mode with an ultra-sharpened Si tip.

References

- Twyman, R.M. *"Atomic Force Microscopy Methodologies"* Elsevier, **2009**
- Gorman, J.J.; Shapiro, B. *"Feedback Control of MEMS to Atoms"* DOI 10.1007/978-1-4419-5832-7_5 Springer, **2012**
- Mittal, V. *"Characterization Techniques for Polymer Nanocomposites"* Wiley-VCH Verlag GmbH & Co, **2012**

Appendix C: Quartz Crystal Microbalance

The quartz crystal microbalance (QCM) is a simple, cost effective, high-resolution mass sensing technique, based upon a piezoelectric effect. The technique possesses a wide detection range. At the low mass end, it can detect monolayer surface coverage by small molecules or polymer films. At the upper end, it is capable of detecting much larger masses bound to the surface.

The possibility of using quartz crystal resonators as quantitative mass measuring devices was first explored by Sauerbrey (1959). The decrease of the resonant frequency of a thickness shear vibrating quartz crystal resonator was found to be proportional to the added mass of deposited film:

$$\Delta f = -\frac{f_q^2 M_f}{N \rho_q S} = -\frac{f_q^2 m_f}{N \rho_q}$$

where f_q is the fundamental resonant frequency of the quartz, N is the frequency constant of the specific crystal cut ($N_{AT} = 1.67 \cdot 10^5$ Hz · cm; $N_{BT} = 2.5 \cdot 10^5$ Hz · cm), $\rho_q = 2.65$ kg/dm^3 is the quartz density, and S is the surface area of the deposited film, the mass of which is M_f. When the deposited film covers the whole sensitive area of the quartz resonator it is easier to use the areal density, $m_f = M_f/S$.

A piezoelectric quartz crystal resonator is a precisely cut slab from a natural or synthetic crystal of quartz. A QCM consists of a thin quartz disk with electrodes plated on it as can be seen in Fig. C.1. The application of an external electrical potential to a piezoelectric material produces internal mechanical stress. As the QCM is piezoelectric, an oscillating electric field applied across the device induces an acoustic wave that propagates through the crystal and meets a minimum impedance when the thickness of the device is a multiple of half wavelength of the acoustic wave. A QCM is a shear mode device in which the acoustic wave propagates in a direction

perpendicular to the crystal surface. To make this happen, the quartz crystal plate must be cut to a specific orientation with respect to the crystal axes. These cuts belong to the rotated Y-cut family: the AT- and BT- cuts shown in Fig. C.2 are representative. Deposition of a thin film on the crystal surface decreases the frequency in proportion to the mass of the film. A typical experimental apparatus set up is shown in Fig. C.3.

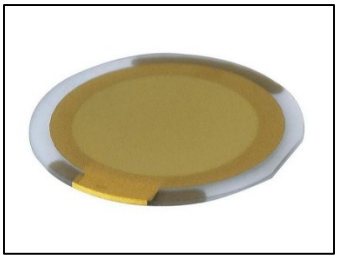

Figure C.1: A typical quartz crystal resonator used for mass measurements.

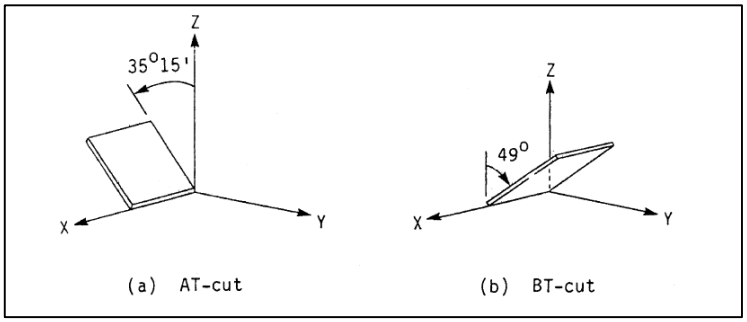

Figure C.2: AT- and BT- quartz crystals.

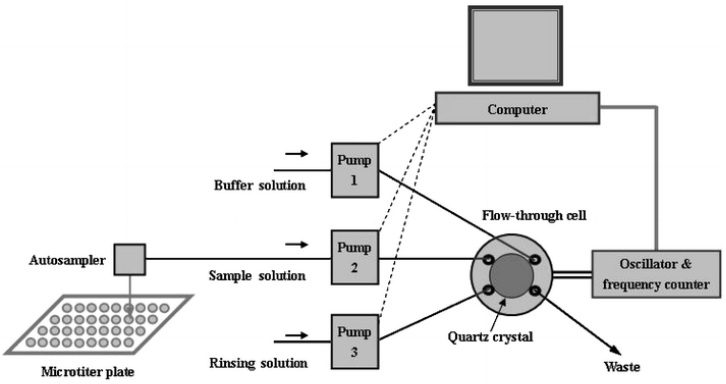

Figure C.3: Typical experimental apparatus set-up of piezoelectric QCM.

Commercial systems are designed to measure mass changes up to ~ 1 ng cm^{-2}.

In this thesis, we have evaluated the recognition properties of the synthesized MIP films by using Attana A100 and Attana A200 QCM, both configured for flow injection analysis. The evaluation was made by measuring the variation in the resonant frequency of gold coated quartz resonators.

References

- Marx, K.A. *Biomacromolecules* **2003**, vol. 4, no. 5
- Mecea, V.M. *Anal. Lett.* **2005,** 38, 753-767
- O'Sullivan, C.K.; Guilbault, G.G. *Biosens. Bioelectron.* **1999,** 14, 663-670

Curriculum vitae

Maria Cantarella was born in November 26, 1987 in Giarre (Catania). She attained her Master Degree in Materials Chemistry with full marks (110/110 cum laude) at the University of Catania in 2011. She worked with a fellowship at the CNR-IPCB institute of Catania since September 2012 to December 2013. In January 2014, she started the PhD course in Materials Science and Nanotechnology at the University of Catania and CNR-IMM under the supervision of Dr. Vittorio Privitera. She spent part of her PhD course at Linnaeus Univeristy (Kalmar, Sweden), with an Erasmus grant, under the supervision of Prof. Ian Nicholls. She is currently working with a fellowship at CNR-IMM under the supervision of Dr. Privitera and Dr. Giuliana Impellizzeri. The main scientific interests are focused on the realization of polymer nanocomposites with photocatalytic properties for water treatment, and the synthesis of molecularly imprinted polymers for the removal of emerging contaminants from water. During the PhD course she presented the results of her research activity, giving both oral and poster contributions, at the following international conferences: IEEE NMDC 2014 (Aci Castello, Italy), E-MRS Spring Meeting 2015 (Lille, France), FisMat 2015 (Palermo, Italy), NanoSEA 2016 (Giardini Naxos, Italy), Materials.it 2016 (Aci Castello, Italy). She won the Young Scientist Award at Symposium B of the E-MRS Spring Meeting 2015: “Materials for Applications in Water Treatment and Water Splitting”. She was a member of the organizing committee of the NanoSEA 2016 conference. Maria Cantarella is author or co-author of several articles, published in international referred scientific journals. She is reviewer of several international scientific journals.

List of publications

- **Cantarella, M.;** Sanz, R.; Buccheri, M.A.; Romano, L.; Privitera, V. "PMMA/TiO_2 nanotubes composites for photocatalytic removal of organic compounds and bacteria from water" *Mater. Sci. Semicond. Process.* **2016,** 42, 58-61
- **Cantarella, M.;** Sanz, R.; Buccheri, M.A.; Ruffino, F.; Rappazzo, G.; Scalese, S.; Impellizzeri, G.; Romano, L.; Privitera, V. "Immobilization of nanomaterials in PMMA composites for photocatalytic removal of dyes, phenols and bacteria from water" *J. Photochem. Photobiol., A* **2016,** 321, 1-11
- Di Mauro, A.; **Cantarella, M.;** Nicotra, G.; Privitera, V.; Impellizzeri, G. "Low temperature atomic layer deposition of ZnO: Applications in photocatalysis" *Appl. Catal., B* **2016,** 196, 68-76
- Fragalà, M.E.; Di Mauro, A.; Cristaldi, D.A.; **Cantarella, M.;** Impellizzeri, G.; Privitera, V. "ZnO nanorods grown on ultrathin ZnO seed layers: Application in water treatment" *J. Photochem. Photobiol., A* **2017,** 332, 497-504
- Di Mauro, A.; **Cantarella, M.;** Nicotra, G.; Pellegrino, G.; Gulino, A.; Brundo, M.V.; Privitera, V.; Impellizzeri, G. "Novel Synthesis of ZnO/PMMA nanocomposites for photocatalytic applications" *Sci. Rep.* **2017,** 7:40895, DOI: 10.1038/srep40895

Acknowledgements

Il mio primo e più grande grazie è rivolto al Dr. Vittorio Privitera, mio tutor scientifico e modello per me da seguire nella vita. Lo ringrazio per la professionalità, la gentilezza, la pazienza e l'entusiasmo con cui mi ha guidato in questi anni, per la fiducia che ha sempre riposto in me, per la serenità con la quale abbiamo affrontato ogni singola sfida di questo percorso e per i suoi innumerevoli consigli. Gli insegnamenti che mi ha dato e i valori che mi ha trasmesso vanno ben oltre le pagine di questa tesi ed è per questo che ritengo il mio dottorato ricco ed io una persona fortunata.

Ringrazio la Dott.ssa Giuliana Impellizzeri, la passione e la determinazione con cui affronta il suo lavoro sono per me un valido esempio. Un grazie va anche agli altri ricercatori del gruppo Water: la Dott.ssa Lucia Romano, il Dr. Massimo Zimbone, il Dr. Ruy Sanz, la Dott.ssa Maria Antonietta Buccheri e la Dott.ssa Viviana Scuderi, sempre disponibili e pronti ad aiutarmi.

Grazie al Prof. Ian Nicholls e al suo gruppo di ricerca, che mi hanno accolta durante il mio tirocinio Erasmus in Svezia, periodo per me di forte crescita personale e professionale. In particolare, ringrazio Alina Sklad, con la quale ho condiviso i successi, ma anche gli insuccessi, di questo periodo.

Ringrazio la Prof.ssa Maria Grazia Grimaldi, valida coordinatrice del dottorato in scienza dei materiali e nanotecnologie. Grazie anche al Prof. Robert Carles e al Dott. Fabio Iacona, che in qualità di referee hanno letto con attenzione la mia tesi fornendomi preziosi suggerimenti.

Ringrazio tutti i professori, i ricercatori, i tecnici e gli amministrativi del CNR-IMM (Università), sempre cordiali e disponibili. Ringrazio anche tutti gli assegnisti e i dottorandi, che hanno fatto o che fanno ancora parte del gruppo, è stato un piacere lavorare, seguire i seminari, partecipare alle riunioni e pranzare con tutti loro. In particolare, desidero ringraziare Alessandro che con la sua allegria e sincerità è stato per me un collega

ideale; Saro e Maria Josè che condividono con me le ansie e le soddisfazioni di questo percorso di dottorato.

Un immenso grazie va agli amici della stanza dottorandi: Vicky, Enrica, Brunilde, Giuseppe Cacciato, Giuseppe Suriani, Marta, Emanuele, Laura e Lucia. Il sorriso, la serenità e la fiducia hanno sempre accompagnato le nostre giornate, per questo non avrei potuto desiderare compagni di stanza migliori.

Grazie alla persona che mi sostiene e mi aiuta da sempre e che più di tutti gioisce ad ogni mio successo, mia madre. Grazie a tutta la mia grande famiglia e soprattutto ai miei dolcissimi nipoti, che nonostante in alcuni periodi non mi vedano per settimane mi aspettano sempre a braccia aperte.

Infine, un grazie speciale va ad una persona unica, Aldo, che mi ascolta e mi incoraggia sempre e che con il suo affetto completa e riempie la mia vita di straordinaria felicità.